Identification and characterization of the genetic alterations underlying neuroendocrine tumors of the small intestine

Dissertation

der Mathematisch-Naturwissenschaftlichen Fakultät

der Eberhard Karls Universität Tübingen

zur Erlangung des Grades eines

Doktors der Naturwissenschaften

(Dr. rer. nat.)

vorgelegt von

Maike Nieser, geb. Hoffmeister

aus Dieburg

Tübingen

2016

Gedruckt mit Genehmigung der Mathematisch-Naturwissenschaftlichen Fakultät der Eberhard Karls Universität Tübingen

Tag der mündlichen Qualifikation:	22.09.2016
Dekan:	Prof. Dr. Wolfgang Rosenstiel
1. Berichterstatter:	Prof. Dr. Bence Sipos
2. Berichterstatter:	Prof. Dr. Hans-Georg Rammensee

Acknowledgements

Prof. Bence Sipos danke ich herzlich für die Überlassung des spannenden Themas dieser Doktorarbeit und die Einführung in die Welt der neuroendokrinen Tumoren. Ich hatte das Glück einer intensiven Betreuung und des gleichzeitigen Einräumens vieler Freiheiten, welche maßgeblich zum Gelingen der Arbeit beigetragen haben. Prof. Bence Sipos ist mir ein Mentor und Vorbild und ich hoffe sehr, dass die anregende Zusammenarbeit noch viele Jahre weitergeht, in denen ich weiter von ihm lernen kann.

Prof. Hans-Georg Rammensee danke ich sehr für die Unterstützung meiner Arbeit als Zweitgutachter.

Prof. Falko Fend danke ich für die Möglichkeit meine Dissertation in der Pathologie zu absolvieren und für die Einbindung in die Molekulare Diagnostik, welche mir ebenfalls viel Freude bereitet.

Großer Dank geht an die AG Sipos & Friends, namentlich Jan Sperveslage, Karen Greif, Christine Beschorner, Dennis Thiele und Bettina Neumayer, für die unglaublich gute (Arbeits-) Atmosphäre, die fortwährend herrschte, sodass auch viele außer-pathologische Tätigkeiten wie Grillfeste, Konzertbesuche und Laufwettbewerbsteilnahmen gemeinsam unternommen wurden. Selbstverständlich bin ich ebenso dankbar für die exzellente und motivierte Unterstützung bei allen labortechnischen Fragestellungen. Je eine bessere Arbeitsgruppe zu finden, wird schwer bis unmöglich.

Barbara Mankel danke ich besonders für ihre tolle Hilfsbereitschaft bei der FISH Durchführung und Auswertung.

Der AG Elektronenmikroskopie, mit Dr. Petra Fallier-Becker, Ria Knittel und Gabi Frommer-Kästle, sowie Susan Noell und Yeliz Donat, danke ich für die angenehme Nachbarschaft, die gute Zusammenarbeit und die schönen Feste, die wir gemeinsam gefeiert haben.

Der AG Molpath, namentlich Dr. Irina Bonzheim, Dr. Julia Steinhilber, Janine Schmidt, Julia Baturin, Achim Rau, Sema Colak und Sieglinde Baisch danke ich für die tolle Zusammenarbeit und die Verlässlichkeit untereinander – auch in stressigen Zeiten.

Mein Dank gebührt ebenso allen übrigen Mitarbeitern des Instituts, mit denen eine sehr angenehme Zusammenarbeit möglich war.

Des Weiteren möchte ich bei allen bedanken, die mir außerhalb der Pathologie in der Zeit der Erstellung meiner Dissertation beigestanden haben:

Meinen Eltern Ina und Wolfgang Hoffmeister danke ich herzlich für die Ermöglichung des Biologiestudiums und die fortwährende Unterstützung in zahlreichen Lebensbelangen! Für das freundschaftliche Verhältnis mit meinen Brüdern Torben und Björn bin ich ebenfalls sehr dankbar und hoffe, dass es immer bestehen bleiben wird.

Meinem Mann Flörg danke ich von Herzen für den immerwährenden Rückhalt, das Aushalten verschiedenster Launen und die gemeinsame Bewältigung zahlreicher Stolpersteine und Abenteuer. Ich freue mich sehr auf die spannende Zukunft mit unserer Familie, die sicher noch viele – hoffentlich vor allem positive – Überraschungen bereithält!

Unserem (noch) kleinen Dalmatiner Elrond danke ich für die Bereicherung des Alltags.

Unserem (noch) ungeborenen Sohn möchte ich sagen, dass ich mich sehr auf ihn freue!

In accordance with the standard scientific protocol, I will use the personal pronoun *we* to indicate the reader and the writer, or my scientific collaborators and myself.

Summary

Neuroendocrine tumors of the small intestine (SI-NETs) have experienced a dramatic increase in incidence over the last three decades. Although defined by a small proliferative index (mostly G1 and G2 tumors), the tumors give frequently and early rise to metastases, which often exceed the size of the primary tumor and kill the patients in the end.

SI-NETs are genetically poorly characterized, the frequent loss of one chromosome 18 (Chr18) being the exception. Therefore, this doctoral thesis focused on this lesion in order to investigate potential tumor suppressors located on this chromosome (SMAD2, SMAD4, Elongin A3, CABLES, PMAIP1, and DCC).

SMAD2 and SMAD4 showed retained expression in the 14 SI-NET samples investigated (12 with loss of Chr18), leaving only haploinsuffiency as possible mechanism in tumor development and progression.

Elongin A3 and *CABLES* mRNAs were differentially expressed between the 1xChr18 and 2xChr18 cohort, suggesting that the loss of Chr18 has an impact on mRNA level. However, western blot analysis of 21 SI-NETs revealed preserved protein expression of Elongin A3 and CABLES. Interestingly, CABLES western blot depicted – in addition to the normal doublet-isoform – an additional isoform at ~55 kDa in the tumor samples, which was not present in the HEK293 control. Among alternative splicing, aberrant splicing of this protein is known in tumors, which could lead to the loss of the CDK-binding domain of CABLES, resulting in enhanced cell growth and tumor formation due to faster progression through the cell cycle [1].

PMAIP1 was not expressed in eight samples investigated. Since a 100% loss of a tumor suppressor is rare, the hypothesis that the lack of PMAIP1 is a normal feature of normal neuroendocrine enterochromaffin cells is favored, rather than the loss being a characteristic of neuroendocrine tumor cells.

Remarkably, the tumor suppressor protein DCC showed total loss or, at least, clearly reduced expression in nearly 30% (6/21) of the tumor samples. Abridged DCC function can result in reduced apoptosis, giving rise to tumor growth and dissemination.

Alternative splicing and mutations in the intronic region of *DCC* [2] render this gene even more interesting.

Further investigations of our lab will focus on the transcriptome and proteome of SI-NETs, and thereby on the differential expression of gene transcripts and proteins between tumors with and without loss of Chr18; hoping to shed light on the role of DCC (and CABLES), which we found to be altered in SI-NETs.

In 2013, Banck et al. published the genomic landscape of SI-NETs with amplifications of the PI3K/AKT/mTOR pathway being the most frequent aberration [3]. Subsequently, we analyzed six genes (*PDGFRα*, *PDGFRβ*, *PIK3CD*, *AKT1*, *AKT2*, *mTOR*) involved in this pathway by FISH; revealing advanced, metastatic tumors as well as more invasive - tumors to harbor significantly more copy number (CN) alterations than tumors of early stage without metastases and less invasive tumors (UICC and T stage comparison). However, no association with protein expression or activation could be identified. One possible explanation for the discrepancy between gene and protein expression might be that epigenetic events play a role in the transcriptional control of amplified genes, thereby preventing protein overexpression.

Since especially the more aggressive tumors (defined by UICC stage IIIB and IV, as well as tumor stage 3 and 4) are lacking effective treatment, the inhibition of the PI3K/AKT/mTOR pathway could be a useful new tool in the therapy of SI-NETs. Therefore, a similar trial to the RADIANT-4 study [4] with the inclusion of functional gastrointestinal neuroendocrine tumors should enlighten the possible effect of everolimus or another inhibitor of the PI3K/AKT/mTOR pathway on the tumor progression.

Zusammenfassung

Neuroendokrine Tumoren des Dünndarms (Dd-NET) haben über die letzten drei Dekaden einen drastischen Anstieg in der Inzidenz erfahren. Obwohl sie durch eine geringe Proliferation gekennzeichnet sind (größtenteils G1 und G2 Tumoren), bilden die Tumore häufig und früh Metastasen, die den Primärtumor in der Größe oftmals übersteigen und den Patienten schließlich töten.

Dd-NET sind genetisch kaum charakterisiert; nur der häufige Verlust eines Chromosoms 18 (Chr18) ist bekannt. Aus diesem Grund beschäftigt sich die vorliegende Doktorarbeit mit dieser Läsion, um potentielle Tumorsuppressoren, die auf diesem Chromosom lokalisiert sind (SMAD2, SMAD4, Elongin A3, CABLES, PMAIP1 und DCC), zu untersuchen.

Die Analyse ergab, dass SMAD2 und SMAD4 in allen 14 untersuchten Dd-NET Proben (12 mit Chr18 Verlust) erhalten sind, sodass nur Haploinsuffizienz als möglicher Mechanismus in der Tumorentwicklung und –progression in Frage kommt.

Elongin A3 und *CABLES* mRNA waren differenziell exprimiert zwischen der 1xChr18 und der 2xChr18 Kohorte, was darauf hindeutet, dass der Verlust des Chr18 einen Einfluss auf das mRNA Level hat. In beiden Fällen zeigte die Western Blot Analyse von 21 Dd-NET jedoch den Erhalt der Proteinexpression. Interessanterweise war im CABLES Western Blot zusätzlich zur normalen Isoform (erscheint als Doppelbande) eine Bande von 55 kDa in den Tumorproben nachweisbar, die in der HEK293 Kontrolle nicht vorhanden war. Neben alternativem Spleißing ist für dieses Protein auch aberrantes Spleißing in Tumoren bekannt, welches zum Verlust der CDK-Bindedomäne von CABLES führen und so in verstärktem Zellwachstum und Tumorformation aufgrund schnellerer Zellzyklusprogression resultieren kann [1].

PMAIP1 war in den acht untersuchten Proben nicht exprimiert. Da ein 100%iger Verlust eines Tumorsuppressors ein seltenes Ereignis darstellt, wird die Hypothese favorisiert, dass die fehlende PMAIP1 Expression eine Eigenschaft einer normalen, neuroendokrinen Enterochromaffin-Zelle darstellt, als dass es sich hierbei um ein Charakteristikum einer neuroendokrinen Tumorzelle handelt.

Bemerkenswert war, dass das Tumorsuppressor-Protein DCC in fast 30% (6/21) der Tumorproben ganz verloren ist oder zumindest eine deutlich verringerte Expression zeigte. Die verminderte Funktion von DCC kann sich in verringerter Apoptose-Tätigkeit niederschlagen, was wiederum zu Tumorwachstum und Metastasierung führen kann. Alternatives Spleißing und Mutationen in der intronischen Region von *DCC* [2] machen das Gen noch interessanter.

Weitere Untersuchungen unserer Arbeitsgruppe werden sich mit dem Transkriptom und Proteom von Dd-NET beschäftigten, genauer gesagt mit der differentiellen Expression von Gentranskripten und Proteinen zwischen Tumoren mit und ohne Verlust von Chr18. Dies soll näheren Aufschluss über die Rolle von DCC (und CABLES), bringen, für welche wir Aberrationen in dieser Tumorart nachweisen konnten.

2013 wurde von Banck et al. die „genomische Landschaft der SI-NETs“ veröffentlicht, in denen Amplifikationen des PI3K/AKT/mTOR Signalwegs als die häufigste Alteration beschrieben wurde [3]. Darauffolgend haben wir sechs Gene, die in diesen Signalweg involviert sind (*PDGFRα*, *PDGFRβ*, *PIK3CD*, *AKT1*, *AKT2*, *mTOR*), mithilfe der FISH Technik analysiert. Fortgeschrittene, mit Metastasen assoziierte Tumoren, als auch invasivere Tumoren beinhalten signifikant mehr Kopienzahl-Alterationen als Tumoren früherer Stadien ohne Metastasierung und weniger invasive Tumoren (UICC und T Stadium Vergleich). Es konnte jedoch keine Assoziation mit Proteinexpression oder -aktivierung festgestellt werden. Eine mögliche Erklärung für diese Diskrepanz zwischen Gen- und Proteinexpression könnte eine epigenetische Kontrolle der Transkription amplifizierter Gene sein, die die Proteinüberexpression verhindert.

Da vor allem für die aggressiveren Tumoren (durch die UICC Stadien IIIB und IV und die Tumorstadien 3 und 4 beschrieben) effektive Behandlungen fehlen, könnte die Inhibierung des PI3K/AKT/mTOR Signalwegs ein brauchbares, neues Werkzeug in der Therapie der Dd-NET sein. Eine mit der RADIANT-4 vergleichbare Studie [4], die funktionelle gastrointestinale neuroendokrine Tumoren einschließt, wäre geeignet um den möglichen Effekt von Everolimus oder einem anderen Inhibitor des PI3K/AKT/mTOR Signalwegs auf die Tumorprogression zu testen.

Publications

Original articles

1. Sperveslage J*, **Hoffmeister M***, Henopp T, Klöppel G, Sipos B. Establishment of robust controls for the normalization of miRNA expression in neuroendocrine tumors of the ileum and pancreas. Endocrine, 2014 Jun;46(2):226-30. IF 3.878 *authors contributed equally to this manuscript

2. Sipos B, Sperveslage J, Anlauf M, **Hoffmeister M**, Henopp T, Buch S, Hampe J, Weber A, Hammel P, Couvelard A, Höbling W, Lieb W, Boehm BO, Klöppel G. Glucagon cell hyperplasia and neoplasia with and without glucagon receptor mutations. J Clin Endocrinol Metab., 2015 May;100(5):E783-8. IF 6.209

3. Noell S, Fallier-Becker P, Mack AF, **Hoffmeister M**, Beschorner R, Ritz R: Water Channels Aquaporin 4 and -1 Expression in Subependymoma Depends on the Localization of the Tumors, Plos One, 2015 Jun 26;10(6):e0131367 IF 3.234

4. Kaemmerer D, Träger T, **Hoffmeister M**, Sipos B, Hommann M, Sänger J, Schulz S, Lupp A. Inverse expression of somatostatin and CXCR4 chemokine receptors in gastroenteropancreatic neuroendocrine neoplasms of different malignancy. Oncotarget, 2015 Sep 29;6(29):27566-79. IF 6.359

Parts of my doctoral thesis are published in the following publication:

5. **Nieser M**, Henopp T, Brix J, Stoß L, Sitek B, Naboulsi W, Anlauf M, Schlitter A.M, Kloeppel, G, Gress T, Moll R, Bartsch D.K, Heverhagen, A.E, Knoefel W.T, Kaemmerer D, Haybaeck J, Fend F, Sperveslage J., Sipos B. Loss of chromosome 18 in neuroendocrine tumors of the small intestine: the enigma remains. Neuroendocrinology, 2016 May 25. [Epub ahead of print] (© 2016 S. Karger AG, Basel) IF 4.498

6. Felix Behling, M.D.; Alonso Barrantes-Freer, M.D., Ph.D.; Marco Skardelly, M.D., Ph.D.; **Maike Nieser**; Arne Christians, M.D., Ph.D.; Florian Stockhammer, Prof., M.D., Ph.D.; Veit Rohde, Prof., M.D., Ph.D.; Marcos Tatagiba, Prof., M.D., Ph.D.; Chrisitan Hartmann, Prof., M.D., Ph.D.; Christine Stadelmann, Prof., M.D., Ph.D.; Jens Schittenhelm, Prof., M.D., Ph.D. Frequency of BRAF V600E mutations in 969 central nervous system neoplasms. Diagnostic Pathology. Accepted 2016 June 16. IF 1.895

7. B. Wolf, K. Krieg, C. Falk, M. Heikenwalder, M. Ringelhahn, K. Breuhahn, H. Keppeler, T. Biedermann, S. Vetter, D. Thiele, **M. Nieser**, E. Schmid, S.W. Warmann, J.Fuchs, M. Avci-Adali, T. Yevsa, Y. Skokowa, S. Hauser, L. Schöls,

U. Kossatz. A new therapeutic approach based on the induction of differentiation in premalignant hepatic cells. Cancer Research. Accepted 2016 July 20. IF 8.556

8. Petra Fallier-Becker, **Maike Nieser**, Ulrike Wenzel, Rainer Ritz and Susan Noell. Is the Aquaporin4-M1 isoform upregulated in gliomas and is this consistent with the absence of typical orthogonal arrays of particles? Accepted 2016 July 25. IF 3.257

Submitted manuscripts

1. Donato Iacovazzo, Sarah E. Flanagan, Rosana Quezado, Emily Walker, Richard Caswell, Fernando de Sousa Barros, Matthew Johnson, Matthew Wakeling, Min Guo, Mary N. Dang, Plamena Gabrovska, Michael Brändle, Bruno Niederle, Emanuel Christ, Stefan Jenni, Bence Sipos, **Maike Nieser**, Andrea Frilling, Ketan Dhatariya, Philippe Chanson, Wouter de Herder, Björn Konukiewitz, Günter Klöppel, Roland Stein, Márta Korbonits, Sian Ellard. Familial insulinomatosis and diabetes mellitus due to a missense MAFA mutation. Submitted to New England Journal of Medicine, 29th of August 2016.

Contributions

I did all the experiments described in this doctoral thesis by myself, if not stated otherwise.

SNP array analysis was performed by Atlas Biolabs (Berlin, DE). Analysis and interpretation of the data with the Chromosome Analysis Suite (Affymetrix, Santa Clara, CA, US) was done by me.

Exome sequencing and SNV calling was performed by CeGaT (Tuebingen, DE). Interpretation and validation of the data was done by me.

All steps for the Liquid chromatography – Mass spectrometry analysis were carried out by the Clinical Proteomics workgroup of Jun.-Prof. Barbara Sitek (Medical Proteom-Center, Bochum, DE).

NFATC1 sequencing was performed by Dr. Laura Stoß.

Content

ACKNOWLEDGEMENTS **3**

SUMMARY **6**

ZUSAMMENFASSUNG **8**

PUBLICATIONS **10**

CONTRIBUTIONS **12**

LIST OF ABBREVIATIONS **16**

FIGURE INDEX **21**

TABLE INDEX **22**

I. INTRODUCTION **23**

General aspects of neuroendocrine tumors (NETs) **23**
Classification **24**
Small intestinal NETs (SI-NETs) **27**
Incidence 27
General aspects of SI-NETs 27
Biological characteristics of (SI-)NETs 29
Genetic characteristics 31
Epigenetic characteristics 37
Therapy 39
Preliminary work (working group Prof. Sipos) **41**
Aim **42**
Part 1: Alterations of Chr18-related tumor suppressors in SI-NETs 42
Part 2: Alterations of the PI3K/AKT/mTOR pathway in SI-NETs 42

II. MATERIAL **43**

2.1 Equipment **43**
2.2 Software and Databases **44**
2.3 Chemical and biological reagents **45**
2.4 Antibodies and FISH probes **47**

2.5 Oligonucleotides **48**
2.6 Kits **52**
2.7 Buffer **53**

III. METHODS **55**

3.1 Clinical Samples **55**
3.1.1 Staging of neuroendocrine tumors of the ileum 55
3.2 HE staining **56**
3.3 Tissue Microarray **56**
3.4 DNA Extraction **56**
3.5 RNA Extraction **57**
3.6 Polymerase chain reaction (PCR) **57**
3.7 Sequencing PCR **57**
3.8 Sanger sequencing **58**
3.9 cDNA synthesis and quantitative Real-time PCR (qRT-PCR) **58**
3.10 Immunohistochemistry (IHC) **58**
3.10.1 IHC staining 59
3.10.2 IHC evaluation 60
3.11 Fluorescence-in-situ-hybridization (FISH) **61**
3.11.1 FISH processing 61
3.11.2 FISH evaluation 63
3.12 Statistical analysis **64**
3.13 Protein extraction **64**
3.14 Western blot **65**
3.15 Cell culture **66**
3.16 Exome sequencing & SNV calling **66**
3.17 Validation by Sanger sequencing **68**
3.18 Oligonucleotides **68**
3.19 SNP array & Data analysis **68**
3.20 Liquid chromatography – Mass spectrometry (LC-MS) **69**

IV. RESULTS - GENERAL CHARACTERIZATION **70**

Clinicopathological data of the patients **70**
Clinical characteristics 70
Expression of immunohistochemical markers 70

IV. RESULTS – GENETIC CHARACTERIZATION **72**

Chr18 is commonly lost in SI-NETs **72**

SNP ARRAY ANALYSIS 72
EXOME SEQUENCING 73
VALIDATION BY SANGER SEQUENCING 74
SANGER-SEQUENCING OF *PML* 81
SANGER-SEQUENCING OF *NFATC1* 81
DATA COMPARISON WITH EXTERNAL DATA SET 82

IV. RESULTS – CHR18-ASSOCIATED TUMOR SUPPRESSORS 84

WESTERN BLOT ANALYSIS OF CHR18-ASSOCIATED PUTATIVE TUMOR SUPPRESSORS 84
SMAD2 AND SMAD4 ARE STRONGLY EXPRESSED IN SI-NETS 84
ELONGIN A3 AND CABLES SHOW STRONG EXPRESSION IN SI-NETS, WHEREAS PMAIP1 IS NOT EXPRESSED 86
DCC EXPRESSION IS LOST/REDUCED IN NEARLY 30% OF SI-NET SAMPLES 88
QUANTITATIVE REAL-TIME PCR (QRT-PCR) ANALYSIS REVEALS *TCEB3C* AND *CABLES* TO BE DIFFERENTIALLY EXPRESSED BETWEEN SAMPLE COHORTS WITH AND WITHOUT LOSS OF CHR18 90

IV. RESULTS - PI3K/AKT/MTOR PATHWAY 94

FISH ANALYSIS OF THE PI3K/AKT/MTOR-PATHWAY 94
COPY NUMBER GAINS OF *PIK3CD, AKT1, AKT2, PDGFRA, PDGFRB*, AND *MTOR* 94
COMPARATIVE ANALYSIS OF PRIMARY TUMOR AND METASTASES 98
ADVANCED TUMORS HARBOR SIGNIFICANTLY MORE CN GAINS THAN TUMORS OF EARLIER STAGE 98
COMPARISON OF FISH RESULTS WITH SNP ARRAY RESULTS 100
COMPARISON OF FISH RESULTS WITH DATA FROM BANCK ET AL. [3] 100
COPY NUMBER VARIATIONS ARE NOT ASSOCIATED WITH POORER OVERALL SURVIVAL 104
PROTEIN EXPRESSION AND ACTIVATION OF AKT, MTOR, AND ITS DOWNSTREAM TARGETS AND ITS ASSOCIATION WITH COPY NUMBER GAINS IN THE PI3K/AKT/MTOR PATHWAY 107
ACTIVATION OF AKT, MTOR, AND ITS DOWNSTREAM TARGETS 107
COPY NUMBER GAINS OF THE PI3K/AKT/MTOR PATHWAY ARE NOT ASSOCIATED WITH PROTEIN EXPRESSION OR ACTIVATION 111

V. DISCUSSION 113

PART 1: CHROMOSOME 18 113
PART 2: PI3K/AKT/MTOR-PATHWAY 121
CONCLUDING REMARKS 125

VI. REFERENCES 127

VII. APPENDIX 137

List of abbreviations

4E-BP1	Eukaryotic translation initiation factor 4E binding protein 1
5-HIAA	5-Hydroxyindoleacetic acid
ADCY5	Adenylate cyclase 5
AJCC-UICC	American Joint Cancer Committee-Union International Contre le Cancer
AKT1	v-AKT murine thymoma viral oncogene homolog 1
AKT2	v-AKT murine thymoma viral oncogene homolog 2
aNET	Appendiceal neuroendocrine tumor
ANKRD30B	Ankyrin repeat domain 30B
ATF7IP	Activating transcription factor 7 interacting protein
AUTS2	Autism susceptibility candidate 2
AZD2014	Mammalian target of rapamycin (mTOR) serine/ threonine kinase (dual TORC1 and TORC2) inhibitor
BCA	Bicinchoninic acid
BDP1	B double prime 1, subunit of RNA polymerase III transcription initiation factor IIIB
BEZ235	Dual ATP-competitive PI3K/mTOR inhibitor
BON-1	Pancreatic carcinoid cell line
bp	base pairs
BSA	Bovine serum albumin
CABLES1	Cdk5 and Abl enzyme substrate 1
CABYR	Calcium binding tyrosine-(Y)-phosphorylation regulated
CACNA1E	Calcium channel, voltage-dependent, R type, alpha 1E subunit
CDKN2A	Cyclin-dependent kinase inhibitor 2A
cDNA	complementary DNA
CDX2	Caudal type homeobox 2
CD56	Cluster of differentiation 56
Cen	Centromere
CEP	Centromere enumeration probe
CgA	Chromogranin A
CIMP	CpG island methylator phenotype
CNV	Copy number variation
Co-Smad	Common-mediator Smad
CORO2A	coronin, actin binding protein, 2A
Cp	Crossing point
CTC	Circulating tumor cells
CYP3A5	Cytochrome P450, family 3, subfamily A, polypeptide 5
C1RL	Complement component 1, r subcomponent-like
C3orf20	Chromosome 3 open reading frame 20
DAB	3,3'-Diaminobenzidine

dapB	dihydrodipicolinate reductase (E.coli gene)
DCC	DCC netrin 1 receptor (“deleted in colorectal cancer”)
DMEM	Dulbecco’s Modified Eagle Medium
DNA	Deoxyribonucleic acid
dNTP	deoxynucleotide triphosphate
DOTATATE	Drug for radionuclide therapy (DOTA: chelating agent, TATE: Octreotide analog)
DOTATOC	Drug for radionuclide therapy (DOTA: chelating agent, TOC: Octreotide analog)
dUTP	deoxyuridine triphosphate
DTCS	Dye Terminator Cycle Sequencing
eIF-4E	Eukaryotic translation initiation factor 4E
ENETS	European neuroendocrine tumor society
EpCAM	Epithelial cell adhesion molecule
FCS	Fetal calf serum
FDA	Food and Drug Administration
Figure	Figure
FISH	Fluorescence-in-vitro-hybridization
FITC	Fluorescein isothiocyanate
FFPE	Formalin-fixed, paraffin embedded
g	gravitational constant
GEP-NET	Gastroenteropancreatic neuroendocrine tumor
HE	Hematoxylin and eosin
HECTD4	HECT domain containing E3 ubiquitin protein ligase 4
HPF	High-power field
HRP	Horseradish peroxidase
IgG	Immunoglobulin G
IHC	Immunohistochemistry
InDel	Insertion / Deletion
LAMA5	Laminin, alpha 5
µg, µl	microgram, microliter
Lu	Lutetium (Radionuclide)
mg, ml	milligram, milliliter
Ki-67 (MIB-1)	Antigen KI-67 (Cellular marker for proliferation)
MAF	Minor allele frequency
MANEC	Mixed adenoneuroendocrine carcinoma
Maspin	Mammary serine protease inhibitor
min	minute
MLST8	MTOR associated protein, LST8 homolog
mRNA	messenger RNA
miRNA	microRNA
mTOR	mechanistic Target Of Rapamycin (serine/threonine kinase)

MS4A14	Membrane-spanning 4-domains, subfamily A, member 14
MUC16	Mucin 16, cell surface associated
NEC	Neuroendocrine carcinoma
(SI-)NET	Neuroendocrine Tumor (of the small intestine)
NCAM	Neural cell adhesion molecule
NFATC1	Nuclear factor of activated T-cells, cytoplasmic, calcineurin-dependent 1
NFYA	Nuclear transcription factor Y, alpha
NGS	Next Generation Sequencing
ns	non-synonymous
nt	nucleotide
OD	Optical density
OR1A1	Olfactory receptor, family 1, subfamily A, member 1
OR5T3	Olfactory receptor, family 5, subfamily T, member 3
OS	Overall survival
p-(protein)	phosphor-(protein)
$p14^{ARF}$	Product of an alternate open reading frame of *CDKN2A*
$p16^{INK4A}$	Product of *CDKN2A*
PBS	Phosphate buffered saline
PCR	Polymerase chain reaction
PDGFRα	Platelet-derived growth factor receptor, alpha polypeptide
PDGFRβ	Platelet-derived growth factor receptor, beta polypeptide
PDK-1	3-phosphoinositide dependent protein kinase-1
PFS	Progression-free survival
pHH3	phosphor-Histone H3
PI3K	Phosphoinositide-3-Kinases
PIEZO2	Piezo-type mechanosensitive ion channel component 2
PIK3CD	Phosphatidylinositol-4,5-Bisphosphate 3-Kinase, Catalytic Subunit Delta
PMAIP1	Phorbol-12-myristate-13-acetate-induced protein 1
PML	Promyelocytic leukemia
PPIB	Peptidylprolyl isomerase B
PRKCH	Protein kinase C, eta
PROVEAN	Protein Variation Effect Analyzer
PRRT	Peptide receptor-mediated radiotherapy
PTEN	Phosphatase and tensin homolog
RASSF1A	Ras association (RalGDS/AF-6) domain family member 1
RB1CC1	RB1-inducible coiled-coil 1
RFC4	Replication factor C (activator 1) 4, 37kDa
RHD	Rel homology domain

RHEB	Ras homolog enriched in brain
RICTOR	RPTOR independent companion of MTOR, complex 2
RNA	Ribonucleic acid
ROX	Carboxy-X-rhodamine
rpm	rounds per minute
RPMI	Cell culture medium, established at **R**oswell **P**ark **M**emorial **I**nstitute
RPTOR	Regulatory associated protein of MTOR, complex 1
RPS6 (S6)	Ribosomal protein S6
RPS6KB1 (S6K1)	Ribosomal protein S6 kinase, 70kDa, polypeptide 1
rs-number	reference SNP cluster ID number
RT	room temperature
RT-PCR	Real Time-PCR
R-SMAD	Receptor-regulated SMAD
s	second
SEER	Surveillance, Epidemiology and End Results
Ser	Serine
SERPINB5	Serpin peptidase inhibitor, clade B (ovalbumin), member 5
SIFT	Sorting Intolerant From Tolerant
siRNA	Small interfering RNA
SMAD2/4	SMAD family member 2/4
SMG5	SMG5 nonsense mediated mRNA decay factor
SNP/SNV	Single Nucleotide Polymorphism / Variation
SRC	SRC proto-oncogene, non-receptor tyrosine kinase
SSTR	Somatostatin receptor
SVEP1	Sushi, von Willebrand factor type A, EGF and pentraxin domain containing 1
SYNPR	Synaptoporin
Table	Table
Taq	*Thermus aquaticus*
TCEB3C	Transcription elongation factor B polypeptide 3C (Elongin A3)
TFA	Trifluoroacetic acid
Thr	Threonin
TKI	Tyrosine kinase inhibitor
TMD	Transmembrane domain
TSC2	Tuberous Sclerosis Complex 2
U	unit
USP44	Ubiquitin specific peptidase 44
USP48	Ubiquitin specific peptidase 48
WB	Western blot
WHO	World Health Organization

XBP1	X-box binding protein 1
Y	Yttrium (Radionuclide)

Figure index

Figure 1: Distribution of NETs by anatomical site from the SEER 1973-2007 tumor registry database; modified according to [6] 23
Figure 2: Human gastrointestinal tract showing parts where GEP-NETs can arise 24
Figure 3: Increase in incidence of neuroendocrine tumors over the past three decades [5] 27
Figure 4: Depiction of neuroendocrine tumors 29
Figure 5: Subgrouping of SI-NETs by their chromosomal aberrations [39] 32
Figure 6: A simplified overview of the PI3K/AKT/mTOR pathway [66] 35
Figure 7: PI3K/AKT/mTOR pathway and the target sites for inhibitory drugs [81] 37
Figure 8: Western blot of the tumor suppressors SMAD2 and SMAD4 in 14 SI-NETs 85
Figure 9: Quantitative western blot analysis for SMAD2 and SMAD4 85
Figure 10: Western Blot analysis of the putative tumor suppressors CABLES, Elongin A3, and PMAIP1 in 8 (of 21) SI-NETs 87
Figure 11: Quantitative western blot analysis for CABLES, Elongin A3, and PMAIP1 88
Figure 12: Western blot of the Chr18-associated tumor suppressor DCC in 21 SI-NETs 89
Figure 13: Quantitative western blot analysis for DCC 90
Figure 14: ΔCp values of the four tumor suppressor genes *DCC*, *TCEB3C*, *CABLES*, and *PMAIP1* 93
Figure 15: Exemplary fluorescent pictures of SI-NETs harboring CN gains 95
Figure 16: Distribution of CN alterations in the PI3K/AKT/mTOR pathway between primary tumors and metastases 97
Figure 17: Comparison of amplifications between primary tumors and matching metastases 98
Figure 18: Distribution of gains by UICC stages 99
Figure 19: Distribution of gains by T stages 99
Figure 20: Percentage of CN gains in SI-NETs 103
Figure 21: Kaplan Meier curves for the six genes of the PI3K/Akt/mTOR pathway investigated 106
Figure 22: Immunohistochemical stainings of AKT2, p-AKT, and p-mTOR in SI-NETs 110
Figure 23: Immunohistochemical stainings of mTOR downstream molecules in SI-NETs 111
Figure 24: Domains of the DCC protein 114

Table index

Table 1: Histopathological grading scale of NETs (WHO Classification 2010) 25
Table 2: TNM classification of neuroendocrine tumors of the lower jejunum and ileum 26
Table 3: UICC-staging of GEP-NETs 26
Table 4: Equipment 43
Table 5: Consumables 44
Table 6: Software and Databases 44
Table 7: Chemical and biological reagents 45
Table 8: Primary Antibodies 47
Table 9: Secondary Antibodies 47
Table 10: FISH probes 48
Table 11: Oligonucleotides for the validation / falsification of mutations found by exome sequencing 48
Table 12: Oligonucleotides for the sequencing of all functional regions of the *PML* gene 51
Table 13: Oligonucleotides for the analysis of potential Chr18-associated tumor suppressor genes by quantitative Real-time PCR (qRT-PCR) 52
Table 14: Commercial Kits 52
Table 15: Buffer 53
Table 16: Cell lines/tissues used as controls for western blot analysis 54
Table 17: Immunoreactive Score (IRS) 60
Table 18: Distribution of UICC stages in the patients' cohort 70
Table 19: SNP array analysis of five primary tumors and three metastases (two matching) 72
Table 20: Stop-gained and non-synonymous somatic variants found by exome sequencing of five SI-NET samples and corresponding normal tissue 73
Table 21: Sanger validation of absence of mutations 75
Table 22: Sanger-validated somatic mutations 79
Table 23: Results of FISH analysis of *PIK3CD*, *AKT1/2*, *PDGFRα/β*, and *mTOR* 96
Table 24: Comparison of FISH results with raw data from Banck et al. 101
Table 25: Expression profile of AKT2, (p-)AKT, p-mTOR, and its downstream signaling molecules (IHC) 108
Table 26: Clinical characteristics 137
Table 27: Expression of immunohistochemical markers 141
Table 28: Quality data of exome sequencing 146
Table 29: Alterations of the five SI-NET samples identified by exome sequencing 147
Table 30: Counts and ratio of FISH signals in samples with CN alterations 147
Table 31: Statistical analysis of the association between gains in the PI3K/AKT/mTOR pathway and subsequent protein expression and activation. 165

I. Introduction

General aspects of neuroendocrine tumors (NETs)

Neuroendocrine tumors (NETs, formerly known as “carcinoids”) are a heterogeneous group of neoplasms arising in the diffuse neuroendocrine system. The term neuroendocrine refers to two qualities of these cells: they share structural similarities with neurons and can produce hormones like endocrine cells. Although the tumors may arise in almost any organ, the majority develops in the pancreas or the gastrointestinal tract and are therefore referred to as gastroenteropancreatic NETs (GEP-NETs; Figure 1) [5].

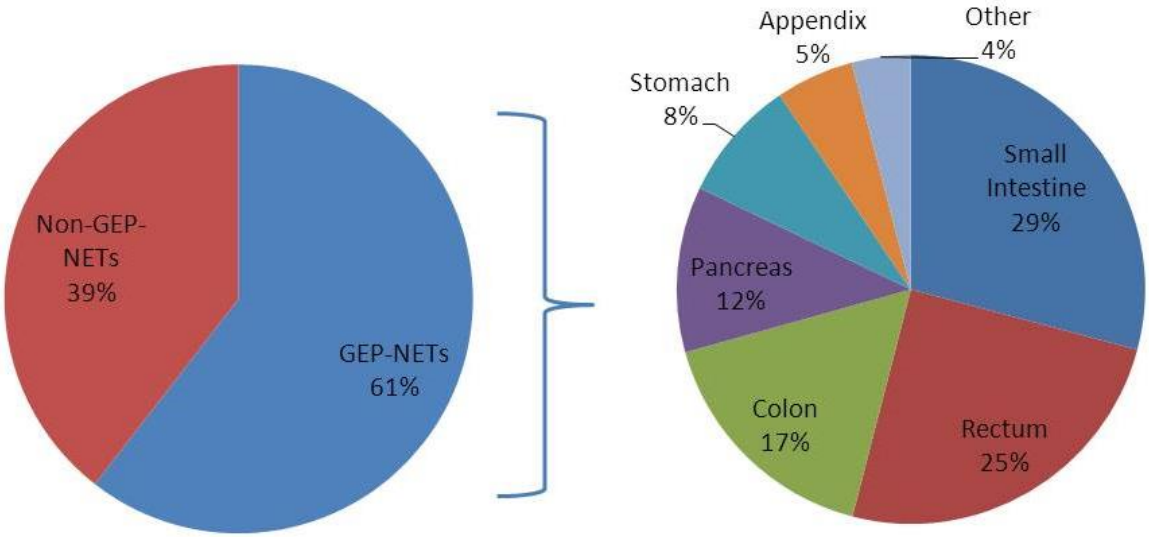

Figure 1: Distribution of NETs by anatomical site from the SEER 1973-2007 tumor registry database; modified according to [6] (GEP-)NET: (gastroenteropancreatic) neuroendocrine tumor, SEER: Surveillance, Epidemiology and End Results

This work focuses on GEP-NETs; in detail on the small intestinal NETs (SI-NETs), which are located in the duodenum, jejunum, or (primarily) the ileum (Figure 2). SI-NETs represent one-third of all GEP-NETs (Figure 1) and they are the most common malignancy in this part of the bowel.

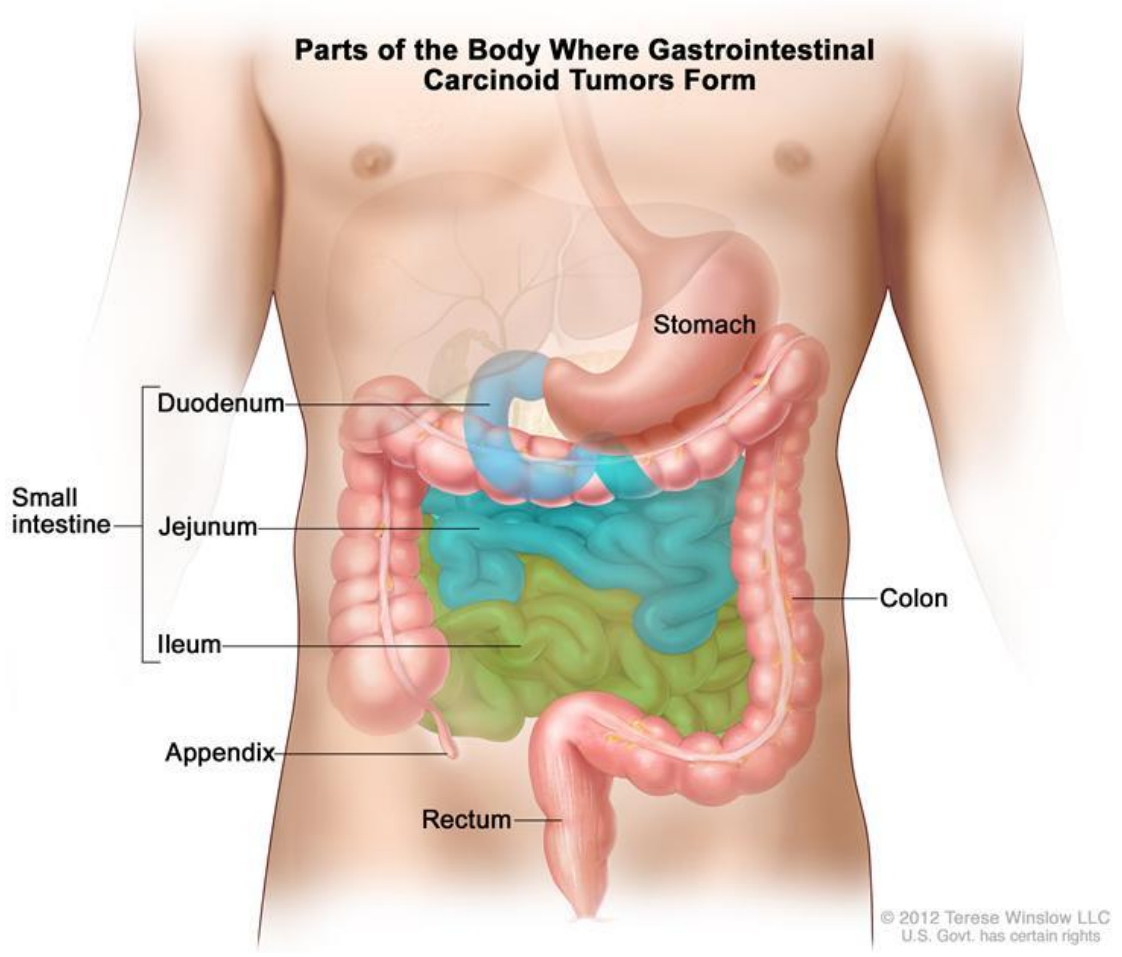

Figure 2: Human gastrointestinal tract showing parts where GEP-NETs can arise
http://www.cancer.gov/images/cdr/live/CDR741567-750.jpg

Classification

The WHO Classification 2010 of GEP-NETs [7] is based on the histological classification, including grading determined by the proliferative behavior of the tumors (Table 1) in combination with site-specific staging. Grade 1 (Ki-67 index ≤2%) and Grade 2 (Ki-67 index 3-20%) NETs are considered well-differentiated neuroendocrine tumors. Grade 3 (Ki-67 index >20%) neoplasms are poorly-differentiated carcinomas. The latter are divided in small and large cell neoplasms. Mixed adenoneuroendocrine carcinomas (MANECs) consist of both a neuroendocrine and an exocrine glandular phenotype (30% of each component at least). The neuroendocrine component may be well or poorly differentiated.

Table 1: Histopathological grading scale of NETs (WHO Classification 2010)
The grading scale is based on proliferation. HPF: high-power field, +: positive, NET: neuroendocrine tumor, NEC: neuroendocrine carcinoma, MANEC: mixed adenoneuroendocrine carcinoma, ENETS: European neuroendocrine tumor society, WHO: World Health Organization

Grade	Mitotic count per 10 HPF	% of cells Ki67+	ENETS/WHO definition
G1	<2	≤2	NET
G2	2-20	3-20	NET
G3	>20	>20	NEC
			MANEC

The proliferative grading has an important impact on the tumor specific overall survival. The 5-year survival rate of jejunoileal NET G1 tumors is 93.8%, of NET G2 83%, and of NET G3 50% [8].

The TNM (T: primary tumor, N: lymph node involvement, M: distant metastasis) staging differs between the different organs/organ parts due to site specific features. A recent publication emphasizes the heterogeneity of jejunal NETs, thereby supporting the distinction between “upper” and “lower” jejunal tumors [9]. The lower jejunal NETs are grouped with ileal NETs, resulting in the TNM classification described in Table 2. This grouping has an important prognostic impact since tumors of the lower jejunum and the ileum are associated with significant shorter survival than tumors of the upper jejunum and duodenum [9].

Table 2: TNM classification of neuroendocrine tumors of the lower jejunum and ileum
T: primary tumor, N: lymph node involvement, M: distant metastasis, AJCC-UICC: American Joint Cancer Committee-Union International Contre le Cancer

T	ENETS/AJCC-UICC classification
TX	Primary tumor cannot be assessed
T0	No evidence of primary tumor
T1	Tumor invades mucosa or submucosa and has a size <1 cm
T2	Tumor invades muscularis propria or size >1 cm
T3	Tumor invades subserosa
T4	Tumor invades serosa/other organs
	For any T add (m) for multiple tumors
N	Regional lymph nodes
NX	Regional lymph nodes cannot be assessed
N0	No regional lymph node metastases
N1	Regional lymph node metastases
M	Distant metastases
MX	Distant metastasis cannot be assessed
M0	No distant metastases
M1	Distant metastases

Following the TNM classification, GEP-NETs (except appendiceal NETs) are classified into stages depicted in Table 3. The staging includes invasiveness and size of the primary tumor, and the involvement of lymph node / distant metastasis.

Table 3: UICC-staging of GEP-NETs

Stage	Primary tumor	Lymph node metastasis	Distant metastasis
Stage I	T1	N0	M0
Stage IIA	T2	N0	M0
Stage IIB	T3	N0	M0
Stage IIIA	T4	N0	M0
Stage IIIB	any T	N1	M0
Stage IV	any T	N1	M1

Comparable to the influence of the proliferative behavior on the survival rate, the staging has an impact on the tumor specific survival. The 5-year survival rate is 100% for stages I and II, 97.1% for stage III, and 84.4% for stage IV [8].

Small intestinal NETs (SI-NETs)

Incidence

Neuroendocrine tumors of the gastrointestinal tract are considered to be rare tumors, representing only 2% of all gastrointestinal neoplasms. However, neuroendocrine tumors of the small intestine are the most common tumors of this part of the gastrointestinal system (Figure 1) [10], and have experienced a dramatic increase in incidence over the past three decades (Figure 3) [5].

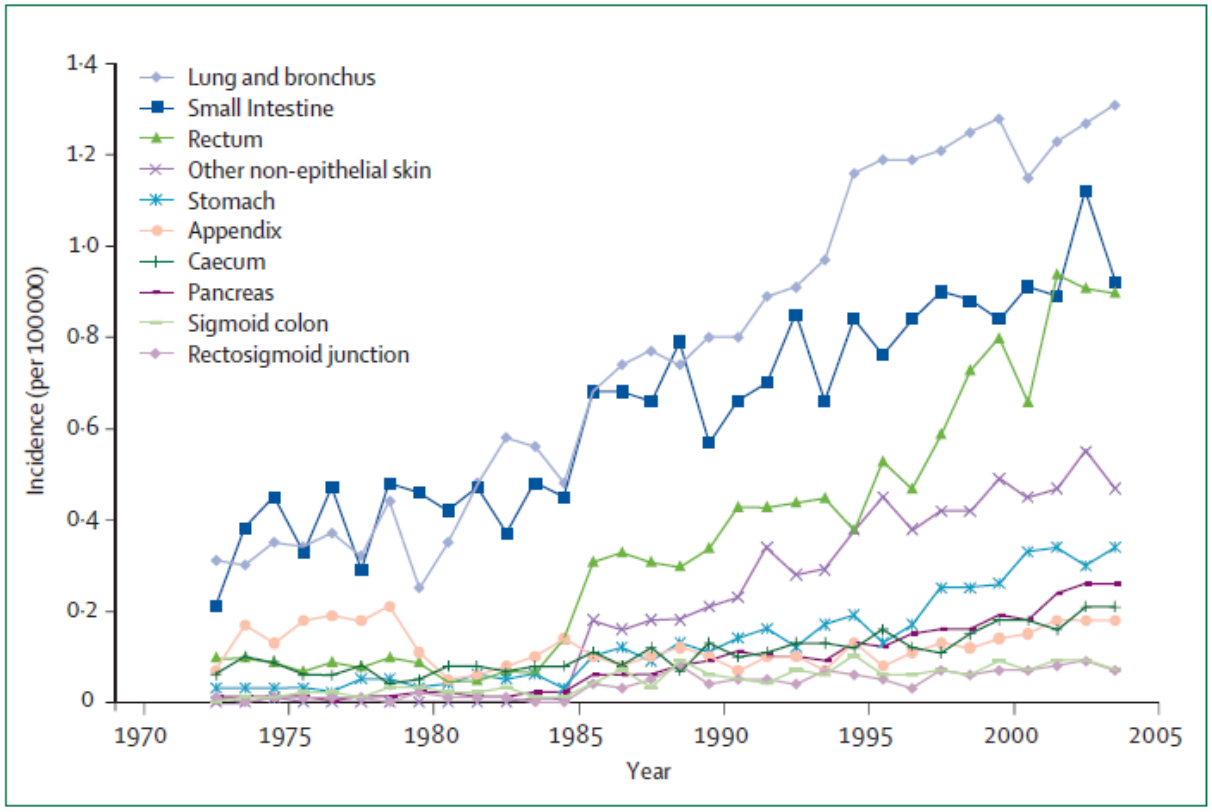

Figure 3: Increase in incidence of neuroendocrine tumors over the past three decades [5]
(US population, Data from SEER database)

2008, the incidence was 1.1/100,000 people per year with a 5-year overall survival (OS) of 62-71%, according to SEER data [11]. It is similar in male and female and peaks between the sixth and seventh decade.

General aspects of SI-NETs

SI-NETs arise mostly sporadic and are not associated with any inherited syndrome, (e.g. multiple endocrine neoplasia (MEN) types 1 and 2, von Hippel-Lindau disease,

and tuberous sclerosis [12], which can give rise to pancreatic NETs), although familial cases have been observed [13].

They are mainly slow-growing tumors (Ki-67 index ≤2%), therefore classified as well differentiated G1 or G2 (Ki-67 index 3-20%) tumors. Despite their low proliferation rate, SI-NETs often present with lymph node and/or distant metastases at various sites (e.g. liver, lung, peritoneum, bones) at the time of diagnosis [13-15].

Cells of well-differentiated neuroendocrine tumors have eosinophilic and granular cytoplasm. The nuclei often depict a typical “salt and pepper” pattern, referring to the chromatin. The growth pattern of the tumor cells depends on the site of origin. Ileal NETs mostly present with an insular pattern (type A) [16], but can also occur in trabecular (type B) or acinar (type C) pattern [17].

NETs are divided into functional and non-functional tumors. Functional tumors secrete hormones, which cause different clinical symptoms. SI-NETs are mostly functional tumors, arising from serotonin-producing enterochromaffin cells (EC) scattered throughout the digestive epithelium. The secretion of serotonin leads to the development of the so called “carcinoid” syndrome. It comes along with the “carcinoid triad” consisting of dry flushing, diarrhea, and cardiac involvement (Hedinger’s syndrome) [18]. This syndrome is often due to liver metastases hampering the inactivation of the secreted peptides which therefore reach the systemic circulation [19]. Figure 4 (A) depicts a neuroendocrine tumor at the ileocecal junction; Figure 4 (B) shows an immunohistochemical staining for serotonin in an ileal NET, which infiltrates the muscular layer.

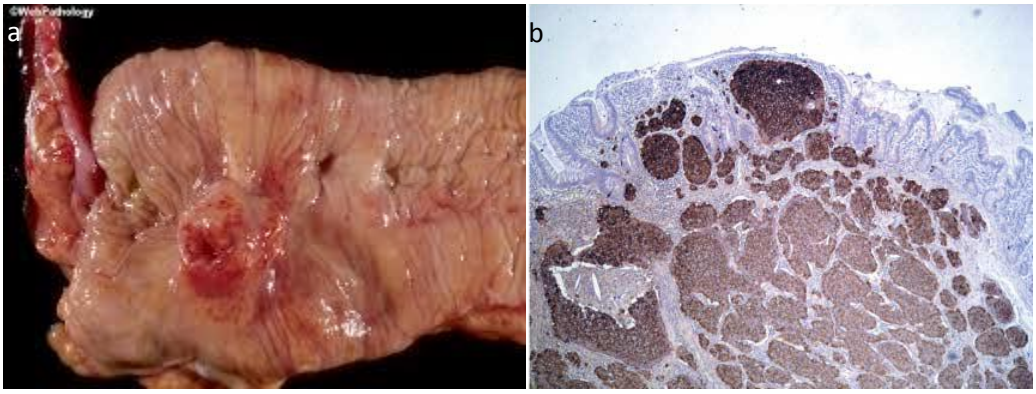

Figure 4: Depiction of neuroendocrine tumors
(A) Neuroendocrine tumor at the ileocecal junction (http://www.webpathology.com/). (B) A functional neuroendocrine tumor, which infiltrates the muscular layer and produces serotonin (brown IHC staining) [13].

Biological characteristics of (SI-)NETs

Biological markers (biomarkers) are disease or patients' characteristics which have prognostic or therapeutic impact. The National Institutes of Health (NIH) Biomarkers Definitions Working Group defined a biomarker as "a characteristic that is objectively measured and evaluated as an indicator of normal biological processes, pathogenic processes, or pharmacologic responses to a therapeutic intervention" [20].

The most usable biomarkers are cell surface and/or secreted proteins. Other potential biomarkers which are expressed in the nucleus or cytoplasm are of limited use due to poor accessibility to clinical assays. The following markers are frequently used for prognostic or predictive implications in SI-NETs.

a) Expression of chromogranin A

One of the most widely used biomarkers in NETs is chromogranin A (CgA). CgA is a member of the chromogranin/secretogranin family of neuroendocrine secretory proteins. It is expressed in secretory vesicles of neurons and endocrine cells. The level of CgA correlates with tumor burden, indicating a worse prognosis [21]. CgA has a medium to high diagnostic sensitivity (60-90%), varying among different primary tumor locations [22]. However, it is not very specific for it is also elevated in a wide variety of benign diseases as well as other malignant tumors of non-neuroendocrine origin [23]. In the pathological diagnostics of NETs immunohistochemical staining of CgA, synaptophysin (b) and haematoxylin-eosin is routinely used [24].

b) Expression of synaptophysin

Synaptophysin is an integral membrane protein of small synaptic vesicles in endocrine cells [25]. Synaptophysin is regarded as the most specific marker of neuroendocrine differentiation, with a much higher sensitivity than CgA [26].

c) Secretion of serotonin and 5-HIAA

Serotonin and its metabolite 5-HIAA are widely explored biomarkers for functional SI-NETs. For a long time, the urinary levels were measured. Recently, a plasma-based method was developed, making the analysis faster and more convenient for the patients [27]. 5-HIAA shows a high specificity (100%), but only low sensitivity (35%) due to diverse expression [28]. Nuclear immunohistochemical positivity for serotonin is supportive for NETs of intestinal origin [24].

d) Expression of CDX2

CDX2, a nuclear transcription factor, plays a crucial role in the regulation of intestine-specific genes involved in cell growth and differentiation. It was found to be a useful marker for intestinal-type differentiation, rarely seen in other tumor types [29]. Furthermore, CDX2 is overexpressed in SI-NETs, independent of clinical stage or phenotype, suggesting it to be an early event in tumor development [30].

e) Expression of Somatostatin receptors (SSTR)

Somatostatin receptors belong to the G-protein coupled receptor 1 family. Up to now, five subtypes of SSTR have been cloned and characterized (SSTR1, 2A, 3, 4, 5). SSTR2A seems to play a pivotal role in low grade NETs of the gastrointestinal tract [31]. The determination of SSTR expression is important for therapeutic considerations (see chapter Therapy).

f) CD56

CD56 (or Neural cell adhesion molecule – NCAM) is a glycoprotein expressed on neurons, natural killer cells and skeletal muscle cells; as well as on cells of the neuroendocrine system. It can be used as marker for tumors of the foregut or midgut with neuroendocrine phenotype [17]. However, CD56 is not specific for the neuroendocrine differentiation [32]; therefore it should always be used in combination with other neuroendocrine markers, such as CgA or synaptophysin.

g) Circulating tumor cells

Recently, circulating tumor cells (CTCs) have become of increasing interest as biomarkers since the development of technology allows for detection in small samples of blood. The technology is based on the expression of the epithelial cell adhesion molecule (EpCAM). In 2013, Khan and colleagues reported 47% of patients with midgut NETs to have ≥2 detectable CTCs [33]. Their results were confirmed by another group [34]. However, since no significant association with therapeutic response could be found, the applicability of CTCs as effective biomarker in neuroendocrine tumors remains to be seen.

Genetic characteristics

a) Chromosomal aberrations

The underlying genetic causes for the development of SI-NETs are still not fully understood. About 70% of SI-NETs display a (partial) loss of chromosome 18 [15, 35-38]. Due to its high frequency it has been postulated that the loss of heterozygosity (LOH) / loss of chromosome 18 represents an early event in tumorigenesis. Other chromosomal aberrations such as gains of chromosome 4, 5, 7, 14, and 20 as well as (partial) loss of chromosome 3, 11, and 13 have been reported in SI-NETs (reviewed in [39]). Gain of chromosome 14 has been shown to be significantly associated with shorter survival [37]. Comparative analysis of the different studies led to the proposal of a molecular progression model for SI-NETs, subdividing the tumors in two groups (Figure 5) [39]. Following this model, most tumors arise from cells which have lost chromosome 18 (Chr18). In a subsequent step these tumors can also loose (parts) of chromosome 3, 11 or 13 and become metastatic (Figure 5, upper illustration). A smaller group of tumors is characterized by different chromosomal gains (Figure 5, lower illustration).

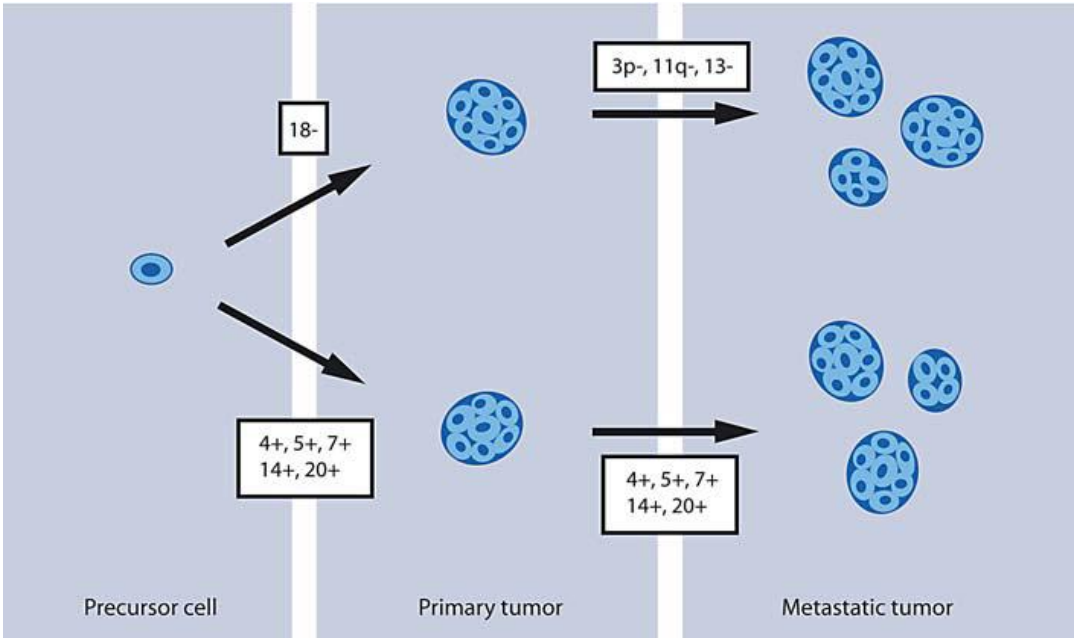

Figure 5: Subgrouping of SI-NETs by their chromosomal aberrations [39]
The majority of tumors is characterized by loss of Chr18, followed by additional losses of e.g. Chr3p, 11q, and 13 (upper illustration). In another, somehow smaller, group gains of Chr4, 5, 7, 14, and 20 were observed (lower illustration)

The role of these frequent genetic aberrations for the tumor progression of SI-NETs has not yet been clarified.

b) Chr18-associated tumor suppressors

The loss of one Chr18 allele could possibly result in the partial loss of tumor suppressor genes located on Chr18, such as the well-known tumor suppressors *SMAD2*, *SMAD4*, *DCC*, and *SERPINB5*.

SMAD2 and *SMAD4* (both located on 18q21.1) encode important signal transduction molecules in the TGFβ pathway [40]. SMAD2 (together with SMAD3) is a receptor regulated SMAD molecule (so-called R-SMADs) which regulates this pathway. R-SMADs become phosphorylated, thereby dissociating from the receptor. Due to phosphorylation these SMADs have a high affinity to so-called “Co-SMADs”, e.g. SMAD4. A complex of R-SMAD and Co-SMAD enters the nucleus, binds to transcription factors, subsequently promoting gene transcription. One main function of TGFβ signaling is the inhibition of cell proliferation and induction of apoptosis, identifying TGFβ as tumor suppressor. In contrast, a disturbed TGFβ signaling pathway can result in promotion of tumorigenesis by induction of epithelial-mesenchymal

transition (EMT), angiogenesis, and suppression of the immune system [41]. SMAD2 and SMAD4 are known to be functionally inactivated in different types of cancers [42-46].

In 1990, *DCC* (18q21.3) was identified to be frequently deleted in colorectal carcinoma [47], a cancer, in which LOH on 18q is a frequent event in tumor progression. *DCC* encodes a netrin-1 receptor, which induces caspase-9-dependent apoptosis in the absence of netrin-1 [48]. Since SI-NETs are characterized by frequent metastases despite of a low proliferation index, reduced apoptosis could be an explanation for the progression of these tumors.

Maspin (encoded by the gene *SERPINB5*, which is located on 18q21.33) has been shown to be deregulated (up- or downregulated) in a myriad of cancers. Intensive studies have shed light on the tumor suppressor function of Maspin by detecting reprogramming of the tumor proteome via Maspin expression, particularly of protein pathways involved in tumor cell extravasation [49]. To evaluate the role of Maspin in SI-NETS, we did western blot analysis in eight tumor samples. No expression of Maspin could be detected in these tumors. However, double immunofluorescence staining with synaptophysin revealed that Maspin is also not expressed in neuroendocrine cells of the normal ileal mucosa ruling out this suspect [50].

Single point mutations or deletions/insertions in genes, especially tumor suppressors, of Chr18 regions that depict a LOH could result in a total loss of function. However, up to now, no mutations were found in *SMAD2*, *SMAD4*, *DCC*, as well as in other genes, located on Chr18 regions (e.g. *SMAD7*, *ONECUT2*, *NEDD4L*) which are frequently deleted in SI-NETs [35, 36, 38].

Other proteins such as PMAIP1 (18q21.32) and CABLES (18q11.2) have been postulated to be candidate Chr18 encoded tumor suppressors. In 2008, *PMAIP1* was identified as a potential tumor suppressor gene in pancreatic cancer by comparative cDNA microarray analysis [51]. *PMAIP1* is a pro-apoptotic gene whose protein functions in a p53-dependent manner [52]. Therefore, loss of PMAP1 could result in a similar outcome as loss of DCC; namely deregulated apoptosis which could give rise to tumor progression due to the development of metastases.

CABLES is a cell cycle regulatory protein that plays a role in proliferation and differentiation [53]; the encoding gene was found to be silenced in ovarian, colorectal, endometrial, and non-small lung cancer [54-57]. In 2013, Zukerberg et al. reported that the (partial) loss of CABLES (detected by IHC) is also a frequent aberration in SI-NETs [58]. Interestingly, alternative as well as aberrant splicing has been described for *CABLES*, resulting in the expression of different isoforms, which can result in abridged protein function due to loss of important protein-protein interacting domains [59].

Imprinted genes requiring only one mutational hit for inactivation are of special interest regarding potential tumor suppressor genes. *TCEB3C* (18q21.1), a maternally imprinted gene [60], functions as a transcription elongation factor and is hence an interesting tumor suppressor candidate [61]. *TCEB3C* encodes the protein Elongin A3, which is known to stimulate the rate of transcription elongation by RNA polymerase II. It was shown that the majority of SI-NETs harbor only one copy of *TCEB3C* and that this results in frequent downregulation of the protein in immunohistochemical experiments. However, some tumor samples with loss of one copy of *TCEB3C* depicted retained protein expression and three samples with two copies showed no protein expression [62].

Taken together, the frequent loss of Chr18 is a suspicious event in the development of SI-NETs. It could result in downregulation of tumor suppressors located on Chr18. A second mutational hit (substitutions, InDels, LOH) then could lead to the loss of tumor suppressor function and thereby to tumor development and progression.

c) PI3K/AKT/mTOR pathway

Members of the PI3K/AKT/mTOR pathway (Figure 6) are known to be frequently altered in tumors, e.g. lung carcinomas, brain tumors, and colorectal cancer [63-65]. Banck and colleagues found that this is also true for SI-NETs with copy number changes in 29% of the analyzed cases [3]. They could show that *PIK3CD*, *PDGFRα/β*, *AKT1/2*, and *mTOR* were amplified in 8 to 17% of the tumors, using whole exome sequencing and array-comparative genomic hybridization (aCGH). Amplifications in the PI3K/AKT/mTOR pathway could lead to constant activation, resulting in enhanced cell proliferation and survival, giving rise to tumor development and progression [66].

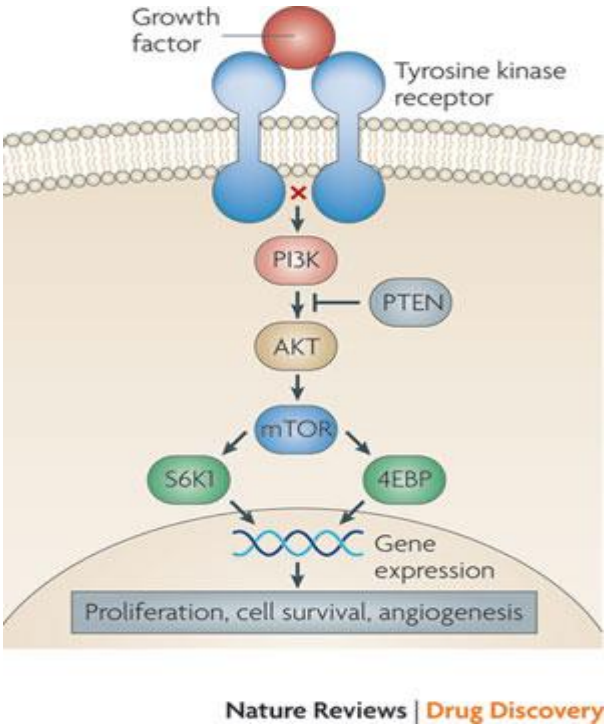

Figure 6: A simplified overview of the PI3K/AKT/mTOR pathway [66]

Platelet-derived growth factor receptors, alpha and beta polypeptide (*PDGFRα* and *PDGFRβ*) encode for cell surface tyrosine kinase receptors, which upon binding of its ligands spur a signaling cascade including activation of Phosphoinositide-3-kinases (PI3K), leading to cell proliferation and growth. Amplifications of *PDGFRα* have primarily been described in glioblastomas [64], but also in lung adenocarcinomas and lung squamous cell carcinomas [67]. *PDGFRβ* amplification has been described in choroid plexus carcinomas [68] and in sarcomatoid non-small cell lung cancer the amplifications have been linked to elevated protein expression [69].

PI3Ks phosphorylate PftdIns(4,5)P2 (Phosphatidylinositol 4,5-bisphosphate) to generate phosphatidylinositol 3,4,5-trisphosphate (PIP3). PIP3 is a key role player, which recruits PH domain containing proteins such as AKT1 to the membrane, thereby activating signaling cascades involved in cell growth, proliferation, survival, and motility. *PIK3CD* encodes the p110δ catalytic subunit belonging to the class I PI3Ks. mRNA overexpression of *PIK3CD*, but no amplification was reported in glioblastomas [70]. A second study also focusing on glioblastomas detected low level copy number gains of *PIK3CD* and *PIK3CA* without gene amplifications [71].

AKT1 and *AKT2* are related genes encoding serine-threonine kinases, which are phosphorylated by PI3K at Thr308. AKT1 is ubiquitously expressed, whereas AKT2 is predominantly expressed in insulin-responsive tissues such as the liver [72]. Upon activation, the AKT proteins translocate to different subcellular compartments and the nucleus, where they regulate numerous cellular functions such as survival, growth, and cell cycle progression through phosphorylation of their target genes. Amplification/overexpression of AKT2 has been reported in different cancers such as non-Hodgkin's lymphoma [73], pancreatic cancer [74], and hepatocellular carcinomas [75]. More recently, amplifications and, more commonly, polysomy of *AKT* genes were described in lung cancer [63].

mTOR belongs to a family of phosphatidylinositol kinase-related kinases. mTOR builds complexes with other proteins, termed mTORC1 (with RPTOR and MLST8), which can be inhibited by the immunosuppressive drug rapamycin and mTORC2 (with RICTOR, MLST8, and mSIN1), which is resistant to rapamycin [76]. mTORC1 is responsible for the activation of S6K1 and 4E-BP1, which are two main downstream targets of mTOR. They function as translation enhancer and repressor, respectively. Activated S6K1 phosphorylates ribosomal protein S6, which initiates protein synthesis. Unphosphorylated 4E-BP1 binds to eIF4E, thereby preventing the protein from docking to the mRNA with subsequent inhibition of the translation-initiation-complex. By phosphorylation, 4E-BP1 releases eIF-4E, which induces translation. It has been shown, that eIF-4E cooperates with other cancer genes to induce tumor formation, identifying the encoding protein as potential oncoprotein [77, 78]. Amplifications of *mTOR* have not been reported in cancers until now. However, it was recently shown, that another component of the mTOR complex mTORC2, *RICTOR*, is amplified in a subset of patients with lung cancer [79]. These patients might benefit from treatment with dual mTORC1/2 or PI3K/mTOR inhibitors, such as AZD2014 and BEZ235, as was shown by *in vitro* experiments.

The constitutive activation of the PI3K/AKT/mTOR survival pathway by amplifications represents an attractive therapeutic target for many different cancers. Everolimus (RAD-001) and temsirolimus (CCI-779) are two approved PI3K/AKT/mTOR inhibitory drugs, which target mTOR. Through the inhibition the synthesis of proteins involved in tumor

cell growth, proliferation, and survival is impaired. Many other anti-cancer drug targeting kinases of this and other pathways are in pre-clinical development [80]. Figure 7 shows the PI3K/AKT/mTOR pathway with the target sites of different inhibitory drugs. The identification of amplifications in SI-NETs could give rise to new possibilities for the treatment of these tumors.

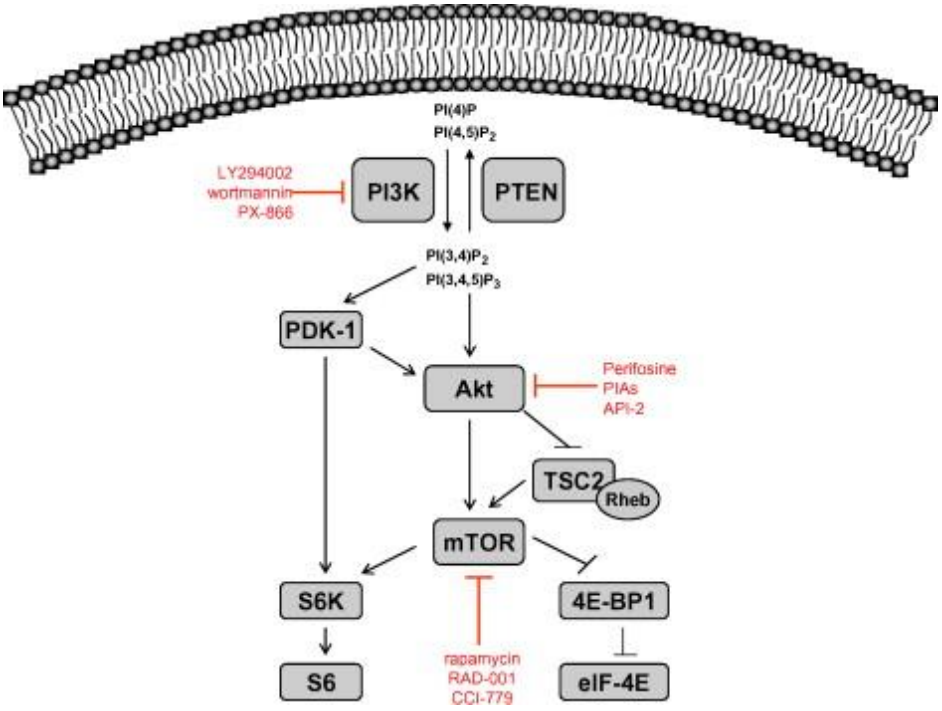

Figure 7: PI3K/AKT/mTOR pathway and the target sites for inhibitory drugs [81]
PI3K, Akt, and mTOR can be inhibited (reversible or irreversible, indicated in red) by different drugs and mechanisms; PI(4)P, $PI(4,5)P_2$, $PI(3,4)P_2$, $PI(3,4,5)P_3$: different phosphoinositides

Epigenetic characteristics

a) MicroRNAs

MicroRNAs (miRNAs) are small (19-25 nt), non-coding RNAs, which function as gene regulators. They can act as oncogenes or tumor suppressors [82]. Li and colleagues found, that five miRNAs (miR-96, -182, -183, -196a, and -200a) are upregulated during tumor progression, whereas four miRNAs (miR-31, -129-5p, -133a, and -215) are downregulated [83].

The loss of Chr18 may result in downregulation of Chr18-related microRNAs involved in tumor progression. Similar effects on miRNA expression by chromosome loss have

been described for gastrointestinal stromal tumors in which the partial loss of chromosome 14 went hand in hand with the downregulation of 38 chromosome 14-related miRNAs [84]. Therefore, we investigated 27 miRNAs located on Chr18 in a cohort of 20 SI-NETs (ten with, ten w/o loss of Chr18), revealing no significant difference in expression between the two cohorts [50].

b) Methylation

Inactivation through methylation is another possible mechanism by which the tumor suppressor function can be lost. Intensive studies revealed methylation of CpG islands (covalent attachment of a methyl group at the 5' position of cytosine residues in CG dinucleotides [85]) in the promoter region to result in downregulation of gene expression [86]. DNA methylation, leading to physical conformation changes, thereby preventing binding of regulatory proteins, works together with histone modifications and chromatin remodeling. The outcome of this interaction is transcriptionally repressed heterochromatin [86, 87].

In 2003, Chan et al. studied the CpG islands of 14 genes and loci (known to be frequently methylated in other gastrointestinal tumors) in seven SI-NETs (and other GEP-NETs) and associated normal mucosa [88]. They found that the *CDKN2A* gene isoform coding for $p14^{ARF}$ was methylated in 57% (4/7) of cases; in contrast, the adjacent normal mucosa was unmethylated. Liu and colleagues confirmed these results; in their cohort 69% (11/16) of ileal tumors were methylated. They also found the alternate isoform of *CDKN2A*, coding for $p16^{INK4a}$, and *RASSF1A* to be methylated in 25% (4/16) and 69% (11/16), respectively, whereas the adjacent normal tissue (if available) was not methylated [89]. Similar findings were reported by Fotouhi et al. [90]. $p16^{INK4a}$ functions as CDK4 kinase inhibitor, whereas $p14^{ARF}$ stabilizes p53 by interacting with the E3 Ubiquitin Ligase MDM2, which is responsible for the degradation of p53. RASSF1A normally inhibits accumulation of Cyclin D1, resulting in cell cycle arrest. Hence, all proteins described above play important roles in the cell cycle G1 control and loss of their function will eventually result in abnormal cell cycle progression and thereby in enhanced cell proliferation and growth.

SERPINB5 is a controversial discussed tumor suppressor gene (see Genetic characteristics b) Chr18-associated tumor suppressors). Verdugo and colleagues reported *SERPINB5* to be methylated in NETs, however, methylation status in the corresponding normal tissue was not applied [91].

Whereas hypermethylation is mostly a local phenomenon, hypomethylation is a global event in cancers [92]. Hypomethylation arises predominantly on highly repetitive DNA sequences, such as Alu and long interspersed elements (LINE)-1 [93, 94]. Choi and colleagues found that these two repetitive sequences are hypomethylated in a subset of “carcinoid” neuroendocrine tumors. LINE-1 methylation was associated with Chr18 loss, methylation of *RASSF1A*, and lymph node metastases [95].

A recent integrative genomic study, published by Karpathakis et al., identified molecular distinct subgroups of SI-NETs [96]. The biggest group comprised SI-NETs with loss of Chr18 and associated CpG island methylator phenotype (CIMP) negativity, whereas CIMP positivity was associated with absence of copy number variations (CNVs); indicating that aberrant global methylation and CNVs are mutually exclusive mutations in SI-NETs.

Although the number of methylome studies rises, the translation to protein expression is often still missing.

Therapy

The only curative therapy for SI-NETs is removal of the primary tumor and the regional lymph node metastases. Unfortunately, this is only possible with 20% of patients [97]. Since SI-NETs are slow-growing tumors systemic chemotherapy is not applicable for most of the patients.

Somatostatin analogues (SSA) can be given to patients with tumors expressing SSTRs. The highest affinity of SST analogues is to SSTR2A [98]. These drugs can help reduce the symptoms of the carcinoid syndrome. In addition, they can inhibit growth of NETs; only in rare cases the reduction of the tumor volume is seen [99]. For octreotide, a widely used SSA, the inhibitory function could be shown in the human midgut carcinoid tumor cell line CNDT2.5 [100]. However, patients may develop resistance to treatment

over time which is partially explained by upregulation of truncated SSTR5 variants in tumors [101].

Radiolabeled SSA therapy or peptide receptor-mediated radiotherapy (PRRT) is another treatment possibility for inoperable and/or metastatic tumors which overexpress SSTR. Radionuclides target the SSTR-expressing tumor cells, get internalized, and thereby inhibit the growth of the tumor by destroying the cells through β- or γ-radiation. The most common used agents are ^{90}Y-DOTATOC and ^{177}Lu-DOTATAE. The side effects of PRRT are mostly mild and self-limiting [102].

The RADIANT-2 study evaluated the effect of the mTOR inhibitor everolimus on progressive SI-NETs [103]. The median progression-free survival (PFS) was 16.4 months with everolimus + octreotide in contrast to 11.3 months with placebo + octreotide. However, no statistical significance was reached (which was probably due to imbalanced informative censoring). Despite this, the study showed that a subgroup of patients with progressive SI-NETs may benefit from treatment with everolimus. The recently published RADIANT-4 study showed that 10 mg everolimus per day leads to significantly prolonged median progression-free survival by 7.1 months compared to the placebo control group in neuroendocrine tumors of the lung or gastrointestinal tract [97]. However, no functional NETs were included, so that the explanatory power for SI-NETs is still a minor one.

In summary, the only curative therapy for SI-NETs, surgery, is only feasible in 1/5 of the patients. All other treatments can reduce the symptoms and prolong the overall survival, but unfortunately do not cure the patients and development of resistance can occur. In this regard, the necessity of new drugs which target tumor specific aberrations or pathways is obvious.

Preliminary work (working group Prof. Sipos)

In preliminary experiments of the working group of Prof. Sipos the effect of the common loss of Chr18 in SI-NETs was addressed.

In order to investigate the protein expression of the well-known tumor suppressors SMAD2, SMAD4, DCC, and Maspin immunohistochemical analyses were performed. DCC and SMAD2 were expressed in all 87 tumors investigated. SMAD4 was expressed in 97% (84/87) of the analyzed cases. However, since the staining results for these proteins were not perfectly convincible due to imperfect antibodies, the results have to be interpreted carefully. Therefore, western blot analysis was the method of choice for the protein investigation in my doctoral thesis, since more reliable antibodies were available for this method.

Maspin was not expressed in any of the 87 tumor samples. Subsequent double immunofluorescence stainings of Maspin and synaptophysin of normal small intestine tissues adjacent to SI-NETs revealed neuroendocrine cells of the ileal mucosa to not express Maspin. This suggests that the lacking Maspin expression in neoplastic SI-NET cells does not reflect an oncogenic event but the phenotype of the non-neoplastic neuroendocrine cells of the mucosa of the small intestine.

My master thesis focused on Chr18-related microRNAs (miRNAs) and their expression in SI-NETs. Therefore, we analyzed the expression of 27 miRNAs coded by regions on Chr18 in quantitative Real-time PCR experiments in an explorative cohort of 20 SI-NETs (with and without loss of Chr18). As no expression differences between the two cohorts could be detected, one allele seems to be sufficient for the expression of the encoded miRNAs.

Aim

Part 1: Alterations of Chr18-related tumor suppressors in SI-NETs

The first part of my doctoral thesis addresses the frequent loss of Chr18 in SI-NETs. Therefore, protein expression of the Chr18-related tumor suppressors DCC, SMAD2, SMAD4, PMAIP1, Elongin A3, and CABLES was analyzed by western blot in a cohort of 8-21 SI-NETs. In addition, mRNA expression of *DCC*, *PMAIP1*, *TCEB3C* (encoding Elongin A3), and *CABLES* was analyzed. The aim of this study was to investigate all known candidate tumor suppressors on Chr18 in view of tumor development. Next generation sequencing and SNP array analysis were performed to investigate alterations on DNA level, which could identify potential (new) tumor suppressors and oncogenes in SI-NETs. In summary, this comprehensive approach to define Chr18-associated genetic alterations should help to improve the understanding of the molecular biology of SI-NETs.

Part 2: Alterations of the PI3K/AKT/mTOR pathway in SI-NETs

The second part of my doctoral thesis focuses on the PI3K/AKT/mTOR pathway in SI-NETs. Since this pathway can be targeted by different FDA approved drugs, it is of special interest for tumor research. Banck and colleagues showed that this pathway is affected by copy number alterations in 29% of SI-NETs by performing next generation sequencing on 48 patients [3]. To take a deeper look at these alterations, Fluorescence-in-situ-hybridization (FISH) analysis was applied to a greater cohort of 217 SI-NETs. Six genes belonging to the PI3K/AKT/mTOR pathway (*PIK3CD*, *PDGFRα*, *PDGFRβ*, *AKT1*, *AKT2*, and *mTOR*) were investigated in order to detect potential gene amplifications and the results were correlated with protein expression and activation of (p-)AKT, p-mTOR, and the downstream signaling proteins p-S6 and p-4EBP1. Gene amplification and/or protein overexpression can be targeted by protein kinase inhibitors such as everolimus (an mTOR inhibitor), which is already approved for treatment of advanced and metastasized pancreatic NETs.

II. Material

2.1 Equipment

Table 4: Equipment

Equipment	Manufacturer
Biofuge primoR (Heraeus)	Thermo Fisher Scientific (Waltham, MA, US)
CM1900	Leica Biosystems, Nussloch, DE
Curix60 (X-ray film processor)	Agfa (Stuttgart, DE)
FlexCycler	Analytik Jena AG (Jena, DE)
Fluorescence microscope Axioplan 2	Carl Zeiss (Jena, DE)
Genesis RSP 100 (Automated liquid handling system)	Tecan Trading AG (Männedorf, CH)
GeXP – Genetic Analysis System	Beckman Coulter (Brea, CA, US)
HybEZ oven	Advanced Cell Diagnostics (Hayward, CA, US)
Hyrax M55 (Microtom)	Carl Zeiss (Jena, DE)
Incubator NuAire-5510E	Integra Biosciences (Fernwald, DE)
Infinity (Gel documentation system)	Vilber Lourmat (Eberhardzell, DE)
Inverse Microscope for Cell culture	Nikon Europe (Düsseldorf, DE)
LightCycler 480 II	Roche (Mannheim, DE)
Microplate Reader	Biorad (Hercules, CA, US)
Microscope	Carl Zeiss (Jena, DE)
Microwave	Severin (Sundern, DE)
MiraxDesk (Scanner)	Carl Zeiss (Jena, DE)
Minispin	Eppendorf (Hamburg, DE)
NanoDrop2000	Thermo Fisher Scientific (Waltham, MA, US)
Pipettes (10, 100,200, 1000)	Eppendorf (Hamburg, DE)
ThermoBrite Stat Spin	Abbott Molecular (Abbott Park, IL, US)
Thermomixer Comfort	Eppendorf (Hamburg, DE)
Tissue-Tek® slide stainer	Sakura (Alphen aan den Rijn, NL)
Tissue Microarrayer	Beecher Instruments (Sun Prairie, WI, US)
Ventana BenchMark System	Ventana Medical Systems (Tucson, AZ, US)
Vortex Genius 3	IKA (Staufen im Breisgau, DE)
Waterbath	GFL (Burgwedel, DE)

Table 5: Consumables

Consumables	Manufacturer
Cell culture flasks T75	Sarstedt (Nümbrecht, DE)
Centrifuge tubes (15 and 50 ml)	Greiner (Frickenhausen, DE)
Cover slips	Menzel (Braunschweig, DE)
Mini-PROTEAN® TGX™ Precast Polyacrylamide Gels	Biorad (Hercules, CA, US)
Pasteur pipettes	Roth (Karlsruhe, DE)
PCR Reaction tubes 0,2ml	Sarstedt (Nümbrecht, DE)
Pipette tips	Starlab (Blakelands, UK)
Reaction Tubes 0,5; 1,5 and 2 ml	Eppendorf (Hamburg, DE)
Serological pipettes 5; 10; 25; 50 ml	Sarstedt (Nümbrecht, DE)
Feather Disposable Scalpels	pfm medical (Köln, DE)
SuperFrost Plus slides	R.Langenbrinck (Emmendingen, DE)

2.2 Software and Databases

Table 6: Software and Databases

Software	Manufacturer
Chromosome Analysis Suite	Affymetrix (Santa Clara, CA, US)
COSMIC	http://cancer.sanDE.ac.uk/cosmic
dbSNP	http://www.ncbi.nlm.nih.gov/projects/SNP/
Ensembl	http://www.ensembl.org/index.html
Exome Variant Server	http://evs.gs.washington.edu/EVS/
Genetic Analysis Software	Beckman Coulter (Brea, CA, US)
GraphPad Prism 4	GraphPad (La Jolla, CA, US)
KEGG	http://www.kegg.jp/
Pathway Maps	http://lsresearch.thomsonreuters.com/maps/
PolyPhen-2	http://genetics.bwh.harvard.edu/pph2/
Primer-BLAST	http://www.ncbi.nlm.nih.gov/tools/primer-blast/
Primer3Plus	http://primer3plus.com/cgi-bin/dev/primer3plus.cgi
PubMed	http://www.ncbi.nlm.nih.gov/pubmed/
SIFT/PROVEAN	http://sift.jcvi.org/
SPSS Statistics	IBM (Armonk, NY, US)
The Human Protein Atlas	http://www.proteinatlas.org/
Tissue Studio XD 2.3.0	Definiens (München, DE)
TMA Designer 2	Alphelys (Plaisir, Fr)
UniProt	http://www.uniprot.org/

2.3 Chemical and biological reagents

Table 7: Chemical and biological reagents

Reagent	Manufacturer
0,25% Trypsin/EDTA Solution (1x)	Gibco, Thermo Fisher Scientific (Waltham, MA, US)
6x Loading Dye	Fermentas (St. Leon-Rot, DE)
Albumin Fraction V	Roth (Karlsruhe, DE)
Agarose	Biozym (Hessisch Oldendorf, DE)
Agencourt AMPure XP Beads	Beckman Coulter (Brea, CA, US)
Agencourt CleanSEQ	Beckman Coulter (Brea, CA, US)
Aqua Phenol pH 4,5 – 5	Roth (Karlsruhe, DE)
BCA Protein Assay Reagent (bicinchoninic acid)	Thermo Fisher Scientific (Waltham, MA, US)
Boric acid	Merck (Darmstadt, DE)
Bovine Serum Albumine (BSA) Standards	Thermo Fisher Scientific (Waltham, MA, US)
β-Mercapthoethanol	Merck Millipore (Darmstadt, DE)
CAS block	Thermo Fisher Scientific (Waltham, MA, US)
CEP hybridization buffer	Abbott Molecular (Abbott Park, IL, US)
Chloroforme / IAA	Roth (Karlsruhe, DE)
Citric acid monohydrate	Merck Millipore (Darmstadt, DE)
cOmplete Tablets EDTA-free, EASYpack (Protease Inhibitor)	Roche (Basel, CH)
Cot-1 DNA (human)	Invitrogen, Life Technologies, Thermo Fisher Scientific (Waltham, MA, US)
Disodium phosphate	Merck Millipore (Darmstadt, DE)
DMEM, high glucose	Gibco, Thermo Fisher Scientific (Waltham, MA, US)
Dulbecco's PBS (1x)	GE Healthcare (Little Chalfont, UK)
Ethylenediaminetetraacetic acid (EDTA)	Merck Millipore (Darmstadt, DE)
Ethanol	Merck Millipore (Darmstadt, DE)
Fetal calf serum (FCS)	Invitrogen, Life Technologies, Thermo Fisher Scientific (Waltham, MA, US)
F-12 Nutrient Mix	Gibco, Thermo Fisher Scientific (Waltham, MA, US)
GelRed Nucleic Acid Stain	Biotium (Hayward, CA, US)
GeneRuler 1kb DNA Ladder	Fermentas (St. Leon-Rot, DE)
Glycin	Roth (Karlsruhe, DE)
Glycogen	Roche (Basel, CH)
Immobilon Western Chemiluminescent HRP Substrate	Merck Millipore (Darmstadt, DE)
Isopropanol	Merck Millipore (Darmstadt, DE)
Methanol	Merck Millipore (Darmstadt, DE)
Monopotassium phosphate	Roth (Karlsruhe, DE)
Nonidet P 40 Substrate (NP-40)	Sigma-Aldrich (St. Louis, MO, US)

Normal goat serum	Cell Signaling (Danvers, MA, US)
Papanicolaous Solution 1a Harris' Haematoxylinsolution	Merck Millipore (Darmstadt, DE)
PageRuler prestained Protein Ladder	Thermo Fisher Scientific (Waltham, MA, US)
Papanicolaou Solution 1A	Merck Millipore (Darmstadt, DE)
Penicillin/Streptomycin Solution	Lonza (Basel, AT)
Pepsin	Sigma-Aldrich (St. Louis, MO, US)
Potassium chloride (KCl)	Merck Millipore (Darmstadt, DE)
ProLong® Gold Antifade mountant with DAPI	Invitrogen, Life Technologies, Thermo Fisher Scientific (Waltham, MA, US)
ProSieve QuadColor Protein Marker	Lonza (Basel, CH)
Proteinase K (50 mg/ml)	Qiagen (Hilden, DE)
Restore Western Blot Stripping Buffer	Thermo Fisher Scientific (Waltham, MA, US)
RNaseOUT™ Recombinant Ribonuclease Inhibitor	Invitrogen, Life Technologies, Thermo Fisher Scientific (Waltham, MA, US)
RnaseZap	Invitrogen, Life Technologies, Thermo Fisher Scientific (Waltham, MA, US)
RPMI1640	Gibco, Thermo Fisher Scientific (Waltham, MA, US)
Skim Milk	BD (Franklin Lakes, NJ, US)
Sodium actetate 3M (NaAc) pH 5,2	Invitrogen, Life Technologies, Thermo Fisher Scientific (Waltham, MA, US)
Sodium azide	Sigma-Aldrich (St. Louis, MO, US)
Sodium chlorid (NaCl)	Merck Millipore (Darmstadt, DE)
Sodium desoxycholat	Roth (Karlsruhe, DE)
Sodium dodecyl sulfate (SDS)	Merck Millipore (Darmstadt, DE)
Sodium fluorid (NaF)	Merck Millipore (Darmstadt, DE)
Sodium hydroxide (NaOH)	Merck Millipore (Darmstadt, DE)
Trisodium citrate dihydrate	Roth (Karlsruhe, DE)
Trizma Base	Sigma-Aldrich (St. Louis, MO, US)
Tween 20	Merck Millipore (Darmstadt, DE)
Xylol	BDH ProLabo (Darmstadt, DE)

2.4 Antibodies and FISH probes

Table 8: Primary Antibodies
M: monoclonal, p: polyclonal, rb: rabbit, ms: mouse, g: goat, IHC: immunohistochemistry, WB: western blot

Antibody	Clone	Dilution	Manufacturer
AKT2 (m, ms)	F-7	1:100 (IHC)	Santa Cruz (Dallas, TX, US)
Anti IK3-1 / Cables1 (p, rb)		1:200 (WB)	Biozol (Eching, DE)
β-Actin (m, ms)	AC-15	1:40.000 (WB)	Sigma-Aldrich (St. Louis, MO, US)
CDX2 (m, rb)	EPR2764Y	1:25 (IHC)	Zytomed (Berlin, DE)
DCC (p, gt)		1:100 (WB)	Santa Cruz (Dallas, TX, US)
DCC (p, rb)		1:500 (WB)	Biorbyt (Cambridge, UK)
Elongin A3 (p, rb)		1:200 (WB)	Santa Cruz (Dallas, TX, US)
Ki-67 Antigen (m, ms)	MIB-1	1:200 IHC	Dako, Agilent Technologies (Santa Clara, CA, US)
pHH3 (p, rb)		1:250 (IHC)	Zytomed (Berlin, DE)
PMAIP1 (p, rb)		1:250 (WB)	Sigma-Aldrich (St. Louis, MO, US)
p-AKT1 (Thr308) (p, rb)		1:200 (IHC)	Santa Cruz (Dallas, TX, US)
p-mTOR (Ser2448) (m, rb)	49F9	1:100 (IHC)	Cell Signaling (Danvers, MA, US)
p-S6 (Ser240/244) (m, rb)	D68F8	1:138 (IHC)	Cell Signaling (Danvers, MA, US)
p-4E-BP1 (Ser65/Thr70) (p, gt)		1:400 (IHC)	Santa Cruz (Dallas, TX, US)
Serotonin (m, ms)	SHT-H209	1:30 (IHC)	Dako, Agilent Technologies (Santa Clara, CA, US)
SMAD2 (m, rb)	86F7	1:1000 (WB)	Cell Signaling (Danvers, MA, US)
SMAD4 (m, ms)	B-8	1:100 (WB)	Santa Cruz (Dallas, TX, US)
SSTR2 (p, rb)		1:100 (IHC)	Zytomed (Berlin, DE)
Synaptophysin (m, ms)	Snp88	1:200 (IHC)	DCS-Diagnostics (Hamburg, DE)

Table 9: Secondary Antibodies
IgG: Immunoglobulin G, HRP: Horseradish peroxidase, H+L: heavy + light chains

Antibody	Conjugation	Dilution	Manufacturer
Streptavidin Alexa Fluor594	Streptavidin	1:500	Thermo Fisher Scientific (Waltham, MA, US)
Goat anti rabbit IgG (H+L)	HRP	1:3000	Thermo Fisher Scientific (Waltham, MA, US)
Goat anti mouse IgG (H+L)	HRP	1:3000	Thermo Fisher Scientific (Waltham, MA, US)
Rabbit anti goat IgG (H+L)	HRP	1:3000	Thermo Fisher Scientific (Waltham, MA, US)

Table 10: FISH probes
Cen: Centromere, CEP: centromere enumeration probe

FISH probe	Fluorophore/Labeling	Manufacturer
AKT1/Cen14q	Texas Red/FITC	Abnova (Taipei, RC)
AKT2/Cen19p	Texas Red/FITC	Abnova (Taipei, RC)
Cen1	SpectrumGreen	Metasystems (Altlussheim, DE)
CEP18	SpectrumGreen	Abbott Molecular (Abbott Park, IL, US)
mTOR	Biotin-labeled	Custom made (CeGaT, Tübingen, DE)
PDGFRA/Cen4p	Texas Red/FITC	Abnova (Taipei, RC)
PDGFRB/PDGFRB (Split)	Texas Red/FITC	Abnova (Taipei, RC)
PIK3CD	Red 5'-ROX dUTP	Empire Genomics (Buffalo, NY, US)

2.5 Oligonucleotides

Table 11: Oligonucleotides for the validation / falsification of mutations found by exome sequencing
The product sizes incl. M13 primers are listed in parentheses

Name	Sequence	Size
ADCY5 M13 for ADCY5 M13 rev	tgtaaaacgacggccagCTGGAAAGCCTGTCTCTGGG caggaaacagctatgacGCTGAGGGCTTCATGCTTTG	165 bp (200 bp)
ATF7IP M13 up ATF7IP M13 lo	tgtaaaacgacggccagTTGGACAATGTACAGTCTAAACGTCGTCGATA caggaaacagctatgacAAGCTCAACCACTTTCTTCAAGTTCTTTCTTTC	251 bp (286 bp)
AUTS2 M13 for AUTS2 M13 rev	tgtaaaacgacggccagGACATTCACCGGAGAGACCC caggaaacagctatgacGAGGGTCCACAGACAGCG	172 bp (207 bp)
BDP1 M13 for BDP1 M13 rev	tgtaaaacgacggccagTGGTCAAGATGCCATGGGTT caggaaacagctatgacCCTCAGTGGTATATTCTTGACAGT	182 bp (217 bp)
CABYR for CABYR rev	TGTGCCTGTGACTGAAGGAG TTGGGACTAACTCGTGGTGA	138 bp
CACNA1E M13 for CACNA1E M13 rev	tgtaaaacgacggccagTTCCCTTAGTCATGGCCCTG caggaaacagctatgacTTTGTCTATCCAGGCACGGT	168 bp (203 bp)
CBLL1 for CBLL1 rev	TAAAGGGGGTGAGCTGTTTG TGTGCATTACTCCAATAAAACATT	150 bp
CORO2A M13 for CORO2A M13 rev	tgtaaaacgacggccagTGGTGTTGAAGGACATGGAGAG caggaaacagctatgacGCATCCTGGCCAGCATGTAA	181 bp (216 bp)
CYP3A5 M13 for CYP3A5 M13 rev	tgtaaaacgacggccagCACCACCATTGACCCTTTGG caggaaacagctatgacTCTGTTTCTTTCCTTCCAGGC	178 bp (213 bp)
C1RL M13 for C1RL M13 rev	tgtaaaacgacggccagTTAGCCAGCCCATCTCCATG caggaaacagctatgacACCGTCAGAATGAGTCCCAT	174 bp (209 bp)
C3ORF20 M13 for C3ORF20 M13 rev	tgtaaaacgacggccagCATTTTTGGGGGCCGTGTTT caggaaacagctatgacCCTCATCCTGCGTGTTTCCT	150 bp (185 bp)
ERCC4 for ERCC4 rev	GCTCGAGCAAGGGTTTATCA TGCACTTTAAATTTCCATACCAAA	157 bp

FLNA for FLNA rev	CTCCGAGTCTCTCCCAACTG CCTGTGTCCTGACTGGGACT	161 bp
HECTD4 for HECTD4 rev	ACAGCAGCAAAGCCAAGTTT CATGGCCCTGCTCAATATCT	160 bp
ITGA7 for ITGA7 rev	AGGTTGGTGACCATCAGCTC AATGGTAGGGGGAGGTGTTC	131 bp
ITGA9 for ITGA9 rev	CACCAAAGGCAGATTCCAAA GCAGTAATGGTCACCCACCT	132 bp
KPNA1 for KPNA1 rev	GCACCTGCAGTGTACAATTCTC TGGGGAAACAGAACCTAACC	110 bp
LAMA3 for LAMA3 rev	CTACCAGCATTTGCCAGTGA ATGACAGGGTGTGCAGGTGT	109 bp
LAMA5 M13 for LAMA5 M13 rev	tgtaaaacgacggccagCTCAGACGGGCAGTGAAGAG caggaaacagctatgacGTTCCCTGTCCAGTCACCTG	191 bp (226 bp)
LARP4 M13 for LARP4 M13 rev	tgtaaaacgacggccagGGCTTAACATTACTAGTAAACAAACCA caggaaacagctatgacTCTGTGTCTGACTGGAAAGTGA	189 bp (224 bp)
MS4A14 M13 for MS4A14 M13 rev	tgtaaaacgacggccagAGCTGCGTCACTCCAAGTTT caggaaacagctatgacTTGAGGGGGCAGGTCATTAG	184 bp (219 bp)
MTOR M13 for MTOR M13 rev	tgtaaaacgacggccagAAGAGGTCCTGATGCAGTGC caggaaacagctatgacAGATGCTGCCTTTAGCCCAA	165 bp (200 bp)
MUC16 M13 for MUC16 M13 rev	tgtaaaacgacggccagACTCATGGGTGAACTTGGACT caggaaacagctatgacCCTCCCCTACCATTGGAAGC	185 bp (220 bp)
MUM1L1 M13 for MUM1L1 M13 rev	tgtaaaacgacggccagTGAGGCAAACATGAATTCTGAAAA caggaaacagctatgacCCGTGAAAGAACCACAACCTATTC	185 bp (220 bp)
MYO10 M13 for MYO10 M13 rev	tgtaaaacgacggccagAGCTGCAGGGACTTGTTCTC caggaaacagctatgacTCGCCACAAAATGCAATCCA	174 bp (209 bp)
NFATC1 for NFATC1 rev	AGGAAGAACACACGGGTACG ACGAACGAAAAGCTGAGAGC	188 bp
NFYA for NFYA rev	AGGCTTCCGTCTCTCTCCTC CACTACCTGGAGGGTCTGGA	190 bp
OR1A1 M13 for OR1A1 M13 rev	tgtaaaacgacggccagCCTAAGATGCTGGCCAACCA caggaaacagctatgacTTGTGTAGTGAAGTGGGCGG	166 bp (201 bp)
OR5T3 M13 for OR5T3 M13 rev	tgtaaaacgacggccagTCCAGCTATGCTTCAGACCA caggaaacagctatgacTGTGAACTCTGACACTCAACA	200 bp (235 bp)
PIEZO2 for PIEZO2 rev	CATTGTCTCTGGTGAGCGATA TGGGAAATTTGTCCGTGAAT	187 bp
PIK3C3 for PIK3C3 rev	TTTCCTTGCTTGTGTAATAATTGTA TGGTTGGTGGATAACTCACA	150 bp
PML for PML rev	AGCAGCAGTGAGTCCAGTGA TTAGAAAGGGGTGGGGGTAG	166 bp

PRKCH M13 for PRKCH M13 rev	tgtaaaacgacggccagGGTTCTCCCGCTGCGAAG caggaaacagctatgacTCACCGTCAGATAGGGGTCC	197 bp (232 bp)
RAD54B M13 for RAD54B M13 rev	tgtaaaacgacggccagACCTGAATGTCAGTGGCTGG caggaaacagctatgacGCAGCAGATTGTTGATGGCT	153 bp (188 bp)
RB1CC1 M13 for RB1CC1 M13 rev	tgtaaaacgacggccagTACAGACCTGTTGTTCCGCA caggaaacagctatgacGTCCTGCCATTGACTCTACCA	174 bp (209 bp)
RFC4 M13 for RFC4 M13 rev	tgtaaaacgacggccagCTTACCCCGGCAATGTCTGT caggaaacagctatgacACAACTCTTTTCTCTTCAGGGAA	150 bp (185 bp)
SEMA3F for SEMA3F rev	GCCACCCACTCATGTACCA CCCAGGAAAAGCACCTCATA	142 bp
SLC27A3 for SLC27A3 rev	GGTGTCCACCAGGAAGATGT TACCCTGGAGGACTCACACC	174 bp
SMG5 M13 for SMG5 M13 rev	tgtaaaacgacggccagTGTCCTTCAGGTGGAGACCA caggaaacagctatgacTCAGCATTGCCCAGTCTGAG	165 bp (200 bp)
SPANXN3 M13 for SPANXN3 M13 rev	tgtaaaacgacggccagTCCCCACTGTCCTGTGAAGA caggaaacagctatgacACTCCATCAATCCAATCCAAAAG	193 bp (228 bp)
SVEP1 M13 for SVEP1 M13 rev	tgtaaaacgacggccagGTGAGTTTTGGAGCACCGTG caggaaacagctatgacCGGGTTTGTCTTGCCAATGG	179 bp (214 bp)
SVIL M13 for SVIL M13 rev	tgtaaaacgacggccagAGGCAGCCTGCTGGAAAAT caggaaacagctatgacAAGAAAGAATTGCCAGGCGC	192 bp (227 bp)
SYNPR M13 for SYNPR M13 rev	tgtaaaacgacggccagCCCCAGACCAGTTCCCTGAT caggaaacagctatgacCCAGTGGCTGCTCAGTATTACA	192 bp (227 bp)
USP44 for USP44 rev	GTAACCACGAAAGGCAGGAA GTGGTGGAGCATCAAAAGGT	188 bp
USP48 for USP48 rev	TGGAAAACTGCTTTACCTGGA CCAAGTGTGGCAAAGGAACT	115 bp
XBP1 M13 for XBP1 M13 rev	tgtaaaacgacggccagACCCTCATCTGTCTAGTTAGGGA caggaaacagctatgacCAGCACTCAGACTACGTGCA	196 bp (231 bp)
ZNF280B M13 for ZNF280B M13 rev	tgtaaaacgacggccagACATGTTCCACACCAACAAAGA caggaaacagctatgacGAAGCATTGGGACTTGTGGC	163 bp (198 bp)
ZNF555 M13 for ZNF555 M13 rev	tgtaaaacgacggccagGCAAACAGTGTGGGAAGACC caggaaacagctatgacCAGTGTGCACCCTCATGTGT	150 bp (185 bp)
M13 for M13 rev	tgtaaaacgacggccag caggaaacagctatgac	35 bp

Table 12: Oligonucleotides for the sequencing of all functional regions of the *PML* gene

Name	Sequence	Size
PML Ex 1 for PML Ex 1 rev	TCCCCTTCAGCTTCTCTTCA CCATCATCCCCTAACCCAAT	219 bp
PML Ex 2.1 for PML Ex 2.1 rev	GACTTCTCCAGGCCTCACCT GCTGCAGACTCTCGAAAAAGA	249 bp
PML Ex 2.2 for PML Ex 2.2 rev	CATGCAGTGCCCCATCTG CTCGTGCTTGAGGAACCACT	232 bp
PML Ex 2.3 for PML Ex 2.3 rev	CTCTGCGCCAAGTGCTTC CGCCCTCTACCTGGTACTTG	218 bp
PML Ex 3.1 for PML Ex 3.1 rev	GAGTCCTAACCCAGGCCAAC CCAAAGGCACTATCCTGCTC	197 bp
PML Ex 3.2 for PML Ex 3.2 rev	ACATCAGCGCAGAGATCCAG GTCCACAGCCTCCAGCAG	224 bp
PML Ex 3.3 for PML Ex 3.3 rev	GCCAGGTGGTAGCTCACG AGGAAACCGTGCATGTCC	205 bp
PML Ex 3.4 for PML Ex 3.4 rev	CAGAGGATGAAGTGCTACGC TTCCCTAGGGTGCAGCAG	240 bp
PML Ex 4 for PML Ex 4 rev	TGCCTGTGACCTTCTTTGTG ACTCACAACCTGCCTGACCT	163 bp
PML Ex 5 for PML Ex 5 rev	GGCTGCTGCCTAGTCATTTC GGAACTCAGGCCTTCAGGAG	237 bp
PML Ex 6.1 for PML Ex 6.1 rev	ACCTGACCTGGCTCTGTGAC GTGAGACTGCCTTGGAGGTG	190 bp
PML Ex 6.2 for PML Ex 6.2 rev	GGAAGGTCATCAAGATGGAGTC CCACTGCCCTACCCACCT	225 bp
PML Ex 7 for PML Ex 7 rev	AGCATGCATCCTAGGCAGTT CTGAGAGTCACCTGCTGTGG	188 bp
PML Ex 8 for PML Ex 8 rev	TGACGCTTGGTTTTTCTGTG TTAGAAAGGGGTGGGGGTAG	213 bp

Table 13: Oligonucleotides for the analysis of potential Chr18-associated tumor suppressor genes by quantitative Real-time PCR (qRT-PCR)
***ACTB* is a housekeeper gene and served as normalization control for qRT-PCR analysis.**

Name	Sequence	Size
ACTB for ACTB rev	accagcttttctgcaagtgc gtttgaggcctgttgctgtg	116 bp
CABLES Ex4 for CABLES Ex5 rev	tgccgtatcgcgacagtac ctttcaaactcactgcaccagt	81 bp
DCC Ex3 for DCC Ex4 rev	acaggaaatgaagcagaagtcag acattggatggtctttgcaga	83 bp
DCC Ex17 for DCC Ex18 rev	accagcttttctgcaagtgc gtttgaggcctgttgctgtg	76 bp
PMAIP1 Ex1 for PMAIP1 Ex2 rev	gcaagaacgctcaaccgag tgtctccaaatctcctgagttg	84 bp
TCEB3C for TCEB3C rev	gcaaggggcacaaatcgtc ctgcagcctctctgactgg	80 bp

2.6 Kits

Table 14: Commercial Kits

Kit	Manufacturer
DAB Substrate Kit	Zytomed (Berlin, DE)
Goat-on-rodent HRP Polymer Kit	Zytomed (Berlin, DE)
High-Capacity cDNA Reverse Transcription Kit	Thermo Fisher Scientific (Waltham, MA, US)
iView DAB Detection Kit	Ventana Medical Systems (Tucson, AZ, US)
QIAamp DNA FFPE Tissue Kit	Qiagen (Hilden, DE)
QuantiTect SYBR Green PCR Kit	Qiagen (Hilden, DE)
ZytoChemPlus HRP Polymer Kit	Zytomed (Berlin, DE)

2.7 Buffer

Table 15: Buffer

Buffer	Composition
Ammonia-ethanol	400 ml 70 % EtOH 12 ml NH_3
Citrate Buffer (10x, pH 6)	29,4 g Trisodium citrate dihydrate ad 1 l ddH_2O
Denaturation Solution (FA/2xSSC, pH 7-8)	70 ml Formamide 10 ml 20xSSC, pH 5,3 ad 100 ml ddH_2O
PBS (10x, pH 7,4)	80 g NaCl 2 g KCl 14,2 g Disodium phosphate 2 g Monopotassium phosphate ad 1 l ddH_2O
Pepsin Buffer (0,9% NaCl pH 2)	0,9 g NaCl ad 100 ml ddH_2O
RIPA Buffer	15 ml NaCl (5 M) 5 ml NP-40 2,5 g Sodium desoxycholat (0,5%) 0,5 g SDS (0,1%) 25 ml Tris (1M) 2 ml EDTA (0,5M) 1,05g NaF ad 500 ml ddH_2O
Running Buffer (5x)	15 g Tris 72 g Glycin 5 g SDS
TBS Buffer (10x, pH 7,6)	24,2 g Tris 80 g NaCl ad 1 l ddH_2O
TEC Buffer (10x, pH 9)	2,5 g Tris 5g EDTA 3,2 g Trisodium citrate dihydrate ad 1 l ddH_2O
Transfer Buffer (10x)	30,3 g Tris 144 g Glycin ad 1 l ddH_2O
Transfer Buffer (1x)	100 ml 10x Transfer Buffer 200 ml Methanol 700 ml ddH_2O
Tris-Borate-EDTA-(TBE-) Buffer (1x)	54 g Tris 28,4 g Boric acid

	3,7 g EDTA ad 5 l ddH_2O
TS-TMBSA	5 ml Tris-HCl 15 ml NaCl 500 µl Tween 20 25 g Skim Milk 10 g BSA 5 ml Sodium azide ad 0,5 l ddH_2O
SDS Loading Buffer Leammli (2x)	2 ml Tris-HCl 400 mg SDS 20 mg Bromphenol blue 2 ml Glycerol ad 10 ml ddH_2O
SDS-Lysis Buffer (5x)	2,5 ml 1 M Tris/HCL pH 8,0 50 µl 0,5 M EDTA 25 ml 20 % SDS 22,45 ml RNase/Dnase free H_2O
Saline Sodium Citrate (SSC) Buffer (20x, pH 7,4)	175,32 g NaCl 88,23 g Na-Citrat ad 1 l ddH2O
Wash Buffer for FISH in general	100 ml 20xSSC, pH 5,3 ad 1 l ddH_2O
Wash Buffer for Post-Hybridization (0,3% NP-40/2xSSC)	100 ml 20xSSC, pH 5,3 3 ml NP-40 ad 1 l ddH_2O
Wash Buffer for Western Blot	1x TBS Buffer 0,05% Tween 20

Table 16: Cell lines/tissues used as controls for western blot analysis

Kit	Control for	Manufacturer
BxPC-3	SMAD4 (negative)	NCI-60
HEK293	CABLES (positive)	ATCC
IMR-32	DCC (positive)	ATCC
K562	SMAD2 (positive)	NCI-60
Kidney tissue	Elongin A3 (positive)	Institute of pathology, Tuebingen
NIH/3T3	SMAD4 (positive)	ATCC
U251	PMAIP1 (positive)	NCI-60

III. Methods

3.1 Clinical Samples

Formalin-fixed, paraffin-embedded (FFPE) tumor specimens of 217 SI-NETs (135 patients) were retrieved from the surgical pathology files of the Institutes of Pathology of Tuebingen, Munich, Duesseldorf, and Marburg. Ethical approval was obtained from the local ethics committee at the University Hospital, Tuebingen (469/2010BO2). The collective comprised 128 primary tumors, 73 lymph node metastases, and 16 distant metastases. For 60 patients, primary tumors and matching lymph node metastases were available. Matching triplets of primary tumors, lymph node, and distant metastases as well as matching pairs of primary tumors and distant metastases were available for seven patients, respectively. For one patient lymph node and distant metastasis were available, but no primary tumor.

Nine fresh frozen tumors (five primary tumors, two matching metastases, and two non-matching metastases from the Institutes of Pathology of Munich and Kiel were used for Genome-Wide Human SNP Array 6.0 (Affymetrix, Santa Clara, CA, US). Five of these samples (two primaries and three non-matching metastases and corresponding normal tissue) were further used for exome sequencing (CeGaT, Tuebingen, DE). For western blot analysis up to 21 fresh frozen samples from the Institutes of Pathology of Tuebingen, Bad-Berka, Graz, and Marburg were used.

3.1.1 Staging of neuroendocrine tumors of the ileum

The SI-NET samples were staged following the TNM criteria defined by the AJCC-UICC and grouped into defined UICC-stages (Appendix Table 26). In addition, the patients were grouped into cohorts, depending on the absence/presence of lymph node/distant metastases at time of diagnosis:

Cohort 1: no lymph node or distant metastases at time of diagnosis
Cohort 2: lymph node metastases at time of diagnosis
Cohort 3: lymph node and distant metastases at time of diagnosis

3.2 HE staining

Hematoxylin and eosin (HE) staining of a representative section was carried out using an automated Tissue-Tek® slide stainer (Sakura, Alphen aan den Rijn, NL) and histologically characterized by a pathologist (Prof. Bence Sipos) to determine the tumor areas of interest.

3.3 Tissue Microarray

Eight tissue microarrays (TMAs) were designed using the FFPE samples described in 3.1 Clinical Samples.

The construction of TMAs was performed as described elsewhere [104]. In short, 1 mm sized tissue biopsies were extracted from the paraffin donor blocks and transferred into pre-punched holes as duplicates (TMA 6-8) / triplicates (TMA 11-14) on recipient paraffin blocks with a tissue microarrayer (Beecher Instruments, WI, US) equipped with a TMA booster (Alphelys, Plaisir, France). Grid layouts for the TMAs were designed with the TMA Designer 2 software (Alphelys, Plaisir, France). The recipient blocks were sealed for 10 min at 56°C and 30 min at 4°C. This procedure was repeated twice. The TMA blocks were cut into 3/3.5 µm sections and placed on SuperFrost Plus slides (Langenbrinck, Emmendingen, DE) for immunohistochemical and fluorescence-in-situ-hybridization analyses, respectively.

TMA 6-8 comprised only primary tumors. TMA 6 consisted of cohort 1 tumors, TMA 7 of cohort 2 and TMA 8 of cohort 3 tumors, respectively. TMA 11.1 and 11.2 comprised mostly primary tumors - but also some metastases - of patients with follow up data. TMA 12 included lymph node metastases corresponding to primary tumors of cohort 2 (TMA 7). TMA 13 included lymph node and distant metastases corresponding to primary tumors of cohort 3 (TMA 8). Finally, TMA14 consisted of metastases (and some primary tumors) corresponding to the tumors on the follow up TMAs 11.1 and 11.2.

3.4 DNA Extraction

For the extraction of DNA, fresh frozen and FFPE tissue samples of SI-NET specimens were cut into 8 µm slices using the CM1900 (Leica Biosystems, Nussloch, DE) and the microtome Hyrax M 55 (Zeiss, Esslingen, DE), respectively. Tumor areas were macro dissected manually from the sections with a sterile scalpel (pfm medical, Cologne, DE)

and further processed for DNA extraction. DNA was extracted using the QIAamp DNA Mini Kit or the QIAamp DNA FFPE Tissue Kit (both Qiagen, Hilden, DE) following the manufacturer's instructions. DNA quantification was performed with the NanoDrop ND-2000 spectrophometer (NanoDrop Technologies, Wilmington, US).

3.5 RNA Extraction

Preparations for RNA extraction were the same as for DNA extraction. RNA was extracted manually with the chloroform/phenol extraction method. Therefore, the tumor sections were deparaffined and macro dissected, followed by proteolysis in 1x SDS-Lysis-buffer over-night. The following day, RNA was extracted through chemical precipitation (chloroform/phenol), washed with 70% ethanol and dissolved in DNase/RNase free water. RNA quantification was performed as described above.

3.6 Polymerase chain reaction (PCR)

For the PCR, the reaction mixture (25 µl in total) included 2.5 µl buffer, 0.5 µl dNTPs, 1 µl of each Primer, 0.25 µl of Gold Taq Polymerase, 17.75 µl of DNase/RNase free water, and 2 µl cDNA (100 ng).

The reaction mixtures were initially heated at 95°C for 5 min to activate the polymerase, followed by 40 cycles including a denaturation step at 94°C for 45 s, an annealing step at 53°C for 45 s and an elongation step at 72°C for 45 s. A final elongation step at 72°C for 5 min was added [105].

The PCR products were illustrated by gel electrophoresis and UV irradiation.

After verification of PCR products (right size of the bands and no band in the negative control), the products were purified with magnetic Agencourt AMPure XP Beads (Beckman Coulter, Brea, CA, US). The purified products were eluted in dH_2O und stored at -20°C until further use.

3.7 Sequencing PCR

For the Sequencing PCR, 2 µl DTCS-Mix, 1 µl Primer (forward/reverse) and 7 µl purified PCR product were mixed together (10 µl reaction mixture in total). The DTCS Mix includes a Thermo Sequenase DNA polymerase I, a pyrophosphatase, dNTPS, dye terminators (ddNTPs), and buffer. The sequencing PCR was carried out for 40 cycles

including a denaturation step at 96°C for 20 s, an annealing step at 50°C for 20 s and an elongation step at 60°C for 4 min. Afterwards the PCR products were purified with Agencourt CleanSEQ (Beckman Coulter, Brea, CA, US), eluted in Sample Loading Solution (SLS) and covered with an oil layer.

3.8 Sanger sequencing

Sanger sequencing was performed with a GenomeLab GeXP machine (Beckman Coulter, Brea, CA, US). Thereby, the single DNA fragments with their fluorescence-labelled ddNTPs become separated by gel electrophoresis. The four different ddNTPs emit light of different wavelengths, which is detected by the instrument and shown as different colored peaks by the software.

3.9 cDNA synthesis and quantitative Real-time PCR (qRT-PCR)

Total RNA (1 µg) was used for reverse transcription with the High-Capacity cDNA RT Kit with RNA Inhibitor (Thermo Fisher Scientific, Waltham, MA, US) for mRNA analysis in a total volume of 20 µl.

QRT-PCR was carried out on 96-well reaction plates in a LightCycler 480 II (Roche, Basel, CH). The reaction mixture included 10 µl of Real-time SYBR Green PCR master mix, 1 µl of each Primer (forward and reverse), 7 µl of DNase/RNase free water and 1 µl of diluted reverse transcription product (20 ng). Each reaction was carried out in triplicates. A negative (water) control was included.

The reaction mixtures were initially heated at 95°C for 15 min to activate the polymerase, followed by 40 cycles including a denaturation step at 94°C for 15 s, an annealing step at 55°C for 30 s, and an elongation step at 70°C for 30 s. A melting curve analysis was carried out with temperatures increasing from 60 to 97°C at 0.11°C interval after the Real-time PCR to assess the specificity of the amplified PCR product [105].

3.10 Immunohistochemistry (IHC)

Immunohistochemical staining was performed on 3 µm thick FFPE-sections mounted on Superfrost® Plus Slides (R. Langenbrinck, Emmendingen, DE).

3.10.1 IHC staining

Immunohistochemical staining of Ki-67 (MIB-1) and pHH3 was performed to characterize the SI-NET samples regarding their proliferative and mitotic status. It has been shown that phosphorylation of histone H3 is a reliable marker for mitotic activity. To verify expression of neuroendocrine markers, the tumors were stained against Somatostatin receptor 2 (SSTR2), synaptophysin, as well as the intestine specific transcription factor CDX2. Since SI-NETs are mostly functional tumors which secrete hormones, the samples were also stained for serotonin.

Immunohistochemical staining of pHH3, Ki-67 (MIB-1), serotonin, synaptophysin, SSTR2, and CDX2 was carried out with the iView DAB Detection Kit on the Ventana BenchMark system (Ventana Medical Systems, Tucson, AZ, US). The antibodies are listed in Table 8 and 9. Cell conditioning solution 1 (CC1) pre-treatment (1 hour) of the tissues was applied for all primary antibodies, except serotonin. For synaptophysin, SSTR2, and pHH3 a Biotin block was applied prior to the staining procedure. Incubation of primary antibodies took place at 37°C for 32 min, incubation of secondary antibodies at 37°C for 8 min. The slides were counterstained with Hematoxylin solution.

In order to determine the involvement of the PI3K/AKT/mTOR pathway in our SI-NET samples, the following proteins were analyzed by immunohistochemical staining:

AKT2, phospho-AKT1 (Thr308), phospho-mTOR (Ser2448), phospho-S6 Ribosomal Protein (Ser240/244), and phospho-4E-BP1 (Ser65/Thr70). The IHC staining against these (phospho-) proteins was performed with the respective antibodies (Table 8) with the ZytoChemPlus Horseradish-peroxidase (HRP) Polymer Kit (Zytomed, Berlin, DE) and the DAB Substrate Kit (Zytomed, Berlin, DE) on the Tecan Genesis RSP 100 system (Tecan Trading, CH). Slides were deparaffined and boiled for 5 min in TEC buffer pH9 (p-AKT, p-4E-BP1) or citrate buffer pH6 (AKT2, p-mTOR, p-S6) for heat-induced antigen-retrieval. The antibodies were diluted in Antibody Diluent (Zytomed, Berlin, DE). The slides were incubated at 4°C over-night. The following day the slides were incubated with the secondary antibody (Table 9) and then with the HRP Polymer for 30 min each at room temperature (RT). The HRP Polymer consists of several molecules of secondary antibody which are covalently attached to several molecules

horseradish peroxidase. After a washing step the slides were incubated with a substrate/chromogen solution two times for 5 min each (16 µl chromogen (DAB) + 200 µl Substrate Buffer per slide). The enzymatic reaction forms a brown staining at the site where the primary antibody has bound. The tissue slides were counterstained with Papanicolaou solution (Merck, Darmstadt, DE) and dehydrated in an ascending ethanol sequence. Finally, the slides were sealed with cover slips for microscopy.

3.10.2 IHC evaluation

pHH3 and Ki-67 (MIB-1) staining were analyzed with the Tissue Studio XD 2.3.0 software (Definiens, Munich, DE). Therefore, whole tumor samples as well as three hotspots (squares à 250 μm^2) were analyzed per slide. The parameter "Nucleus Classification" was chosen to differentiate between low and medium staining as well as between medium and high staining. The results were imported into Excel (Microsoft, Redmond, US). Nuclei, which were called "medium" and "high" by the software were determined positive and therefore summed up and divided through all detected nuclei. The results represent the percentage of pHH3/Ki-67 positive cells in the respective tumor sample/hotspot.

AKT2, p-AKT, as well as p-mTOR, p-4E-BP1, and p-S6 immunohistochemical staining was evaluated using the immunoreactive score (IRS) resulting in staining values ranging between 0 and 12 (Table 17).

Table 17: Immunoreactive Score (IRS)

Staining intensity		# of positive cells		IRS	
0	no reaction	0	no	0-2	negative
1	weak reaction	1	less than 10%	3-4	weakly positive
2	moderate reaction	2	between 10 and 50%	6-8	moderately positive
3	strong reaction	3	between 50 and 80%	9-12	highly positive
		4	more than 80%		

Synaptophysin and serotonin were scored 0 for negative staining, 1 for weak staining, 2 for moderate staining, and 3 for strong staining. CDX2 expression was valued with + for

positive staining and - for negative staining. Finally, SSTR2 staining was evaluated with 0 for negative staining, 1 for partial staining, 2 for incomplete membrane staining, and 3 for >10% of the cells showing strong membranous staining.

3.11 Fluorescence-in-situ-hybridization (FISH)

3.11.1 FISH processing

For all FISH analyses, deparaffined slides were heated in sodium citrate buffer and proteins were enzymatically digested with pepsin (Sigma-Aldrich, St. Louis, MO, US).

Chr. 18 FISH

To determine how many samples of our cohort exhibit loss of chromosome 18, a Chr18 centromere FISH probe was used (Table 10).

For Chr18 centromere FISH, whole tissue slides as well as TMAs were used. With a HE stained slide of the same sample the tumor area was determined and the FISH slide was marked on the back side with a diamond pen (~25 mm^2). The slides were denatured for 10 min in 70% formamide/2x SSC at 72°C. The CEP 18 FISH probe was diluted in CEP hybridization buffer (# 07J36-001, Abbott Molecular Inc., Abbott Park, IL, US) and distilled water in a 1:2:7 ratio (probe:dH_2O:CEP hybridization buffer) and the mix was denatured for 5 min at 72°C. The hybridization was carried out at 42°C for at least 15 h. All hybridizations were carried out with a ThermoBrite hybridizer (Abbott Molecular Inc., Abbott Park, IL, US). The following day the slides were washed in 2x SSC Buffer as well as in 2x SSC with 0.3% NP-40 at 72°C for 5 min to wash away non-specific hybrids which are less stable than specific bindings. After slides were air-dried in darkness, they were counterstained and mounted with ProLong® Gold Antifade mountant with DAPI (Life Technologies, Waltham, MA, US) and a cover slip was placed over the target area.

PI3K/AKT/mTOR-pathway FISH

For the evaluation of amplifications in the PI3K/AKT/mTOR-pathway, commercial probes for *PIK3CD*, *AKT1*, *AKT2*, *PDGFRα*, and *PDGFRβ*, and a custom made probe for *mTOR* were used (see Table 10). The FISH analysis for these six genes was carried out on the eight TMAs described in 3.3 Tissue Microarray.

AKT1/2, PDGFRα/β FISH

The probes for *AKT1*/Cen14q, *AKT2*/Cen19p, *PDGFRα*/Cen4p, and *PDGFRβ* (split probe) were ready to use (all Abnova, Taipei, RC). The slides and probes were co-denatured for 5 min at 75°C and the hybridization was carried out at 37°C for 15 h at least. The post-hybridization wash and the DAPI counterstaining were carried out as described above.

PIK3CD FISH

The *PIK3CD* FISH (Empire Genomics, Buffalo, NY, US) was used together with the Cen-1 probe (Metasystems, Altlussheim, DE). The hybridization mix included 2 µl PIK3CD probe, 2 µl Cen-1 probe, and 10 µl hybridization buffer. The mix and the slides were co-denatured at 83°C for 3 min. Hybridization, post-hybridization wash, and the DAPI counterstaining took place as described above.

mTOR FISH

The *mTOR* FISH probe was a customized probe which was developed by CeGaT (Tuebingen, DE) in cooperation with Prof. Dr. Perner (Institute of Pathology, University Hospital Bonn).

The probe mix for the *mTOR* detection included 2 µl *mTOR* probe, 2 µl CEP1 probe, 1 µl Cot-1 (Thermo Fisher Scientific, Waltham, MA, US), and 10µl CEP hybridization buffer. Cot-1 is used to suppress non-specific hybridizations to probes derived from BAC clones, resulting in improved signal-to-background-ratio. The slides and the probe were co-denatured at 84°C for 6 min. The hybridization was carried out as described above.

Post-hybridization wash was performed with 2x SSC for 6 min at 75°C and 0.5x SSC at RT. Afterwards the slides were blocked with CAS block (Thermo Fisher Scientific, Waltham, MA, US) including 10% normal goat serum (Cell Signaling, Danvers, MA, US). The secondary antibody Streptavidin Alexa Fluor 594 (Thermo Fisher Scientific, Waltham, MA, US) (Table 9) was used for the detection of *mTOR* (Biotin labelled). It was diluted 1:1000 in CAS block before it was applied to the slides. The detection took place for 1 h at RT in a humidified chamber. After another washing step, the nuclei were counterstained with DAPI.

3.11.2 FISH evaluation

The evaluation of the FISH assays was achieved with a Zeiss Axioskop fluorescent microscope (Zeiss, Jena, DE).

Chr. 18 FISH

To determine whether an SI-NET sample has lost one Chr18 at least 100 cells were counted. If >80% cells showed two signals, the sample was considered to have a normal set of two Chr18, and vice versa (if >80% of the cells showed only one signal, the sample was considered to have a loss of Chr18). If the count of one (two) signal(s) was between 20% and 80% of cells, the sample was considered to have a mosaic pattern of Chr18.

PI3K/AKT/mTOR-pathway FISH

The number of specific signals per cell as well as the number of the respective centromeric probe was counted. At least 30 cells per tumor were counted and a gene-reference-ratio was established. The ratio and the average number of gene and centromere specific signals were taken into account for statistical analyses. The gaps between the target specific and the centromere probe were of different size for each gene.

PDGFRα (69 kb) is located on 4q12, whereas the chromosome reference probe is located on 4p13, leaving a gap of 9,200 kb. *AKT1* (26 kb) is located on 14q32.33, the chromosome reference probe on 14q11.2, resulting in a gap of 71,800 kb. *AKT2* (55kb) is located on 19q13.13, the chromosome reference probe on 19p13.11, resulting in a gap of 17,800 kb. Since a split probe was used for *PDGFRβ* (42 kb, located on 5q33.1) no gap was present between the two probes. *mTOR* (155 kb) and *PIK3CD* (77 kb) are located both on 1p36.2. The centromere enumeration probe, which was used for Chr1, was located on the long arm of Chr1, at position 1q12.

Gene amplifications are defined as an increase in the copy number of a specific chromosomal region, that is commonly linked to overexpression of the respective gene [106]. Polysomy, however, describes the condition when extra copies of a whole chromosome are present. The centromere probes, included in every gene specific FISH analysis, were used as reference for the presence of polysomy. These basic definitions in mind, we grouped our samples into the following three categories:

Samples were defined as “amplified”, when the centromere signal count was ≤72 and target/centromere signal ratio >1.2, counting 30 cells. “Amplified + polysomy” refers to samples with a centromere signal count >72 and target/centromere signal ratio >1.2. Samples defined as “polysomy” had a target signal count >72, but a target/centromere signal ratio ≤1.2.

The ratio of 1.2 for the amplification threshold was based on evaluation of target/centromere signal counts in normal neuroendocrine cells, since this ratio was significantly different from the signal ratios in the non-tumorigenic cells.

For *PDGFRβ*, only one parameter was available, resulting in the conditions “not amplified” (target/reference signal ≤72) and “amplified” (target/reference signal >72) for statistical analysis.

3.12 Statistical analysis

Pearson’s Chi-square test was applied (SPSS, IBM, Armonk, NY, US) for FISH and IHC results and Kaplan-Meier estimation for survival were performed with SPSS (IBM SPSS Statistics for Windows, Version 22.0). For multivariate analyses Bonferroni correction was applied.

For statistical analysis of association between FISH results and immunohistochemical stainings, two cut offs were chosen for IHC: a) no/weak staining (Remmele score 0-3) against moderate/strong staining (Remmele score 4-12) and b) dichotomic distribution (0-6 vs. 7-12).

3.13 Protein extraction

Frozen tissues of SI-NET samples were cut into 15x10 µm slices for protein isolation. 100-150 µl RIPA-buffer (charged with protease inhibitor (Roche, Basel, CH)) was added to the tissues. Tissues were homogenized by pipetting up and down on ice. After centrifugation at 4°C and 13.000 rpm the supernatants containing the protein lysates were used for further processing. BCA reaction was carried out to determine protein concentration using Bovine Serum Albumin (BSA) Standards (Thermo Fisher Scientific, Waltham, MA, USA). Absorption was measured at 560 nm with the Microplate Reader (Biorad, Hercules, CA, US).

3.14 Western blot

20 µg protein were charged with 1 Vol of 2x Laemmli Sample Buffer (Biorad, Hercules, CA, US) and 1/10 Volume of β-mercaptoethanol (Merck, Darmstadt, DE) and denatured at 95°C for 10 min.

For western blotting the protein lysates were separated on 7.5%, 10% or 12% SDS gels (Biorad, Hercules, CA, US), depending on the predicted protein size, at 200 V. Proteins were transferred to a PVDF membrane at 100 V for 1 h. Membranes were blocked with 5% Skim Milk (BD, Franklin Lakes, NJ, US) diluted in 1x TBS/Tween 0.05% buffer for 1 h at RT. After an over-night incubation at 4°C with the primary antibody (SMAD2 (86F7) Rabbit mAb (1:1000), #3122, Cell Signaling, MA, US; SMAD4 (B-8) Mouse mAb (1:100), #sc-7966, Santa Cruz, CA, US; PMAIP1 Rabbit pAb (1:250), #HPA051063, Sigma, MO, US; Anti-IK3-1 / CABLES1 Antibody (Lys588), Rabbit pAb (1:1000), #LS-C176874, Biozol, DE; Elongin A3 (S-16) Rabbit pAB (1:200), #sc-84811, Santa Cruz, CA, US; DCC, Rabbit pAb (1:500), #orb10519, Biorbyt, Cambridge, UK; 2. DCC (A-20), Goat pAb (1:100), #sc-6535, Santa Cruz, CA, USA with Blocking Peptide sc-6535 P) the membranes were washed with 1x TBS/Tween 0.05% buffer for 3x 10 min and incubated with the secondary antibody at RT for 1 h (Goat anti-mouse (1:3000) IgG (H+L) HRP conjugated, #G-21040 or Goat anti-rabbit (1:3000) IgG (H+L) HRP conjugated, #G-21234, both from Life Technologies, Carlsbad, CA, US). All antibodies are listed in Table 8 and 9. The membranes were washed for 3x 10 min and Immobilon Western Chemiluminescent HRP Substrate (Merck Millipore, Darmstadt, DE) was added. Darkroom development techniques were used for image acquiring.

To ensure that the gels were properly loaded with equal amounts of protein, the membranes were stripped with Stripping Buffer (Thermo Fisher Scientific, Waltham MA, US), washed, blocked, and incubated with an antibody against β-Actin (clone AC-15 (1:40000), # A5441, Sigma-Aldrich, St.-Louis, MO, US). The blotting procedure was carried out as explained above.

As positive controls for western blot analysis K562 and NIH/3T3 cell line for SMAD2 and SMAD4 were used, respectively. The human pancreatic carcinoma cell line BxPC-3 lacking expression of SMAD4 [44] was used as a negative control in SMAD4 western

blots. As positive controls for western blot analysis of Elongin A3, PMAIP1, and CABLES kidney tissue, U-251 cell line, and HEK293 cell line were used, respectively. The neuroblastoma cell line IMR-32 served as positive control for DCC western blot. The cell lines K562, BxPC-3, and U251 were retrieved from the NCI-60 cell line panel. NIH/3T3, HEK293, and IMR-32 were bought from ATCC (Middlesex, UK).

Due to difficulties in distinguishing the bands between 180 and 250 kDa of the second DCC western blot, a competition with the matching peptide was performed.

Since the β-Actin expression of the samples varied slightly between the samples, a semi-quantitative analysis of the western blot results was done. Therefore, the western blot pictures were loaded into Adobe Photoshop (Mountain View, CA, USA), inverted and analyzed with the histogram setting. The background noise was subtracted from the protein bands. Then, the specific bands of the tumor suppressor proteins were normalized to the respective β-Actin band, resulting in a percentage value. A value <20% was determined as lost/reduced expression of the protein.

3.15 Cell culture

For western blot analyses different cell lines were used as positive/negative controls (3.14 Western blot). NIH/3T3 and HEK293 were maintained in DMEM plus 10% FCS and 1% Penicillin/Streptomycin. IMR-32, K562, BxPC-3, and U251 were maintained in RPMI plus 10% FCS and 1% Penicillin/Streptomycin. All cell lines were cultured at 37°C and 5% CO_2. For protein extraction cells were trypsinized, washed in 1x PBS, and pelleted through centrifugation. Protein extraction was performed as explained in 3.12 Protein extraction.

3.16 Exome sequencing & SNV calling

Exome sequencing of five SI-NET samples (tumor content between 70% and 90%) and the corresponding normal tissues was performed by CeGaT (Tuebingen, DE) using the SOLiD 5500xl machine (Thermo Fisher Scientific, Waltham, MA, US). For the sequencing performance DNA was enriched with the Agilent SureSelect ExomeKit v.4. Mapping was done by LifeScope v2.5.1 (Thermo Fisher Scientific, Waltham, MA, US). SNV/InDel calling was performed with diBayes in LifeScope v2.5.1 (Thermo Fisher Scientific, Waltham, MA, US) as well as with samtools mpileup 0.1.18 with bcftools and

vcfutils.pl [107]. Annotation was achieved with dbSNP137, ESP6500 (Exome Variant Server), Ensembl v69, and the inhouse database of CeGaT. The comparison between tumor and normal sample output was done with the following settings: in tumor samples, SNVs with a coverage >10 and a minimal novel allele frequency of 1% were considered for further analysis, when the SNVs in the normal tissue samples (coverage >20) showed a maximal novel allele frequency of 1%. Minimum distance between the novel allele frequencies was set to 0.3 (min. 3x normal allele frequency < tumor frequency). Lists of “real” somatic mutations were achieved by filtering SNVs and InDels according to the following four steps.

1) SNVs with bad quality
2) SNV function (non-synonymous, (essential) splice site, stop gain/loss)
3) SNVs and InDels with rs-number (dbSNP database)
4) SNVs and InDels against SNVs and InDels found in the corresponding normal tissue

3.17 Validation by Sanger sequencing

High value somatic SNVs (achieved by the steps laid out above) were validated by Sanger sequencing with the GeXP – Genetic Analysis System (Beckman Coulter, Brea, CA, US).

3.18 Oligonucleotides

High value somatic SNVs (achieved by the steps laid out above) were validated by Sanger sequencing. PCR primers were designed using the program Primer3Plus (http://primer3plus.com/cgi-bin/dev/primer3plus.cgi) generating amplicons between 110 bp and 250 bp.

Two targets [*PML* (Chr15) and *NFATC1* (Chr18)] were further analyzed (sequencing of all functional regions) in a set of 30 SI-NETs (including 15 primaries, eight matching distant metastases and seven non-matching lymph node metastases). (The sequencing of *NFATC1* was subject of the doctoral thesis of Dr. Laura Stoß).

For the potential tumor suppressor genes *DCC*, *PMAIP1*, *TCEB3C*, and *CABLES* primers were designed which were used for qRT-PCR. The specificity of all primers was tested with Primer-BLAST (http://www.ncbi.nlm.nih.gov/tools/primer-blast/). All primers are listed in tables 11-13.

3.19 SNP array & Data analysis

The SNP array analysis (Atlas Biolabs, Berlin, DE) was performed to identify chromosomal aberrations in SI-NETs. The data was analyzed and interpreted with the Chromosome Analysis Suite (Affymetrix, Santa Clara, CA, US). To evaluate additional smaller losses, the parameter “copy number marker count” was set to 10 and the “sizes” to 100, 50, and 40kb, respectively. Nine fresh frozen tissues (five primary tumors and four metastases of SI-NETs) from Kiel and Munich were used for SNP Array analysis (named Tu1, Tu1 Met, Tu2, Tu3, Tu4, Tu5 Met, Tu6 Met, Tu7, and Tu7 Met).

3.20 Liquid chromatography – Mass spectrometry (LC-MS)

All steps for the Liquid chromatography – Mass spectrometry analysis were carried out by the Clinical Proteomics workgroup of Jun.-Prof. Barbara Sitek (Medical Proteom-Center, Bochum, DE).

Sample preparation

Cell lysis was performed in lysis buffer (7 M urea, 2 M thio-urea, 0.1 % SDS, 30 mM Tris-HCl, pH 8.5) by sonication on ice for 10 min. Protein concentration was carried out using Bradford assay. Subsequently, 40 µg of cell lysate were loaded on ProGel Tris Glycin 18%, 1 mm gel two times. Samples were allowed to run for 1 h. After Coomassie staining, three gel bands were cut between 150-250 kDa and in-gel digestion was performed with trypsin (37°C, 16 h). The resulting tryptic peptides were extracted from the gel by sonication in 50% acetonitrile in 0.1% trifluoroacetic acid (TFA) two times. Fractions of the same molecular weight were pooled together and dried in vacuum. Peptides were reconstituted in 40 µl 0.1% TFA.

LC-MS/MS analysis

LC-MS analysis was performed on Ultimate 3000 RSLCnano system online coupled to an Orbitrap Elite instrument (Thermo Fisher Scientific, Waltham, MA, US). 15 µl of the reconstituted samples were loaded onto a trap column and the peptides were then separated on an analytical C18 column using a 90 min gradient from 5–40% solvent B at a flow rate of 300 nl/min (solvent A: 0.1% formic acid, solvent B: 0.1% formic acid 84% acetonitrile).

Protein Identification

Thermo Scientific Proteome Discoverer™ version 1.4 was used to search MS/MS spectra against UniProtKB/Swiss-Prot human database using Mascot® search engine. Mascot parameters were set as: Tryptic digestion with up to one missed cleavage, precursor ion mass tolerance of 5 ppm and fragment ion mass tolerance of 0.4 D with Oxidation (M) and prominamide (C) as dynamic modification. To estimate the confidence of peptide identifications a decoy database search was performed. Peptides with false discovery rate (FDR) > 1% were discarded.

IV. Results - General characterization

Clinicopathological data of the patients

Clinical characteristics

The clinical characteristics of the patients are summarized in Appendix Table 26. For the 135 patients, whose tissues were used for TMA design, IHC, FISH, qRT-PCR, and Sanger sequencing, the mean age at the time point of diagnosis was 60.5 (range 20-87). 51 were female, 50 were male, and for 32 patients the sex was not available. The patients' samples were classified according to TNM stage and UICC stage. The UICC classification is summarized in Table 18.

Table 18: Distribution of UICC stages in the patients' cohort
TMA: Tissue micro array, FFPE: formalin-fixed, paraffin embedded, NA: not available

Sample group	Stage I	Stage IIA	Stage IIB	Stage IIIA	Stage IIIB	Stage IV	NA
FFPE	9	6	8	1	52	46	4
Cryo	3	1	1	0	11	8	1

The grading was determined by Ki-67 staining, which was evaluated with the Hotspot method by using the Tissue Studio software (Definiens, Munich, DE). Most of the samples were G1 tumors, which is in line with the literature concerning ileal NETs; few were G2. Additionally, pHH3 was analyzed, which ranged between <0.00 and 2.14, indicating that the mitotic activity is really low in these tumors (Appendix Table 26).

Concerning the cryo samples used for western blot and SNP analysis, as well as sequencing, the mean age of the patients was 61.2 and ranged between 26 and 85 (for three patients the age was not available). 15 patients were female, seven were male, and for three the sex was not available. Again, UICC classification is shown in Table 18.

Expression of immunohistochemical markers

Seven potential tumor samples were excluded before evaluating the immunohistochemical results of the neuroendocrine tumor markers (Appendix Table 27, indicated in grey), due to lacking tumor tissue or detachment of the tissue from the

slide. 95% (198/208) of the tumor samples expressed synaptophysin (for 2/210 samples the staining was not applicable). Hereof, 87 samples exhibited strong, 78 moderate, and 33 weak expression. 5% (10/208) showed no expression of synaptophysin. The samples with no synaptophysin expression are rare examples of tumors, for which the diagnosis of a SI-NET is confirmed by the immunohistochemical marker CgA alone.

The nuclear transcription factor CDX2 was expressed in 91% (181/198) of SI-NETs (for 12 samples no evaluation was feasible). 9% (18/198) did not express CDX2.

Somatostatin receptor 2 (SSTR 2) was expressed by 76% (155/203) of SI-NETs (for seven samples the analysis was not feasible). Hereof, 100 samples showed strong, 26 moderate, and 29 weak expression. 24% (48/203) showed no expression of SSTR2.

86% (179/208) of the tumors were positively stained for serotonin, indicating that the majority of the SI-NET cohort comprises functional tumors, as expected (for two samples the staining was not applicable). Only 17% (36/208) were negative for serotonin.

IV. Results – Genetic characterization

Parts of the results described on page 71-91 are already published in [50].

Chr18 is commonly lost in SI-NETs

Focusing on this characteristic lesion, FISH analysis with a Chr18 centromeric enumeration probe was performed in 121 SI-NET samples. The analysis revealed that 64% of the tumor samples (77/121) had suffered loss of one Chr18 (Appendix Table 26). 12% showed mosaicism regarding their Chr18 status (14/121); 18% exhibited the normal count of two copies of Chr18 (22/121). In 7%, it was not possible to determine the Chr18 status. In the three cohorts, 57% of cohort 1, 65% of cohort 2, and 65% of cohort 3 showed a loss of Chr18.

SNP Array analysis

Nine SI-NET samples (including five primary tumors and four metastases with two matching primary-metastasis pairs) were analyzed by SNP array 6.0 technology (Affymetrix, Santa Clara, CA, US). One sample (Tu6 Met) was of bad quality and therefore excluded from further analysis. In Table 19 the results of the remaining eight samples are shown.

Table 19: SNP array analysis of five primary tumors and three metastases (two matching)
Chr: Chromosome, CN: Copy number, -: no gain/loss

Chromosome	Tu1	Tu1 Met	Tu2	Tu3	Tu4	Tu5 Met	Tu7	Tu7 Met
Chr4	CN3	CN3	CN3	-	-	-	CN3	CN3
Chr5	CN3	CN3	-	-	-	-	CN3	CN3
Chr9	-	-	CN1: p11.2-q13	-	-	-	-	-
Chr10	CN3	CN3	-	-	-	-	-	-
Chr12	CN1: p.13.31-p11.1	CN1: p.13.31-q11	-	-	-	-	-	-
Chr14	-	-	CN3	-	-	-	-	-
Chr17	CN3: q21.32-q25.3	CN3: q21.32-q25.3	-	-	-	-	-	-
Chr18	CN1	CN1	-	Mosaic	CN1	CN1	CN1	CN1
Chr20	CN3	CN3	CN3	-	-	-	CN3	CN3

Tu1 and its matching metastasis showed copy number gain of Chr4, 5, 10, 20, and part of the long arm of Chr17. Both samples depicted loss of Chr18 and partial loss of

Chr12. Remarkably, in the metastasis the partial loss of Chr12 comprised both the short and the long arm of the chromosome, whereas in the primary tumor only the short arm was affected. Tu7 and the matching metastasis also showed CN gain of Chr4, 5, and 20 and loss of Chr18. Tu2 shared the CN gain of Chr4 and 20, but depicted additionally gain of Chr14. In this tumor a partial loss of Chr9 was present, which was not found in any of the other tumors. Tu2 was the only tumor with a normal count of two for Chr18. Finally, Tu4 and Tu5 Met depicted loss of Chr18 as sole chromosomal aberration. In Tu3 a mosaic pattern regarding Chr18 was present without additional alterations.

Exome sequencing

Exome sequencing was performed with five different SI-NETs and corresponding normal tissue samples. Statistics concerning the mean coverage on target and underrepresented bases (total and in percent) are shown in Appendix Table 28.

Appendix Table 29 gives an overview over the alterations detected by exome sequencing, but were not included in the further analysis (e.g. intergenic, intronic, synonymous, etc.).

Only stop-gained and non-synonymous variants were included in the further analysis and evaluation. The following table (Table 20) shows the workflow and the type (transition vs. transversion) of substitutions. The filtering for adjacent SNVs was necessary, because the detection of these artifacts is a known problem of the SOLiD 5500xl machine.

Table 20: Stop-gained and non-synonymous somatic variants found by exome sequencing of five SI-NET samples and corresponding normal tissue
w/o: without, rs-number: dbSNP database entry

Sample	All SNVs (w/o rs-number)	Coverage ≥20	Filtering for adjacent SNVs	Transitions (A/G – C/T)	Transversions (A/C, A/T, G/C, G/T)
1	118 (95)	81 (67)	63 (49)	27	36
2	100 (76)	68 (53)	49 (35)	16	33
3	129 (91)	85 (66)	76 (57)	26	50
4	122 (94)	83 (66)	68 (51)	22	46
5	55 (36)	54 (35)	38 (23)	17	21

Validation by Sanger sequencing

The selection of target genes for validation by Sanger sequencing was achieved by extensive review of the literature concerning cancer context and pathways. Additionally, the SNVs had to be determined “deleterious” or “damaging” by the protein variation prediction programs PROVEAN and SIFT (http://provean.jcvi.org/index.php), respectively plus “probably/possibly damaging” by Polyphen-2, a tool for annotating coding non-synonymous SNVs (http://genetics.bwh.harvard.edu/pph2/bgi.shtml). In contrast to the other prediction tools, PROVEAN can also predict impacts of InDels.

PolyPhen-2 predicts the functional significance of an allele substitution by Naïve Bayes classifier trained using supervised machine-learning. It consists of two dataset pairs. The first pair is called HumDiv and includes all damaging alleles with known effects on the molecular function causing human Mendelian diseases, present in the UniProtKB database, together with differences between human proteins, which are assumed to be non-damaging. The second pair, HumVar, consists of all human disease-causing mutations from UniProtKB, together with common human ns-SNVs (MAF>1%) without known involvement in disease and which are therefore treated as non-damaging (http://genetics.bwh.harvard.edu/pph2/dokuwiki/overview).

All primers for validation/falsification of NGS data were designed using the program Primer3Plus (http://primer3plus.com/cgi-bin/dev/primer3plus.cgi). The list of primers is shown in Table 11-13. (Some primers had an additional gene-unspecific tail, called “M13”, attached to the gene-specific sequence for easing of the sequencing PCR.)

Firstly, the focus lay on variations which were found in more than one patient. This basic approach was soon to be discarded, because Sanger sequencing revealed that none of these “common” alterations were “true” mutations, but artifacts (Table 21).

Table 21: Sanger validation of absence of mutations
Chr: chromosome, Ref: reference base, Mut: mutated base, Aa: amino acid

Chr	Position	Type	Ref	Mut	Aa1	Aa2	Aa pos.	Gene	Sample	PROVEAN/SIFT	PolyPhen-2 (HumDiv/HumVar)
Chr1	11206838	SNV	G	C	D	E	1527	*MTOR*	3	neutral/tolerated	probably damaging
Chr1	153749658	SNV	C	G	S	C	380	*SLC27A3*	5	deleterious/damaging	probably damaging
Chr3	37512566	SNV	T	G	F	C	85	*ITGA9*	1,2,3,4	deleterious/damaging	probably damaging
Chr3	122180112	SNV	A	C	F	V	131	*KPNA1*	1,2,3,4	deleterious/damaging	probably/possibly damaging
Chr3	122180113	SNV	C	A	R	S	130	*KPNA1*	1,2,3,4	deleterious/damaging	probably/possibly damaging
Chr3	50222175	SNV	C	A	R	S	462	*SEMA3F*	1,2,3,4	neutral/tolerated	benign
Chr5	16877777	SNV	G	C	P	A	21	*MYO10*	4	deleterious/tolerated	possibly damaging
Chr7	107393921	SNV	C	G	R	G	83	*CBLL1*	1,2,3,4	neutral/damaging	probably damaging
Chr8	95392469	SNV	C	A	L	F	717	*RAD54B*	5	deleterious/damaging	probably damaging
Chr10	29843781	SNV	T	C	T	A	31	*SVIL*	1	neutral/tolerated	probably damaging
Chr12	50834274	SNV	A	T	E	V	237	*LARP4*	5	deleterious/damaging	probably damaging
Chr12	56088728	SNV	A	C	F	C	676	*ITGA7*	1,2,3,4	deleterious/damaging	probably damaging
Chr16	14026096	SNV	T	A	S	R	352	*ERCC4*	5	neutral/damaging	benign
Chr18	39576604	SNV	T	A	. (splice site)	.	298	*PIK3C3*	5	neutral/tolerated	-
Chr18	39576605	SNV	A	T	I	F	299	*PIK3C3*	5	deleterious/damaging	probably damaging
Chr18	21407328	SNV	C	G	A	G	907	*LAMA3*	1,2,3,4	neutral/tolerated	benign
Chr19	2853229	SNV	C	T	T	I	389	*ZNF555*	1	deleterious/tolerated	benign

Chr22	22843692	SNV	G	T	P	H	11	*ZNF280B*	1	neutral/damaging	benign
ChrX	105450788	SNV	G	A	V	M	455	*MUM1L1*	1	neutral/tolerated	probably damaging
ChrX	142596781	SNV	T	G	N	H	97	*SPANXN3*	1	neutral/damaging	possibly damaging/benign
ChrX	153596042	SNV	C	T	M	I	229	*FLNA*	1	deleterious/damaging	probably damaging
ChrX	153596044	SNV	T	C	M	V	229	*FLNA*	1	deleterious/damaging	probably damaging

Next, the focus lay on mutations in genes located on Chr18. Three somatic mutations in Chr18-associated genes could be identified and verified by Sanger sequencing (Table 22). The SNVs in *CABYR* and *NFATC1* were found in one patient (Tu5) whereas the deletion in *PIEZO2* was found in another patient (Tu3).

NFATC1 had a mutational count of 66% in the exome sequencing of the respective tumor. The SNV in *NFATC1*, which results in an amino acid change from arginine to cysteine at position 552 (p.R552C, c.1720G>A), was predicted to be deleterious/damaging (PROVEAN/SIFT) and probably damaging (PolyPhen-2). The database COSMIC (Catalogue of Somatic Mutations) revealed p.R552C not to be described in any tumor type. However, this SNV could be a unique feature of SI-NETs.

The mutation in *CABYR* (p.I318V, c.1104T>C) showed a allele frequency of 46% in the tumor sample. This SNV was predicted to have no damaging effect on protein structure/function (neutral/tolerated/benign). Isoleucine and valine are both essential amino acids with hydrophobic side chains. The similar chemical features reduce the possibility, that the substitution has a negative impact on the protein function. This prediction is in line with the finding that this mutation is not listed in the COSMIC database.

The deletion of three bases in *PIEZO2* (p.E2727del, c.8181_8183del) was present in nearly 19% of the tumor sample. Prediction with the program PROVEAN revealed a deleterious effect on protein structure/function, but since the deletion of three bases does not result in a frameshift the protein function will probably be preserved nonetheless. This mutation is also not reported in COSMIC. Additionally, no distinct protein features, such as phosphorylation/acetylation/etc. sites, are described for this amino acid position and the mutation is positioned at the very end of the gene, indicating that the damaging impact on the whole protein is probably small.

The remaining three SI-NETs did not show any SNVs or InDels in Chr18-related genes.

Thereafter, mutations affecting Chr18 independent genes with relation to tumor development and/or progression and classification as “damaging” were investigated by

Sanger sequencing. Table 21 (falsified SNVs) and Table 22 (validated SNVs) include all genes/mutations which were subject of this approach.

Table 22: Sanger-validated somatic mutations
Chr: chromosome, Ref: reference, Mut: mutated base, Aa: amino acid, *germ line

Chr	Position	Type	Ref	Mut	Aa1	Aa2	Aa pos.	Gene	Sample	PROVEAN/SIFT	PolyPhen-2 (HumDiv/HumVar)
Chr1	22056254	SNV	T	C	M	V	415	*USP48*	5	deleterious/damaging	probably damaging
Chr1	156228800	SNV	C	T	R	Q	813	*SMG5*	1	neutral/tolerated	benign
Chr1	181680146	SNV	G	A	R	Q	371	*CACNA1E*	5	deleterious/damaging	probably damaging
Chr3	14803089	SNV	T	C	M	T	821	*C3orf20*	1	deleterious/damaging	benign
Chr3	63437756	SNV	T	A	F	Y	11	*SYNPR*	4	deleterious/NA	-
Chr3	123071419	SNV	T	G	N	H	382	*ADCY5*	4	deleterious/damaging	probably damaging
Chr3	186509587	SNV	G	A	T	I	243	*RFC4*	2	deleterious/damaging	probably damaging
Chr5	70849070	SNV	G	A	D	N	2375	*BDP1*	3	neutral/tolerated	benign
Chr6	41048582	SNV	G	T	Q	H	36	*NFYA*	1	neutral/damaging	possibly damaging
Chr7	70255539	SNV	G	T	D	Y	1113	*AUTS2*	5	deleterious/damaging	probably damaging
Chr7	99250323	SNV	A	G	V	A	369	*CYP3A5*	1	deleterious/tolerated	benign
Chr8	53558307	SNV	A	T	N	K	1314	*RB1CC1**	5	neutral/tolerated	probably damaging
Chr9	100895449	SNV	C	T	M	I	173	*CORO2A*	1	neutral/tolerated	benign
Chr9	113169164	SNV	C	T	D	N	2906	*SVEP1*	5	neutral/tolerated	possibly damaging
Chr11	56020625	SNV	C	T	P	L	317	*OR5T3*	1	deleterious/damaging	probably damaging
Chr11	60183406	SNV	C	T	S	F	322	*MS4A14*	4	neutral/damaging	probably/possibly damaging
Chr12	7249343	SNV	C	T	G	S	370	*C1RL*	4	deleterious/tolerated	probably/possibly damaging

Chr12	14589163	SNV	A	T	D	V	590	*ATF7IP*	1	deleterious/damaging	probably damaging
Chr12	95926819	SNV	A	G	M	T	405	*USP44*	1	deleterious/damaging	benign/possibly damaging
Chr12	112632704	SNV	C	G	A	P	2490	*C12orf51*	5	neutral/damaging	probably/possibly damaging
Chr14	61788886	SNV	C	T	Q	*	23	*PRKCH**	5	NA/NA	-
Chr15	74335379	SNV	T	A	L	Q	587	*PML*	1	neutral/damaging	probably damaging
Chr17	3119215	SNV	A	G	M	V	101	*OR1A1*	4	neutral/damaging	benign
Chr18	21736417	SNV	A	G	I	V	318	*CABYR*	5	neutral/tolerated	benign
Chr18	77211057	SNV	C	T	R	C	552	*NFATC1*	5	deleterious/damaging	probably damaging
Chr18	10671600-10671602	Del	GAG	-	E	-	2727	*PIEZO2*	2	deleterious/NA	-
Chr19	9087465	SNV	C	A	Q	H	1450	*MUC16*	1	neutral/damaging	probably damaging/benign
Chr20	60886124	SNV	G	A	P	L	3372	*LAMA5*	5	neutral/tolerated	benign
Chr22	29192093	SNV	A	C	S	A	181	*XBP1*	4	neutral/tolerated	possibly damaging/benign

After 29 of the 51 genes chosen for re-sequencing by Sanger sequencing could be validated, two genes were picked for further analysis; *PML* (promyelocytic leukemia) and *NFATC1* (Nuclear factor of activated T-cells, cytoplasmic, calcineurin-dependent 1).

Sanger-sequencing of *PML*

Next generation sequencing and subsequent Sanger sequencing revealed tumor sample 1 to have a p.L587Q (c.1760T>A) mutation in *PML*. This mutation was predicted to be (probably) damaging by the programs PolyPhen-2 and SIFT, respectively (whereas PROVEAN predicted the substitution to be tolerated).

Therefore, and since *PML* is a well-known tumor suppressor gene, it was chosen to be object of further sequencing analysis in a cohort of 30 SI-NET samples. The cohort consisted of 15 primary tumors, eight matching distant metastases, and seven non-matching lymph node metastases. Primers were designed for Exon 1-8 of the gene, including all important domains (e.g. coiled coil domain, essential for core assembly of PML Nuclear Bodies (PML-NBs), Nucleus localization signal, Sumo interaction motif, and different Zinc finger motifs).

In one distant metastasis the somatic mutation p.T130I (c.389C>T) could be detected, whereas the primary tumor depicted the wild type allele, as did both matching normal tissues. This variation was predicted to be benign by PolyPhen-2; the SIFT result was in agreement (tolerated). Only the PROVEAN prediction suggested a deleterious effect on protein function.

No further mutations in *PML* could be found in our cohort of SI-NETs. The p.L587Q mutation is not located in any important domain. p.T130I is located within the B box-type binding domain which mediates the interaction with PIAS1, together with the coiled coil domain.

Sanger-sequencing of *NFATC1*

The somatic mutation in *NFATC1* (p.R552C, c.1720G>A) was of great importance for our research, because the gene is located on Chr18 and the mutation was predicted to be deleterious/damaging for the function of the altered protein. It is positioned in the Rel-homology domain (RHD), which is found in a family of eukaryotic transcription factors (incl. NFAT). Dr. Laura Stoß (former doctoral student) sequenced all important

domains of *NFATC1* (phosphorylation sites, DNA-binding sites, Calcineurin-binding site, and transactivation domain A, nucleus localization signal and nucleus export signal) in the same cohort of 30 SI-NET samples described above. A germ line mutation (p.L344V, c.1030C>G) in a primary tumor as well as in the matching distant metastasis (and the matching normal tissue) was detected. This mutation is not located in any distinct domain and since it was also present in the normal tissue, no tumor-specific background of the SNV was expected.

Data comparison with external data set

During the preparation of my doctoral thesis, Banck et al. published the first study concerning the genomic landscape of SI-NETs. They detected 197 somatic alterations in 48 patients [3].

The only gene bearing mutations in both the cohort of Banck et al. and ours was *ADCY5* (*Adenylate cyclase 5*). Both mutations lie in the Adenylyl cyclase N-terminal extracellular and transmembrane region. Partridge et al. pointed out that primarily the loss of polar residues in transmembrane domains (TMD) can lead to severe protein malfunction, since these residues are able to form membrane-inserted H-bonds, thereby stabilizing the α-helices of TMDs [108].

The mutation found in our sample (p.N382H, c.1144A>C, 19%) lead to an amino acid substitution from asparagine (polar) to histidine (basic), which therefore could result in a destabilized protein structure. The mutation found by Banck et al. (p.V312I) is a valine to isoleucin substitution (both hydrophobic amino acids), meaning that amino acids with similar chemical functionalities are replaced by another, diminishing the potential disadvantageous impact of this mutation.

Concerning Chr18 Banck and colleagues identified only one SNV. The gene *ANKRD30B* (*Ankyrin repeat domain 30B*) depicted a T>A substitution at genomic position 14796361 (p.V625D, predicted to be benign). No Pfam annotations are known for this gene (http://cancer.sanger.ac.uk/cosmic). The tumor, in which the mutation was found, showed no loss of Chr18.

Our exome sequencing of five patients with SI-NETs revealed two SNVs and one deletion in genes on Chr18 in two patients. Patient Tu5, which had one mutation in *NFATC1* and *CABYR*, respectively, also showed loss of one Chr18 (FISH and SNP array analysis). Patient Tu3 (with a 3-base pair-deletion in *PIEZO2*) showed a mosaic pattern concerning Chr18 status.

IV. Results – Chr18-associated tumor suppressors

Western blot analysis of Chr18-associated putative tumor suppressors

In order to analyze, whether Chr18 loss is accompanied with loss of protein expression of the known putative tumor suppressors located on this chromosome, western blot analysis was performed with protein lysates from up to 21 SI-NET samples.

SMAD2 and SMAD4 are strongly expressed in SI-NETs

First, the protein expression of the two tumor suppressors SMAD2 and SMAD4 was investigated by western blot analysis with protein lysates from 14 SI-NET samples (ten with loss of Chr18, confirmed by Chr18 centromere FISH, two without loss of Chr18 and two samples with mosaicism regarding Chr18 status). Both tumor suppressor proteins were detected in varying amounts in all samples investigated (SMAD2: 60 kDa, SMAD4: 61 kDa, β-actin: 42 kDa; Figure 8).

SMAD2

SMAD2 could be detected in varying amounts in all samples investigated (Figure 8, upper panel). SMAD2 appears as double band in western blot analysis; one band at ~55 kDa, one at ~70 kDa. To determine if either bands or only one band is specific for SMAD2, the CML cell line K562 was used as positive control. The protein lysate of this cell line showed a single band at ~55 kDa in western blot analysis; therefore, this band was defined as specific for SMAD2 (Figure 8, indicated by the red arrow). Although no loss of expression was detected in the SI-NET samples, the tumor samples showed differences in strength of expression of SMAD2, whereas the β-Actin expression only varied slightly between the samples. The quantitative western blot analysis revealed one sample to be negative for SMAD2 (sample 6, <20% of β-Actin, Figure 9). This sample depicted loss of Chr18.

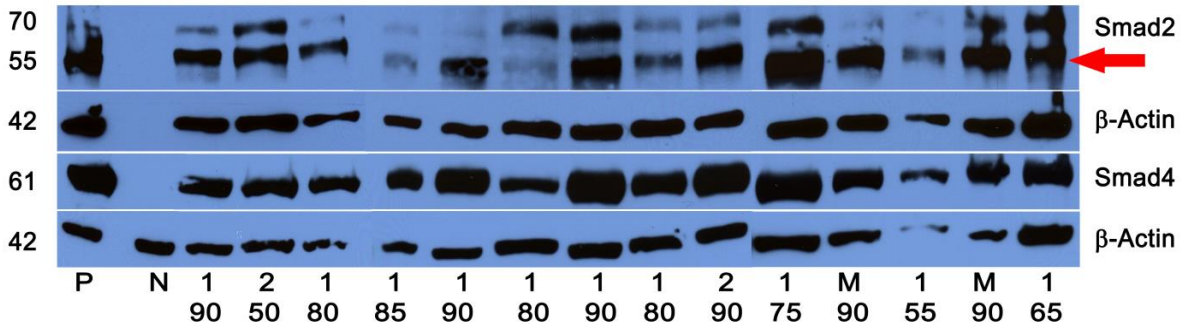

Figure 8: Western blot of the tumor suppressors SMAD2 and SMAD4 in 14 SI-NETs
The samples show variable strength of expression of SMAD2 and SMAD4 (SMAD2: 60 kDa, indicated by the red arrow, SMAD4: 61 kDa, β-actin: 42 kDa). P: positive control, N: negative control, M: mosaic, 1: 1xChr18, 2: 2xChr18, numbers below indicate tumor content (%)

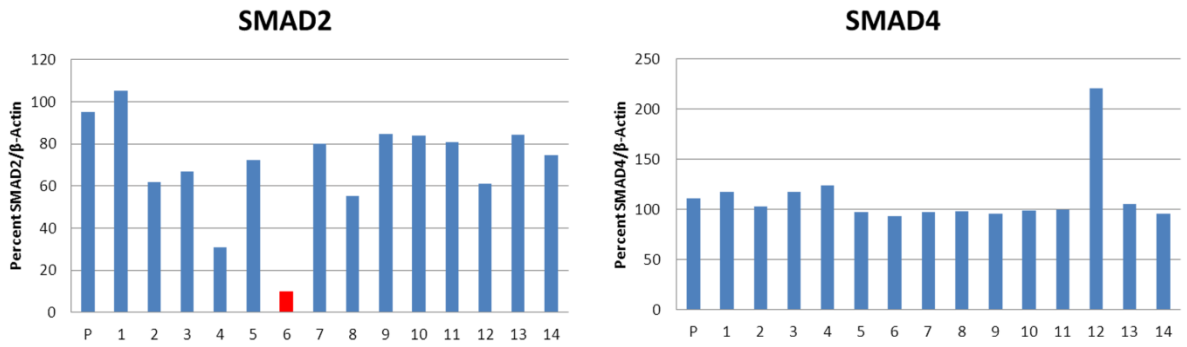

Figure 9: Quantitative western blot analysis for SMAD2 and SMAD4
The ratio of the distinct protein expression (SMAD2/SMAD4) to the respective β-Actin expression per sample is shown (%). P: positive control; red bar indicates protein expression <20% of β-Actin

SMAD4

Western blot analysis of SMAD4 revealed a similar result: all 14 SI-NET samples showed strong expression of this protein, regardless of the count of Chr18 (Figure 8, lower panel). Half of the samples showed (slightly) higher SMAD4 expression than expression of the housekeeping protein β-Actin (>100% of β-Actin expression), whereas the other half of the samples showed similar expression for both proteins (Figure 9). NIH/3T3 was used as positive control for this Western blot, whereas the pancreatic carcinoma cell line BxPC-3 was used as negative control for SMAD4 [44].

Elongin A3 and CABLES show strong expression in SI-NETs, whereas PMAIP1 is not expressed

Western blot analyses of the two tumor suppressors Elongin A3 and CABLES were performed with 21 fresh frozen tissues. CABLES was detected in varying amounts in all analyzed samples (Figure 10, upper panel, Figure 11, first picture; only the first eight samples are shown). For CABLES multiple isoforms are described, which often show as doublets in western blot analyses. Whereas the positive control (HEK293 T cell lysate) only depicts the upper doublet band at ~67 kDa, all NET samples showed an additional aberrant band of varying strength at ~55 kDa.

Since two different bands were visible in the Elongin A3 western blot (but only one isoform is known), a competition analysis with a peptide was performed, identifying the upper band to be the specific one (Figure 10, middle panel, Figure 11, second picture; only the first eight samples are shown). Elongin A3 exhibited distinct positive results in 20 of the 21 samples; one sample was negative (not shown).

Western blot analysis of PMAIP1 revealed negativity (<20% of β-Actin expression) of the first eight samples, whereas the protein lysate of U251 showed a distinct band (Figure 10, lower panel, Figure 11, third picture); therefore, no further samples were tested.

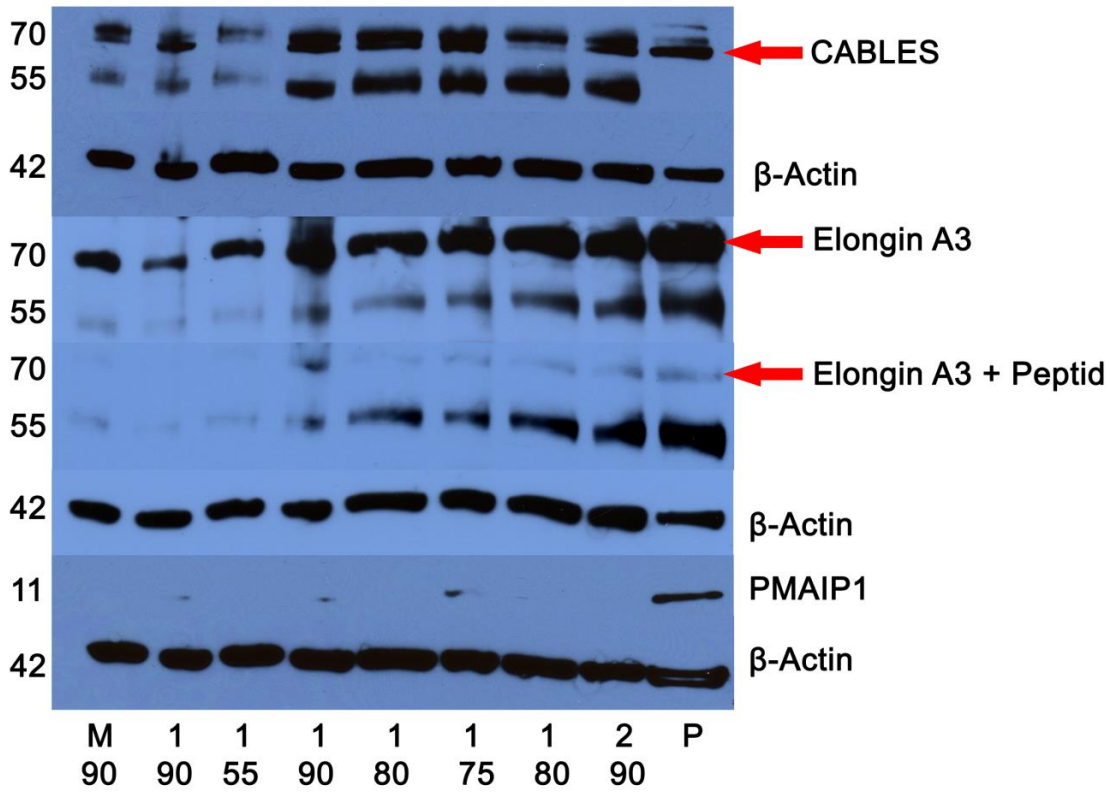

Figure 10: Western Blot analysis of the putative tumor suppressors CABLES, Elongin A3, and PMAIP1 in 8 (of 21) SI-NETs CABLES and Elongin A3 are mostly strongly expressed, whereas PMAIP1 is negative in all samples (CABLES: 67 kDa, indicated by the red arrow, Elongin A3: 60 kDa, with and without competing peptide, indicated by the red arrow, PMAIP1: 15 kDa) P: positive control, M: mosaic, 1: 1xChr18, 2: 2xChr18, numbers below indicate tumor content (%)

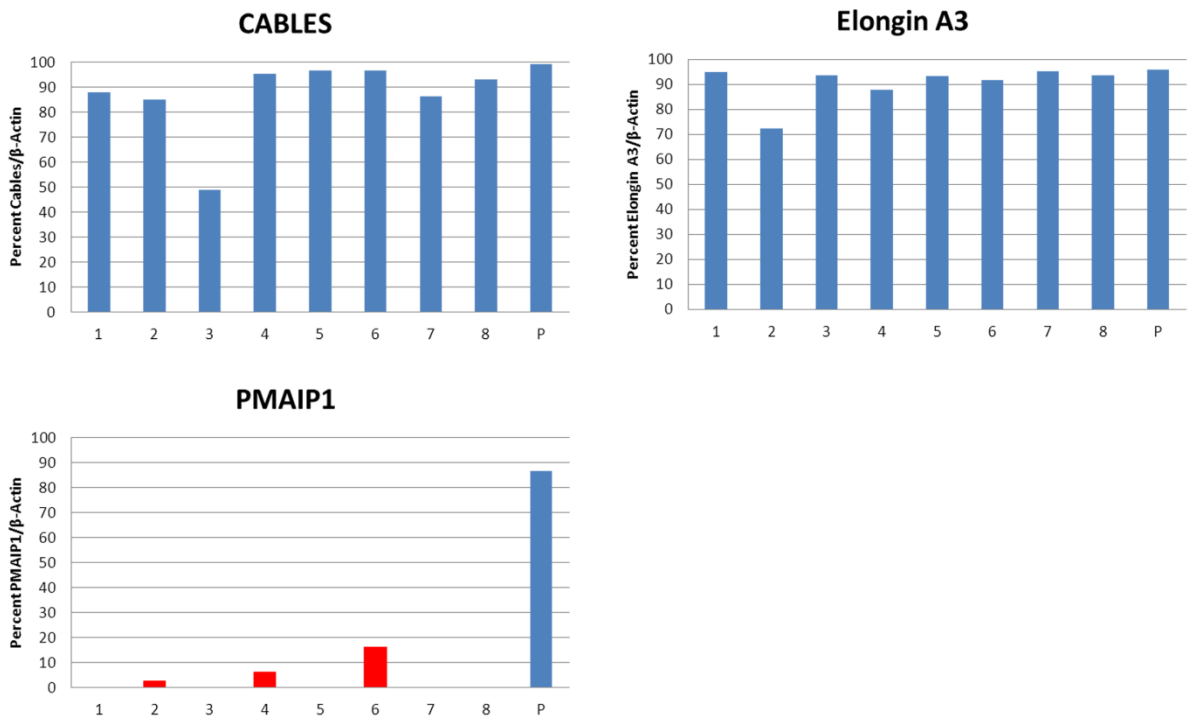

Figure 11: Quantitative western blot analysis for CABLES, Elongin A3, and PMAIP1
The ratio of the distinct protein expression (SMAD2/SMAD4) to the respective β-Actin expression is shown (%). P: positive control; red bars indicate protein expression <20% of β-Actin; Sample 1, 3, 5, 7, and 8 depicted no band at all for PMAIP1.

DCC expression is lost/reduced in nearly 30% of SI-NET samples

Western blot analysis of DCC using the first antibody was performed with 21 tumor samples. The evaluation of the western blot results revealed total loss or reduced DCC expression (<20% of β-Actin expression) in 29% (6/21) of samples (Figure 12A, Figure 13: DCC 1A, 2, 3).

With the first eight tumor samples a second western blot was performed, using another antibody (Figure 12B, Figure 13: DCC 1B). Due to difficulties in distinguishing the bands between 180 and 250 kDa, a competition with the matching peptide was applied. In addition, a label-free identification of DCC-specific peptides in the positive control IMR-32 by mass spectrometry was performed. The mass spectrometry confirmed DCC to be present in the gel bands at ~190 kDa.

The second western blot analysis revealed sample 5 and 7 to have lost DCC expression. This result is supported by the first western blot: sample 7 has lost DCC expression as well and sample 5 exhibits reduced expression of DCC. Since the background signal was very high, sample 3 and 6 were not analyzable in the second

western blot. All samples with lost/reduced expression of DCC depicted only one copy of Chr18.

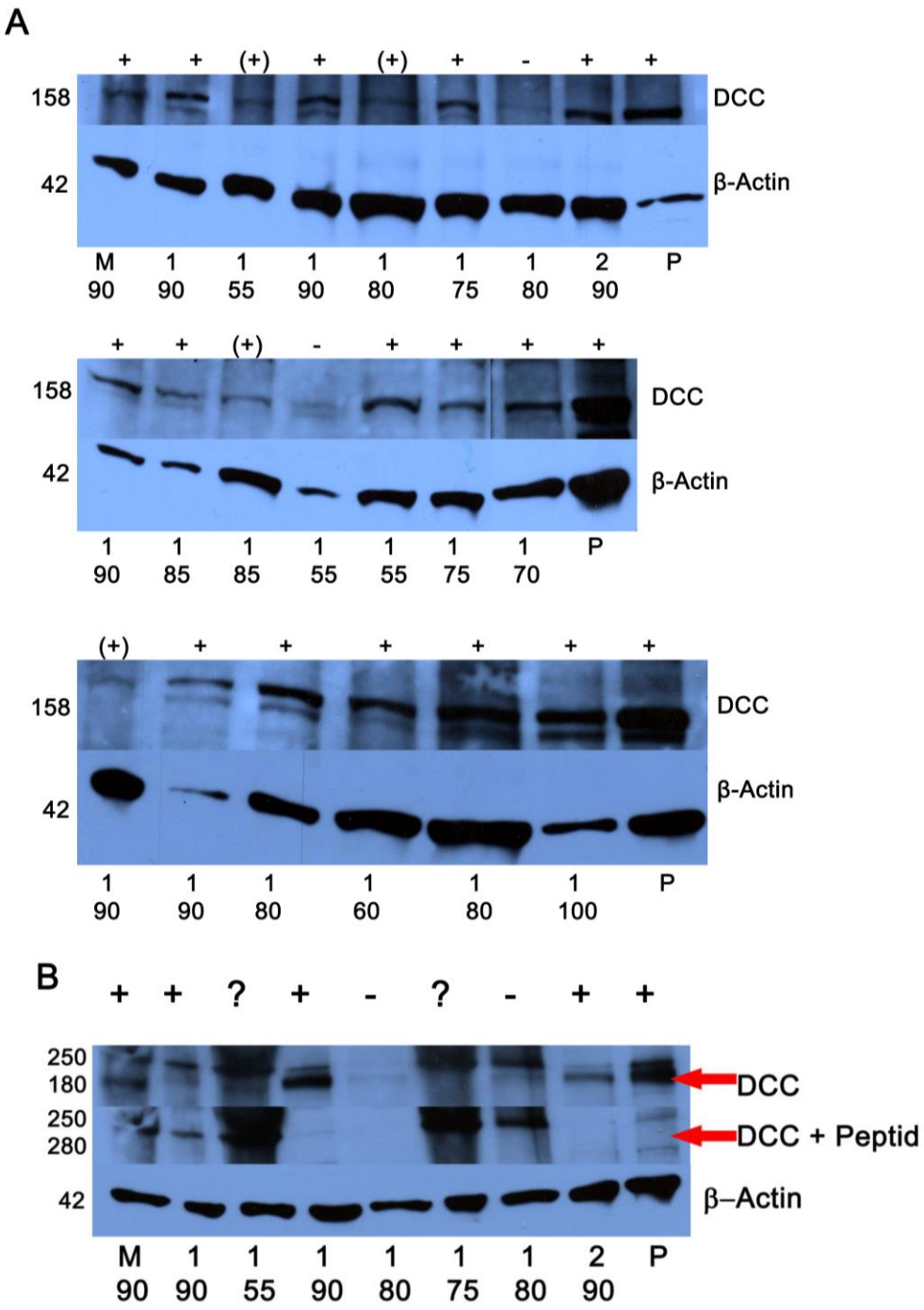

Figure 12: Western blot of the Chr18-associated tumor suppressor DCC in 21 SI-NETs
A) DCC is lost in sample 7 and 12. The samples 3, 5, 11, and 16 show greatly reduced expression of DCC (158 kDA). B) DCC western blot of the first eight tumor samples, using a second antibody (190 kDa). A competition analysis with matching peptide was carried out to determine the right protein band (indicated by the red arrow). DCC is lost in sample 5 and 7. Due to strong background, the samples 3 and 6 are not analyzable. P: positive control, M: mosaic, 1: 1xChr18, 2: 2xChr18, numbers below indicate tumor content (%)

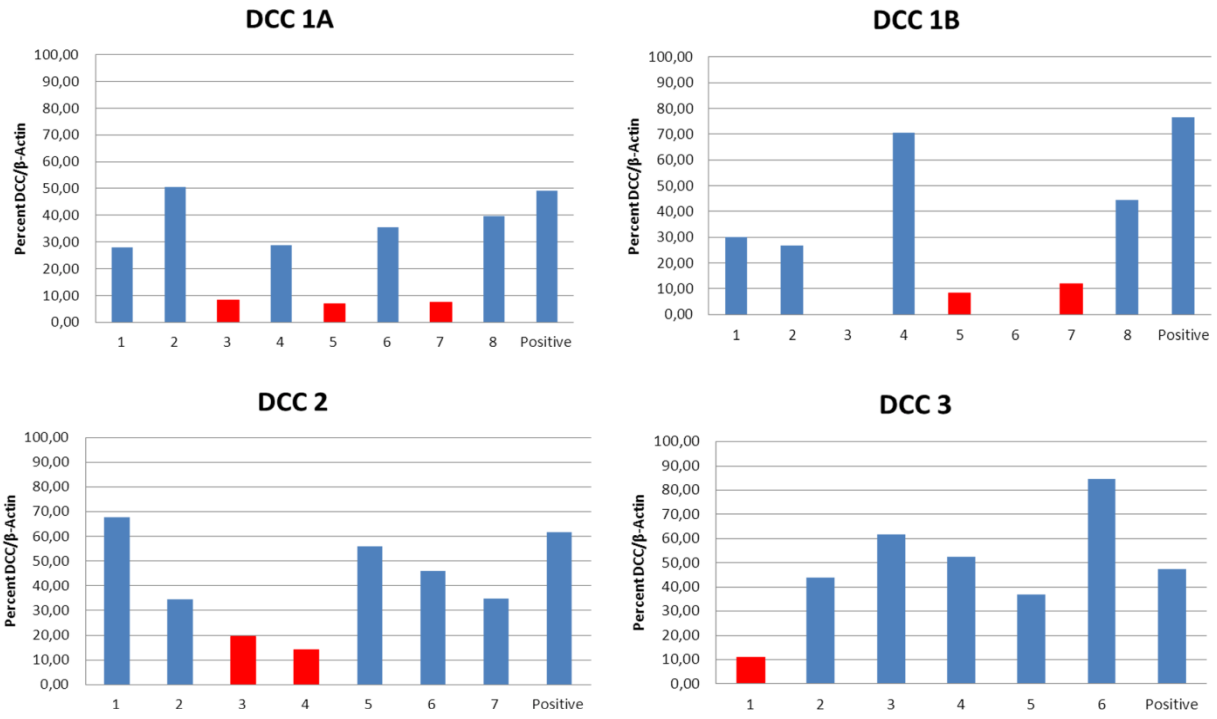

Figure 13: Quantitative western blot analysis for DCC
Red bars indicate protein expression <20% of β-Actin. Sample 3 and 6 of DCC western blot 1B (second antibody) were not analyzable due to high background, therefore no bar is shown.

Quantitative Real-time PCR (qRT-PCR) analysis reveals *TCEB3C* and *CABLES* to be differentially expressed between sample cohorts with and without loss of Chr18

Since only one cryo-conserved sample with the normal count of Chr18 was available for western blot analyses of Elongin A3, PMAIP1, DCC, and CABLES, an additionally qRT-PCR was performed to further investigate the influence of the Chr18 loss on these tumor suppressors. qRT-PCR for *TCEB3C* (coding for Elongin A3), *PMAIP1*, *DCC*, and *CABLES* was done in a greater cohort of 69 FFPE samples.

The Cp-values ranged between 22 (high expression) and 35 (low expression). The raw Cp-values were normalized to *β-Actin*, resulting in ΔCp values. The statistical setup was designed that lower ΔCp values indicate an upregulation, whereas higher ΔCp values display a downregulation.

Four samples depicted Cp values >30 for the normalization control *β-Actin* and were therefore excluded from further analysis (the high Cp values of the ubiquitously

expressed housekeeping gene *β-Actin* suggest that the RNA of the respective samples is somehow degraded). Of the remaining 65 samples, 38 exhibited the loss of one Chr18, 13 samples depicted the normal count of two chromosomes 18, and 12 tumors showed mosaicism regarding their Chr18 status, determined by FISH analysis (it was not possible to ascertain the Chr18 status for two samples). For the comparative analysis of cohorts with/without loss of Chr18, the mosaic samples were excluded.

DCC seems to be weakly expressed in SI-NETs: *DCC* Ex3-4 exhibited average Cp values of 34.29 and 34.65 for samples with 1xChr18 and 2xChr18, respectively. Similar results were achieved, when comparing the mRNA coding for the exon boundary between Ex17 and Ex18 of the *DCC* gene: average Cp value of 33.51 and 34.02 for 1xChr18 and 2xChr18, respectively. The mean ΔCp values were 10.41 (1xChr18) and 9.86 (2xChr18) for *DCC* Ex3-4 and 9.59 (1xChr18) and 9.22 (2xChr18) for *DCC* Ex17-18 (Figure 14, upper panel). The difference of expression between the two cohorts were not significant for *DCC* (p=0.22 for Ex3-4 and p=0.31 for Ex17-18, respectively).

TCEB3C (the gene coding for Elongin A3) exhibited strong expression in SI-NETs with average Cp values of 24.62 (1xChr18) and 24.71 (2xChr18). Although the Cp values were nearly the same for both cohorts, the normalization revealed a significant downregulation of this gene in the cohort with loss of Chr18 (p=0.01, with average ΔCp values of 0.9 for 1xChr18 and 0.07 for 2xChr18; Figure 14, middle panel, first picture).

CABLES was weakly expressed in SI-NETs with average Cp values of 34.2 (1xChr18) and 34.38 (2xChr18). However, comparative analysis revealed significantly different mRNA expression between the two cohorts (ΔCp values of 10.47 and 9.68 for 1xChr18 and 2xChr18, p=0.03; Figure 14, middle panel, second picture).

Finally, *PMAIP1* expression was analyzed by qRT-PCR. Since western blot analysis revealed negativity for eight tested SI-NETs, weak mRNA expression was to be expected regarding this gene. This was confirmed by the Cp values: mean Cp values were 34.37 (1xChr18) and 34.75 (2xChr18). The normalization resulted in average ΔCp values of 10.52 (1xChr18) and 9.97 (2xChr18). The difference between the two cohorts showed a tendency towards higher *PMAIP1* expression in the cohort with preserved Chr18 status, but was not significant (p=0.07; Figure 14, lower panel).

In summary, only *TCEB3C* mRNA seems to be strongly expressed in SI-NETs, all other genes exhibited high Cp values, suggesting a weak expression. However, all genes investigated showed a trend towards lower ΔCp values in the cohort with two Chr18 compared to the cohort with loss of Chr18, meaning higher expression. This difference was significant concerning *TCEB3C* and *CABLES.*

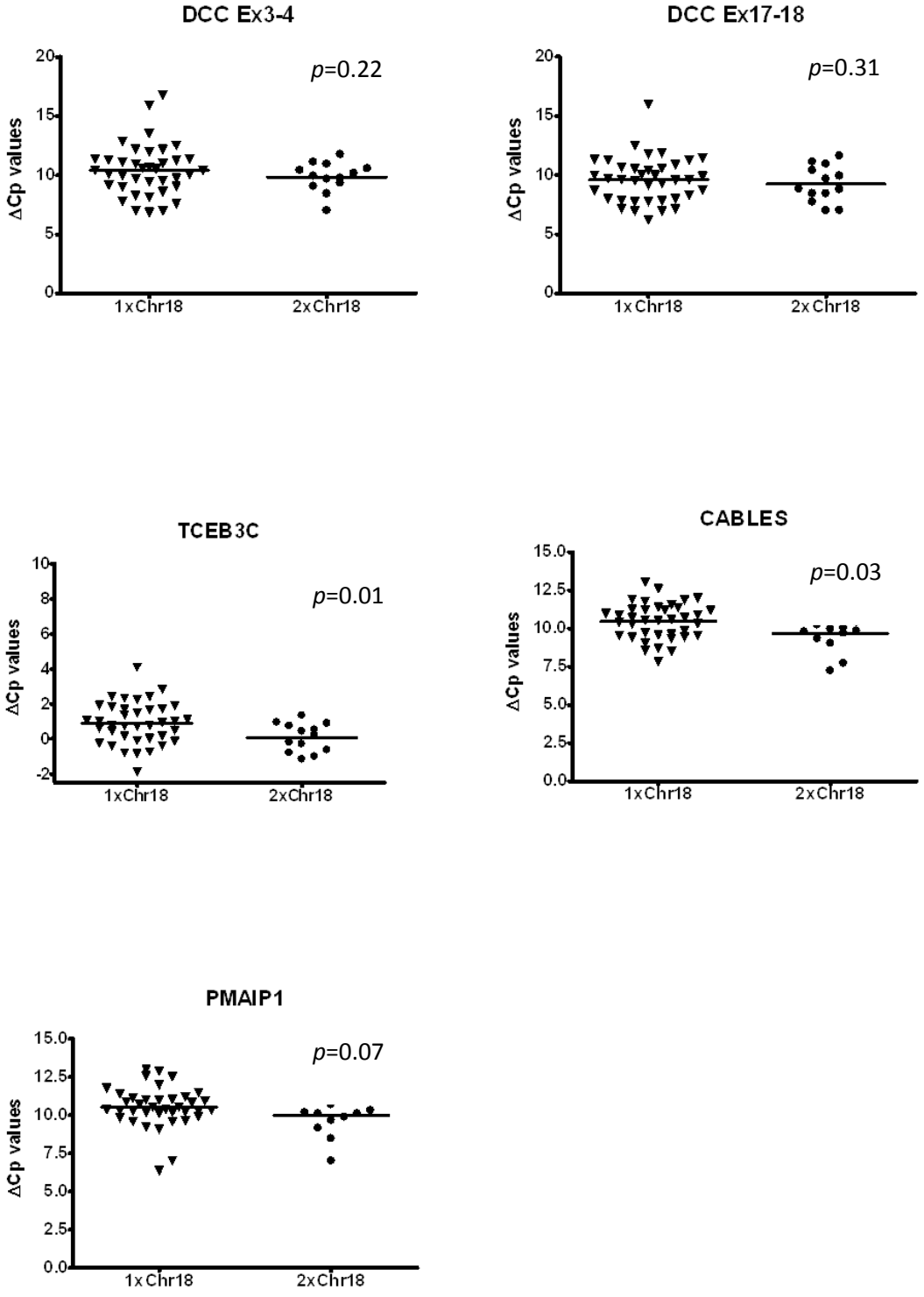

Figure 14: ΔCp values of the four tumor suppressor genes *DCC*, *TCEB3C*, *CABLES*, and *PMAIP1*
The Cp values of the genes were normalized to *β-actin*. For *DCC*, two primer pairs amplifying different exon boundaries of the gene were tested (exon 3-4 and exon 17-18). *TCEB3C* and *CABLES* were significantly downregulated (*p*=0.01 and *p*=0.03, respectively) in the cohort with loss of Chr18 compared to the cohort with a normal count of Chr18.

IV. Results - PI3K/AKT/mTOR pathway

FISH analysis of the PI3K/AKT/mTOR-pathway

Copy number gains of *PIK3CD, AKT1, AKT2, PDGFRα, PDGFRβ*, and *mTOR*

Eight TMAs with 217 SI-NETs (comprising 135 patients) were analyzed for amplifications of the PI3K/AKT/mTOR-pathway. To cover the whole pathway, the tyrosine kinase receptors *PDGFRα* and *PDGFRβ*, the PI3K delta isoform *PIK3CD*, and the serine/threonine kinases *AKT1* and *AKT2,* and *mTOR* were analyzed.

Evaluation of FISH results revealed low level amplifications in a subset of SI-NETs, meaning that most of the nuclei showed 3-6 gene specific signals per cell (Figure 15). No high level amplifications with >9 signals per cell could be detected. These amplifications were sometimes associated with additional signals for the reference chromosome probes, indicating chromosome polysomy. (The ratios of gene specific signals to reference chromosome signals ranged between 1.03 and 1.6. This evaluation was not achieved for *PDGFRβ* since only a split probe was available for this gene.)

Henceforth, the term copy number (CN) variation is used for the variations found in the tumors, since single gene amplifications (centromere signal count ≤72, target/centromere ratio >1.2), amplifications in combination with polysomy (centromere signal count >72, ratio target/centromere signals >1.2), or polysomy (target signal count >72, ratio target/centromere signals ≤1.2) occurred in our samples.

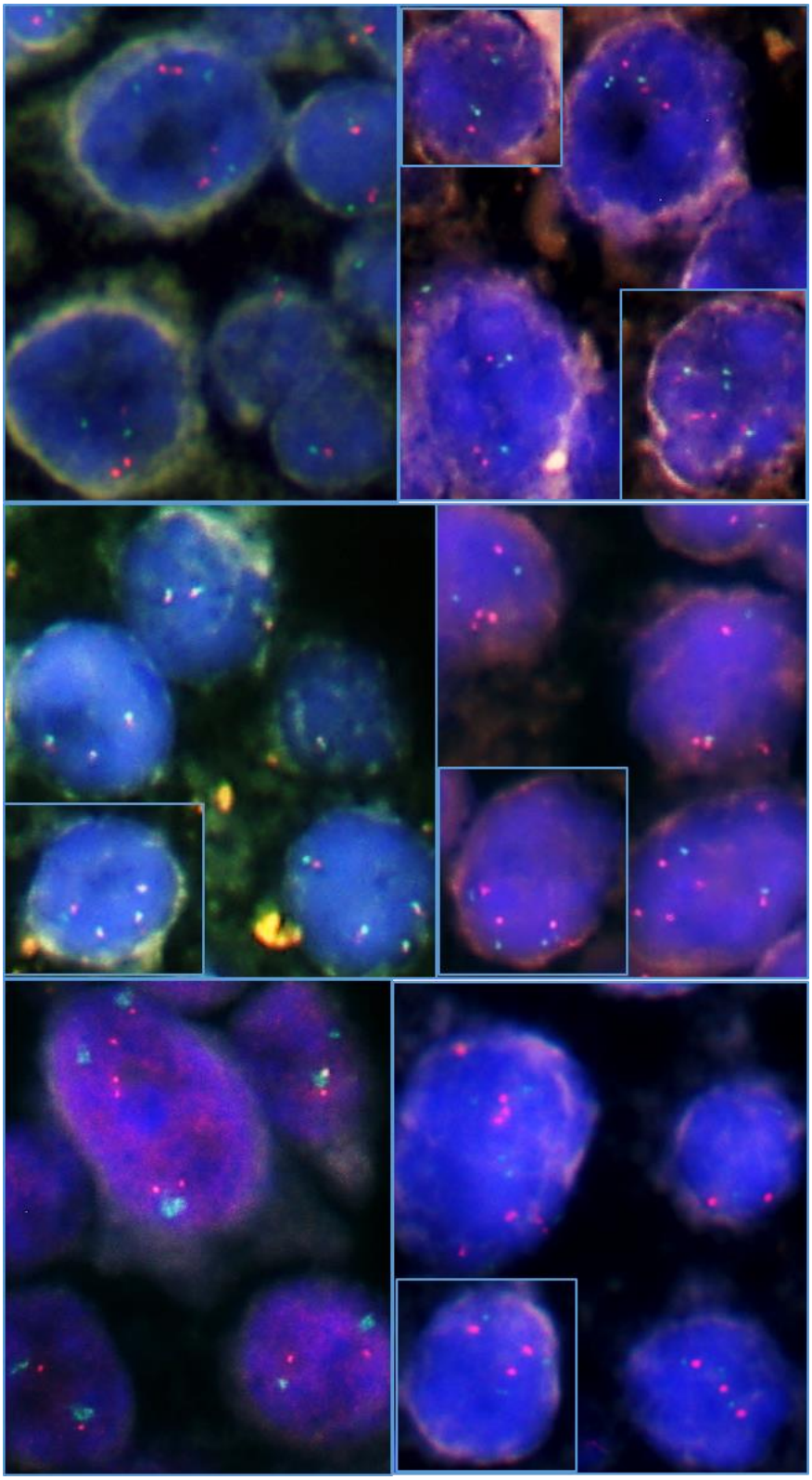

Figure 15: Exemplary fluorescent pictures of SI-NETs harboring CN gains
(A) *AKT1*, (B) *AKT2*, (C) *PDGFRβ*, (D) *PDGFRα*, (E) *mTOR*, and (F) *PIK3CD*; magnification: 1000x; red: gene specific signals, green: reference chromosome signals

The percentage of CN variations in our cohort ranged between 12% (*PDGFRα*) and 24% (*PDGFRβ*). *PIK3CD* and *AKT1* depicted CN variations in 18% each, *AKT2* in 14% and *mTOR* in 16% (Table 23 last line). Table 23 gives a detailed overview over the variations found in the SI-NETs.

Table 23: Results of FISH analysis of *PIK3CD*, *AKT1/2*, *PDGFRα/β*, and *mTOR*
The upper panel shows the number of samples which were applicable for FISH analysis. In the lower panels the percentage and total number of samples with gene CN variations are given. P: primary tumor, LN: lymph node metastasis, DM: distant metastasis, CN: copy number, any: any CN variation for the gene, amplified: centromere signal count ≤72, ratio target/centromere signals >1.2, amplified+polysomy: centromere signal count >72, ratio target/centromere signals >1.2, polysomy: target signal count >72, ratio target/centromere signals ≤1.2

	PIK3CD	*AKT1*	*AKT2*	*PDGFRα*	*PDGFRβ*	*mTOR*
Applicable cases	P: 94	P: 91	P: 96	P: 83	P: 96	P: 95
	LN: 57	LN: 56	LN: 58	LN: 59	LN: 63	LN: 58
	DM: 13	DM: 13	DM: 10	DM: 12	DM: 14	DM: 12
	any: 113	any: 110	any: 112	any: 104	any: 112	any: 110
Amplified cases [%]	P: 7% (7/94)	P: 9% (8/91)	P: 2% (2/96)	P: 1% (1/83)	P: 14% (13/96)	P: 7% (7/95)
	LN: 19% (11/57)	LN: 14% (8/56)	LN: 9% (5/58)	LN: 3% (2/59)	LN: 27% (17/63)	LN: 7% (4/58)
	DM: 15% (2/13)	DM: 23% (3/13)	DM: 10% (1/10)	DM: 0%	DM: 36% (5/14)	DM: 8% (1/12)
Amplified + polysomy [%]	P: 0%	P: 1% (1/91)	P: 1% (1/96)	P: 0%	-	P: 1% (1/95)
	LN: 0%	LN: 4% (2/56)	LN: 0%	LN: 0%	-	LN: 0%
	DM: 0%	DM: 0%	DM: 0%	DM: 0%	-	DM: 0%
Polysomy [%]	P: 0%	P: 0%	P: 4% (4/96)	P: 2% (2/83)	-	P: 4% (4/95)
	LN: 2% (1/57)	LN: 0%	LN: 3% (2/58)	LN: 10% (6/59)	-	LN: 2% (1/58)
	DM: 0%	DM: 0%	DM: 10% (1/10)	DM: 17% (2/12)	-	DM: 0%
All CN variations	P: 7% (7/94)	P: 10% (9/91)	P: 7% (7/96)	P: 4% (3/83)	P: 14% (13/96)	P: 13% (12/95)
	LN: 21% (12/57)	LN: 18% (10/56)	LN: 12% (7/58)	LN: 14% (8/59)	LN: 27% (17/63)	LN: 9% (5/58)
	DM: 15% (2/13)	DM: 23% (3/13)	DM: 20% (2/10)	DM: 17% (2/12)	DM: 36% (5/14)	DM: 8% (1/12)
	any: 18% (20/113)	any: 18% (20/110)	any: 14% (16/112)	any: 12% (12/104)	any: 24% (27/112)	any: 16% (17/110)

The distribution of CN alterations in the PI3K/AKT/mTOR pathway between primary tumors, lymph node metastases, and distant metastases is depicted in Figure 16. For

five of the six genes, CN alterations were more abundant in metastases (lymph node and distant metastases combined) than in primary tumors, with *mTOR* being the exception. This observation was statistically significant for *AKT1* (p=0.005), *AKT2* (p=0.014), *PDGFRα*, and *PDGFRβ* (both p<0.000). Additionally, the percentage of amplified genes was mostly slightly higher in distant than in lymph node metastases, but statistical significance was not reached. The values of lymph node/distant metastases for the different genes were: *PIK3CD* 21/15%, *AKT1* 18/23%, *AKT2* 12/20%, *PDGFRα* 14/17%, *PDGFRβ* 27/36%, and *mTOR* 9/8%.

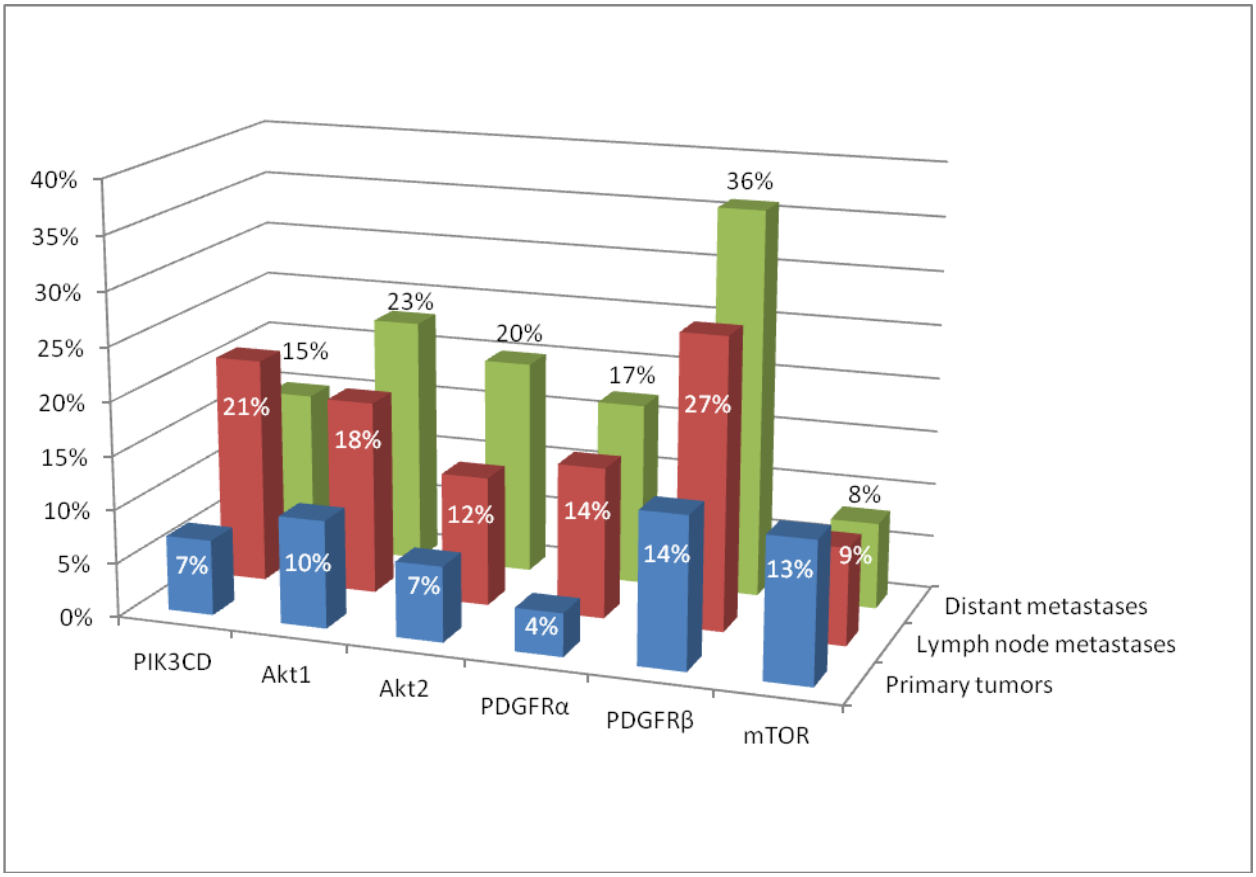

Figure 16: Distribution of CN alterations in the PI3K/AKT/mTOR pathway between primary tumors and metastases
Blue: primary tumors, red: lymph node metastases, green: distant metastases

Comparative analysis of primary tumor and metastases

The FISH analysis showed that metastases mostly harbor more CN variations than primary tumors. To take a closer look at the time point of this event, we did a comparative analysis of primary tumors and matching metastases.

For the comparison, 37 to 50 analyzable samples were available. The evaluation revealed *AKT1*, *AKT2*, and *PDGFRα* CN gains to occur more often in metastases than in matching primary tumors (Figure 17). *PIK3CD* and *PDGFRβ* CN gains were present fifty-fifty either in primary tumors or metastases. Interestingly, gains of *PDGFRα* were predominantly seen in both primary tumors and matching metastases (60%); in contrast no overlap of gains could be observed in matching primary-metastases pairs for *PIK3CD*.

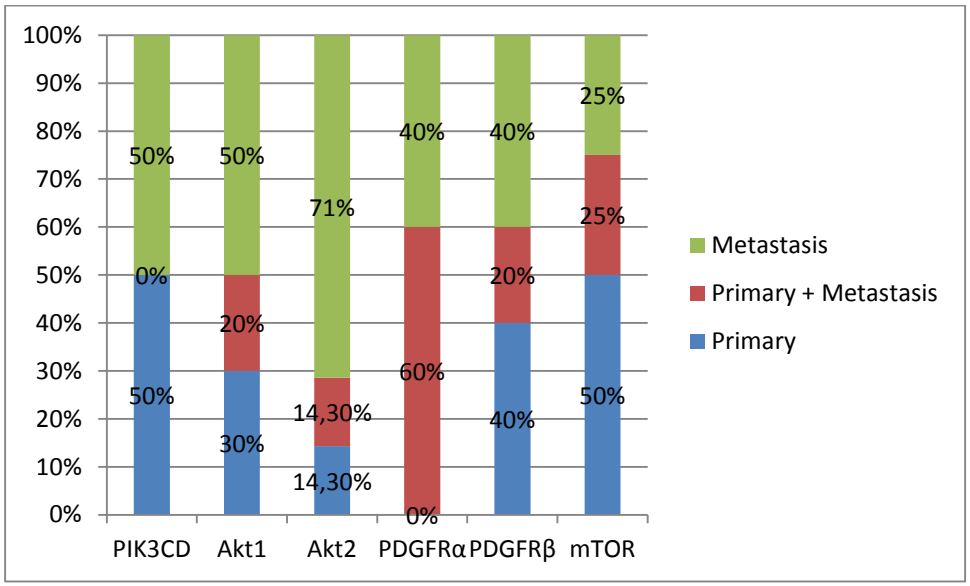

Figure 17: Comparison of amplifications between primary tumors and matching metastases
P: primary tumor, M: metastasis

Advanced tumors harbor significantly more CN gains than tumors of earlier stage

The next step was a comparative evaluation of the distribution of gains in different tumor stages. Advanced tumors (UICC stage IIIB and IV) depicted significantly more gains in the PI3K/AKT/mTOR pathway than earlier tumors (UICC stage I-IIIA grouped together, p=0.014, Figure 18).

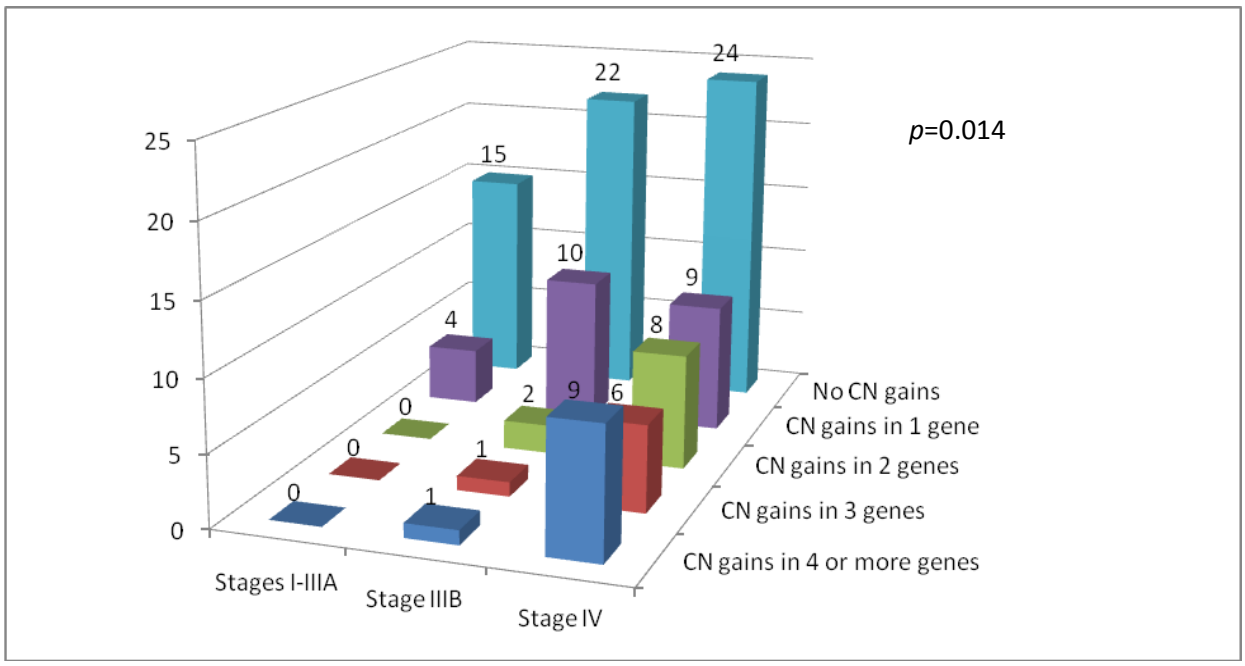

Figure 18: Distribution of gains by UICC stages
Advanced tumors (UICC stage IIIB and IV) show significantly more CN gains in the PI3K/AKT/mTOR pathway in contrast to tumors of earlier stages (*p*=0.014).

Furthermore, when comparing early T stages (T1+T2) with higher T stages (T3+T4) concerning their amplification status, a significant association was seen between gains and higher T stages (*p*=0.028, Figure 19).

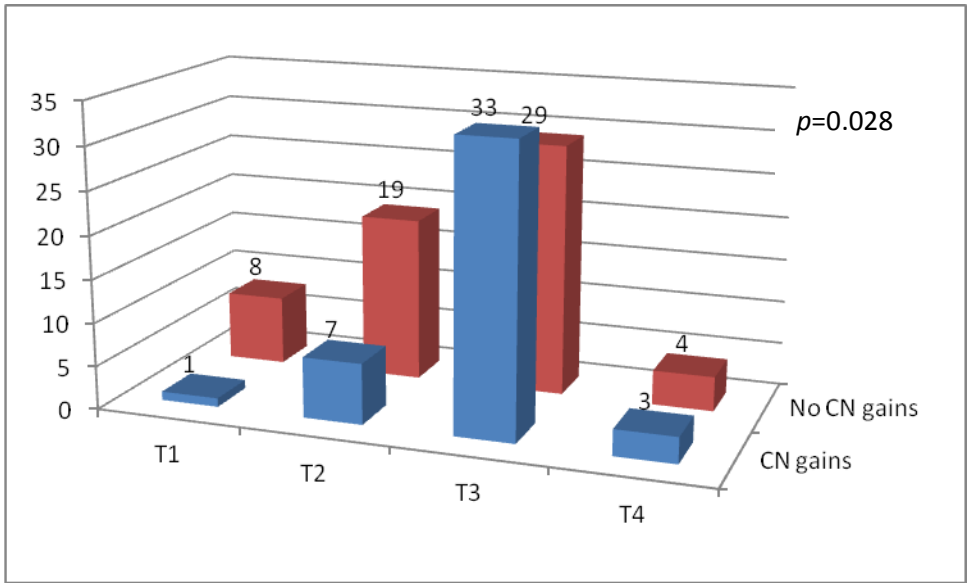

Figure 19: Distribution of gains by T stages
Higher T stages (T3+T4) depicted significantly more CN gains than T1 and T2 stages (*p*=0.028).

These results indicate that the CN variations are prevalent in tumors with advanced stage (with lymph node / distant metastases) and invasion in the (sub-)serosa / other organs.

Comparison of FISH results with SNP array results

In order to get a better understanding of the events underlying the CN variations received by FISH analysis, the SNP array samples Tu1 und Tu7, and their matching metastases, as well as Tu2 (samples showing multiple CNVs), were analyzed in regard of the PI3K/AKT/mTOR signaling pathway gene variations.
Therefore, SNP array data was compared with the exact chromosomal locations of the genes investigated by FISH.

PDGFRα, which is located on Chr4, was affected by a huge CN gain, comprising the region 4p11-q12 and 4p11-q13.2, in Tu1(Met) and Tu7(Met) respectively. Comparable results were achieved for *PDGFRβ*, located on Chr5: the regions 5q32-q33.1 and 5q31.1-q33.1 were affected in the respective tumors. For both regions, CN gains of 3 were detected. Tu2, which also depicted CN of 3 for Chr4 and Chr14, showed no amplification of *PDGFRα* and *AKT1*, indicating that the amplified regions were dissimilar to the locations of these two genes.

mTOR, *PIK3CD* (both located on Chr1), and *Akt1* (Chr14) were not affected by CN gains in any of the samples investigated. *Akt2* (Chr19) was amplified (CN=3) within a region of 3,642 kb (19q13.2) in Tu1(Met), but not in Tu7(Met) or Tu2.

Comparison of FISH results with data from Banck et al. [3]

Banck and colleagues' publication, stating gene alterations in the PI3K/AKT/mTOR pathway to be the most frequent with 29% (14/48) of patients affected, prompted us to verify their findings in a greater cohort of 135 patients (217 tumor samples) and with another method, the Fluorescence-in-situ-hybridization. Subsequently, a comparison of the results, achieved by the different methods and in the different cohorts, is performed.
The exact locations of the six genes of the PI3K/AKT/mTOR pathway were compared with the data of Supplemental Table 12 of Banck et al., which depicted "1013 Somatic Copy Number Variations (SCNA) in 48 SI-NET" (adjusted in Table 25, fold change was not given by Banck et al., but calculated by us).

Table 24: Comparison of FISH results with raw data from Banck et al.
Table adapted after Supplemental Table 12 of Banck et al. [3]
Pt-ID: Patients identification, Chr: Chromosome, m.log2: ratios between tumor and normal tissue reads per exon, normalized to mean ratio and log(2) transformed, 2^x: fold change, calculated on basis of m.log2, bp: base pairs, pval: p-value.

Pt-ID	Chr	Start	End	Exons	m.log2 (x)	Fold change (2^x)	Event size [bp]	Call	pval	Gene
13	1	6.488.285	28.843.236	3066	0.2686	1.205	22.354.951	amp	1.34E-09	mTOR/PIK3CD
17	1	14.362	11.710.001	1539	0.2662	1.203	11.695.639	amp	7.77E-22	mTOR/PIK3CD
35	1	14.362	13.182.960	1818	0.2571	1.195	13.168.598	amp	8.21E-50	mTOR/PIK3CD
45	1	14.362	28.843.236	4011	0.3777	1.299	28.828.874	amp	5.23E-19	mTOR/PIK3CD
4	4	53.226	190.947.538	7842	0.3628	1.286	190.894.312	amp	NA	PDGFRα
7	4	53.226	190.947.538	7844	0.402	1.321	190.894.312	amp	NA	PDGFRα
20	4	678.271	190.947.538	7783	0.256	1.194	190.269.267	amp	NA	PDGFRα
36	4	40.058.650	190.947.538	5983	0.341	1.267	150.888.888	amp	NA	PDGFRα
2	5	94.982.582	180.687.001	4944	0.4715	1.387	85.704.419	amp	NA	PDGFRβ
4	5	140.372	180.687.001	8828	0.3525	1.277	180.546.629	amp	NA	PDGFRβ
7	5	140.372	180.687.001	8816	0.3881	1.309	180.546.629	amp	NA	PDGFRβ
9	5	140.372	180.687.001	8783	0.3219	1.25	180.546.629	amp	NA	PDGFRβ
20	5	34.684.611	180.687.001	7773	0.2831	1.217	146.002.390	amp	NA	PDGFRβ
22	5	140.372	180.687.001	8760	0.319	1.247	180.546.629	amp	NA	PDGFRβ
34	5	6.651.954	180.687.001	8430	0.329	1.256	174.035.047	amp	NA	PDGFRβ
4	14	50.175.876	106.950.170	4314	0.3994	1.319	56.774.294	amp	NA	Akt1
7	14	89.029.994	106.950.170	1714	0.3538	1.278	17.920.176	amp	NA	Akt1
14	14	103.998.918	106.950.170	355	0.7003	1.625	2.951.252	amp	NA	Akt1

20	14	19.377.593	106.950.170	6164	0.3067	1.237	87.572.577	amp	NA	Akt1
21	14	77.679.788	106.950.170	2007	0.4777	1.393	29.270.382	amp	NA	Akt1
35	14	104.037.959	106.950.170	355	0.3055	1.236	2.912.211	amp	NA	Akt1
41	14	104.640.484	106.950.170	237	0.3641	1.287	2.309.686	amp	NA	Akt1
42	14	103.801.989	106.950.170	401	0.3866	1.307	3.148.181	amp	NA	Akt1
13	19	30.018.117	59.092.611	6103	0.4087	1.327	29.074.494	amp	NA	Akt2
16	19	110.678	59.092.611	11624	0.4449	1.361	58.981.933	amp	NA	Akt2
22	19	110.678	59.092.611	11496	0.3157	1.245	58.981.933	amp	NA	Akt2
45	19	17.598.268	43.967.277	3274	0.4959	1.41	26.369.009	amp	2.11E-26	Akt2

PIK3CD and *mTOR* were co-amplified in the patients 13, 17, 35, and 45, resulting in a frequency of 8% (4/48). *PDGFRα* and *AKT2* were amplified in four out of 48 samples, as well. *AKT1* was the most amplified gene in 17% (8/48) of the samples, *PDGFRβ* the second most amplified gene in 14.5% (7/48).

Figure 20 summarizes the different frequencies of CN gains, which were found in the study of Banck et al. [3] and by us.

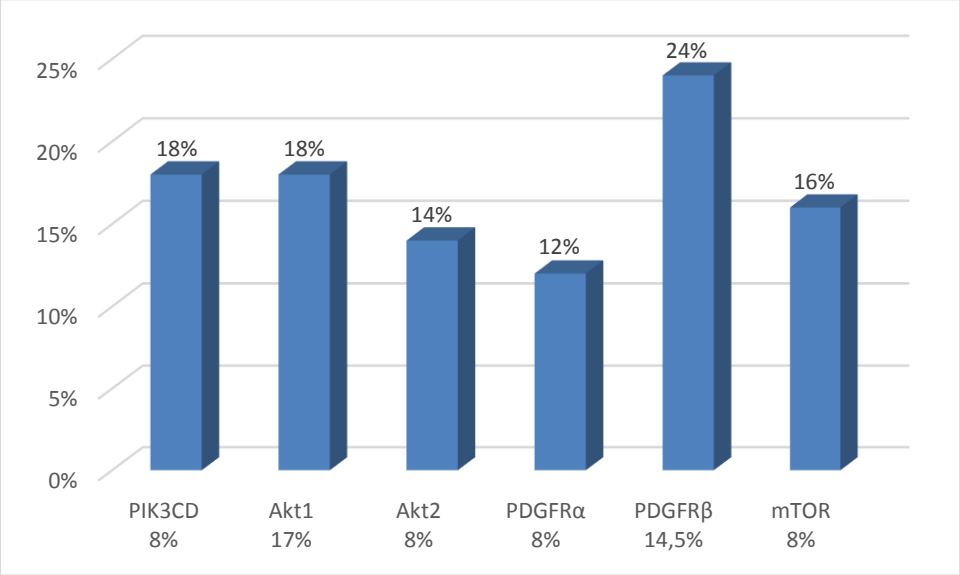

Figure 20: Percentage of CN gains in SI-NETs
Percentages over the blue bars depict the results of the FISH evaluation in our cohort of 217 tumor samples. Values under the gene names refer to the percentage of amplified cases (raw data analysis) detected by Banck et al. [3] in 48 tumor samples.

The frequencies achieved by FISH are slightly higher than the ones achieved by NGS and array CGH, which is probably due to the different collectives and sample sizes.

In our cohort, the majority of the variations were defined as “amplified” (Table 23), indicating that, albeit increased reference centromere signals occasionally occurred (Appendix Table 30), these additionally signals did not exceed the threshold of 72 signals per cell (see Methods 3.11.2 FISH evaluation).

In order to evaluate, if this was also true for the gains found by Banck et al., we again looked at the raw data of the CNVs (Table 24). The event size and number of exons give an impression of the regions which were affected by these CN gains. At least, 237

exons were affected and the smallest event size was 2,310 kbp (patient 41, *AKT1* amplification). One gene includes an average of 8.8 exons [109], so that the mentioned region might statistically comprise 27 different genes. This result suggests that Banck et al. did not identify single gene amplifications, but CN variations, which are due to (partial) chromosomal gains.

The last part of the data set comparison regarding gene amplifications in the PI3K/AKT/mTOR pathway focused on the level of amplifications, because our FISH results revealed predominant low-level amplifications of 3-6 signals per cell. Banck and colleagues provided an m.log2 value, which was calculated by counting the reads per exon in tumor and in normal tissue and determining the ratio between counts from normal tissue to tumor tissue. The ratios were then normalized to the mean ratio and log2-transformed (Supplemental data of Banck et al. [3]). All samples with an m.log2 ≥0.25 were defined as "amplified". For easing of the interpretation, the m.log2 values were converted to fold changes (2^x) by us. m.log2 ≥0.25 results in a fold change of 1.189. The fold changes of the regions, in which the six signaling genes are located, ranged between 1.194 and 1.625; meaning that these huge CN gains depicted only low amplification amplitudes (the authors describe that only small/focal amplifications, which included mostly only two exons, depicted higher amplitudes up to 16-fold). To sum up, Banck et al. observed gene gains in conjunction with gains of larger chromosomal regions, comparable to our SNP array results. Our FISH results, however, revealed mostly gene specific amplifications, in contrast to polysomy or combined occurrence of amplification and polysomy, according to our definition of the different CN statuses. All detected amplifications/gains (by Banck et al., as well as our SNP array and FISH results) were defined as "low-level".

Copy number variations are not associated with poorer overall survival

To test whether single CN gains are associated with reduced overall survival, a Cox-Regression analyses for all six genes was performed. For patients with CN gains no significant differences in survival were seen compared to patients without any gains. Figure 21 depicts the Kaplan Meier plots for A) *AKT1*, B) *AKT2*, C) *PDGFRα*, D) *PDGFRβ*, E) *mTOR*, and F) *PIK3CD*. The analysis included all CN variations (amplification, amplification + polysomy, polysomy) in any tumor sample of a patient

(primary tumor, lymph node, and/or distant metastasis). The *p*-values are given in the legends.

In addition, investigation of all CN variations involved in the PI3K/AKT/mTOR pathway did not reveal any significant association with reduced overall survival (no amplification vs. amplification *p*=0.218, no amplification vs. 1xamplification vs. multiple amplifications *p*=0.458, no amplification vs. 1xamplification vs. 2xamplification vs. 3x+amplification *p*=0.598, no amplification vs. 1xamplification vs. 2xamplification vs. 3xamplification vs. 4x+amplification *p*=0.755, no amplification vs. 1xamplification vs. 2xamplification vs. 3xamplification vs. 4xamplification vs. 5x+amplification *p*=0.841, high amplifications (3-6) vs. low amplifications (0-2) *p*=0.455; no figures shown).

To sum up, CN gains in the PI3K/AKT/mTOR pathway do not seem to have a negative (or positive) impact on overall survival of the patients.

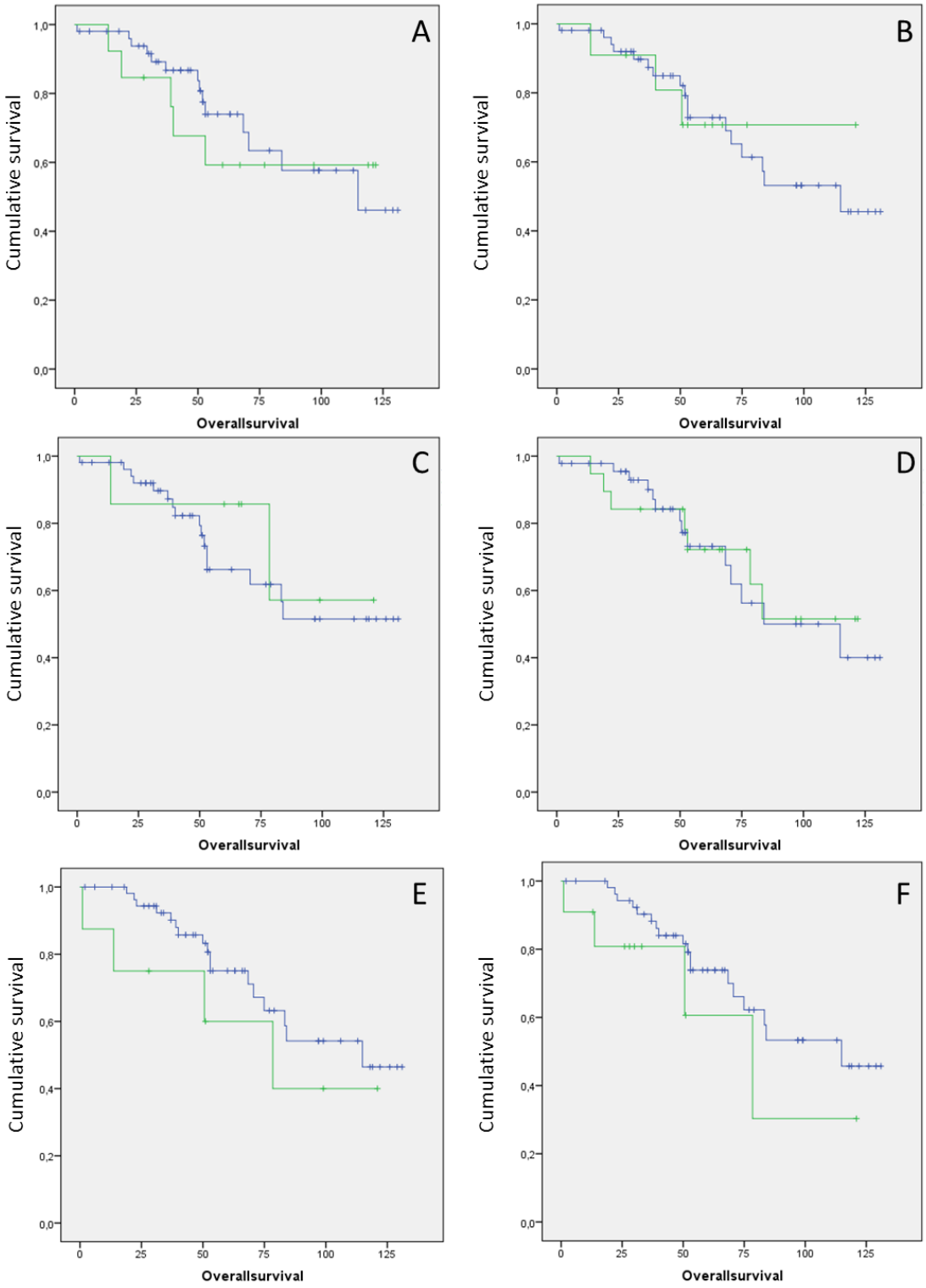

Figure 21: Kaplan Meier curves for the six genes of the PI3K/Akt/mTOR pathway investigated
A) *AKT1* *p*=0.77, B) *AKT2* *p*=0.90, C) *PDGFRα* *p*=0.60, D) *PDGFRβ* *p*=0.85, E) *mTOR* *p*=0.30, F) *PIK3CD* *p*=0.22; green: CN gain, blue: no CN gain, overall survival in months

Protein expression and activation of AKT, mTOR, and its downstream targets and its association with copy number gains in the PI3K/AKT/mTOR pathway

Activation of AKT, mTOR, and its downstream targets

The last aim was to determine if there is an association between gains of the above mentioned genes and expression of the encoded proteins. Therefore, a statistical analysis of gene gains with subsequent protein expression was performed. The protein expression was evaluated according to the immunoreactive score (see Table 17). Two cut offs were chosen for immunohistochemical staining: a) no/weak staining (Remmele score 0-3) against moderate/strong staining (Remmele score 4-12) and b) dichotomic distribution (0-6 vs. 7-12).

AKT2 was moderately to strongly expressed in 69% of primary tumors, 56% of lymph node metastases, and 79% of distant metastases. p-AKT showed moderate to strong expression in 42.5%, 37%, and 58% of primary tumors, lymph node, and distant metastases, respectively (Table 25, line 3). Dichotomic evaluation revealed strong expression of AKT2 in only 16, 11, and 7% of primary tumors, lymph node, and distant metastases, respectively. For p-AKT, the values were even lower with 9% (primary), 2% (lymph node), and 0% (distant metastases) (Table 25, line 5).

Moderate to strong (0-3 vs. 4-12) activation of mTOR was seen in 47% of primary tumors, 44% of lymph node, and 58% of distant metastases for p-mTOR. p-S6 was moderately to strongly expressed in only 8% of primary tumors and lymph node metastases, and 33% of distant metastases. In contrast, p4E-BP1 depicted strong expression in 69% of primary tumors, 23% and 30% of lymph node and distant metastases, respectively. However, when applying the dichotomic cut off (0-6 vs. 7-12), only 4% of primary tumors, 7% of lymph node, and 0% of distant metastases showed strong expression for p-mTOR. All samples showed only weak staining for p-S6, when using the dichotomic evaluation. p-4E-BP1 was strongly expressed in 12.5% of primary tumors; the metastases depicted only weak expression in this setting.

When looking at protein expression of the AKT/mTOR pathway in any tumor sample of one case (primary or lymph node or distant metastases), moderate to strong expression (4-12) of AKT2 and p-AKT was seen in 74% and 48%, respectively. In contrast, strong

expression was only detected in 21 and 8.5%, respectively. p-mTOR was moderately to strongly expressed in 55% of the SI-NET samples. Only 6.5% showed expression with staining scores of 6-12. Similar results were achieved for p-4E-BP1 with 67% (4-12) and 11% (6-12) moderate to strong expressed samples. For p-S6 both cut offs resulted in 14% of moderately to strongly expressed samples.

The difference of the results achieved with the two different cut-off values indicate that most of the samples showed moderate staining with scores of 4-6 for the different (phosphor-)proteins evaluated.

Table 25: Expression profile of AKT2, p-AKT, p-mTOR, and its downstream signaling molecules (IHC)

	AKT2	p-AKT (Thr308)	p-mTOR (Ser2448)	p-S6 (Ser240/244)	p-4E-BP1 (Ser65/Thr70)
Applicable cases	P: 98	P: 87	P: 89	P: 88	P: 88
	LN: 61	LN: 54	LN: 43	LN: 60	LN: 39
	DM: 14	DM: 12	DM: 12	DM: 12	DM: 10
	any: 113	any: 106	any: 107	any: 108	any: 104
No/weak stained cases [0-3]	P: 31% (30/98)	P: 57.5% (50/87)	P: 53% (47/89)	P: 92% (81/88)	P: 31% (27/88)
	LN: 44% (27/61)	LN: 63% (34/54)	LN: 56% (24/43)	LN: 92% (55/60)	LN: 77% (30/39)
	DM: 21% (3/14)	DM: 42% (5/12)	DM: 42% (5/12)	DM: 67% (9/12)	DM: 70% (7/10)
	any: 26% (29/113)	any: 52% (55/106)	any: 45% (48/107)	any: 86% (93/108)	any: 33% (34/104)
Moderate/strong stained cases [4-12]	P: 69% (60/98)	P: 42.5% (37/87)	P: 47% (42/89)	P: 8% (7/88)	P: 69% (61/88)
	LN: 56% (34/61)	LN: 37% (20/54)	LN: 44% (19/43)	LN: 8% (5/60)	LN: 23% (9/39)
	DM: 79% (11/14)	DM: 58% (7/12)	DM: 58% (7/12)	DM: 33% (4/12)	DM: 30% (3/10)
	any: 74% (84/113)	any: 48% (51/106)	any: 55% (59/107)	any: 14% (15/108)	any: 67% (70/104)
No-to-moderate stained cases [0-6]	P: 84% (82/98)	P: 91% (79/87)	P: 96% (85/89)	P: 100% (88/88)	P: 87.5% (77/88)
	LN: 89% (54/61)	LN: 98% (53/54)	LN: 93% (40/43)	LN: 100% (60/60)	LN: 100% (39/39)
	DM: 93% (13/14)	DM: 100% (12/12)	DM: 100% (12/12)	DM: 100% (12/12)	DM: 100% (10/10)
	any: 79% (89/113)	any: 91.5% (97/106)	any: 93.5% (100/107)	any: 86% (93/108)	any: 89% (93/104)
Strong stained cases [6-12]	P: 16% (16/98)	P: 9% (8/87)	P: 4% (4/89)	P: 0% (0/88)	P: 12.5% (11/88)

	LN: 11% (7/61)	LN: 2% (1/54)	LN: 7% (3/43)	LN: 0% (0/60)	LN: 0% (0/39)
	DM: 7% (1/14)	DM: 0% (0/12)	DM: 0% (0/12)	DM: 0% (0/12)	DM: 0% (0/10)
	any: 21% (24/113)	any: 8.5% (9/106)	any: 6.5% (7/107)	any: 14% (15/108)	any: 11% (11/104)

In Figure 22, exemplary stainings of AKT2, p-AKT (Thr308), and p-mTOR are shown. Figure 23 shows immunohistochemical staining of the mTOR downstream signaling proteins p-4E-BP1 (with and without complementary peptide) and p-S6.

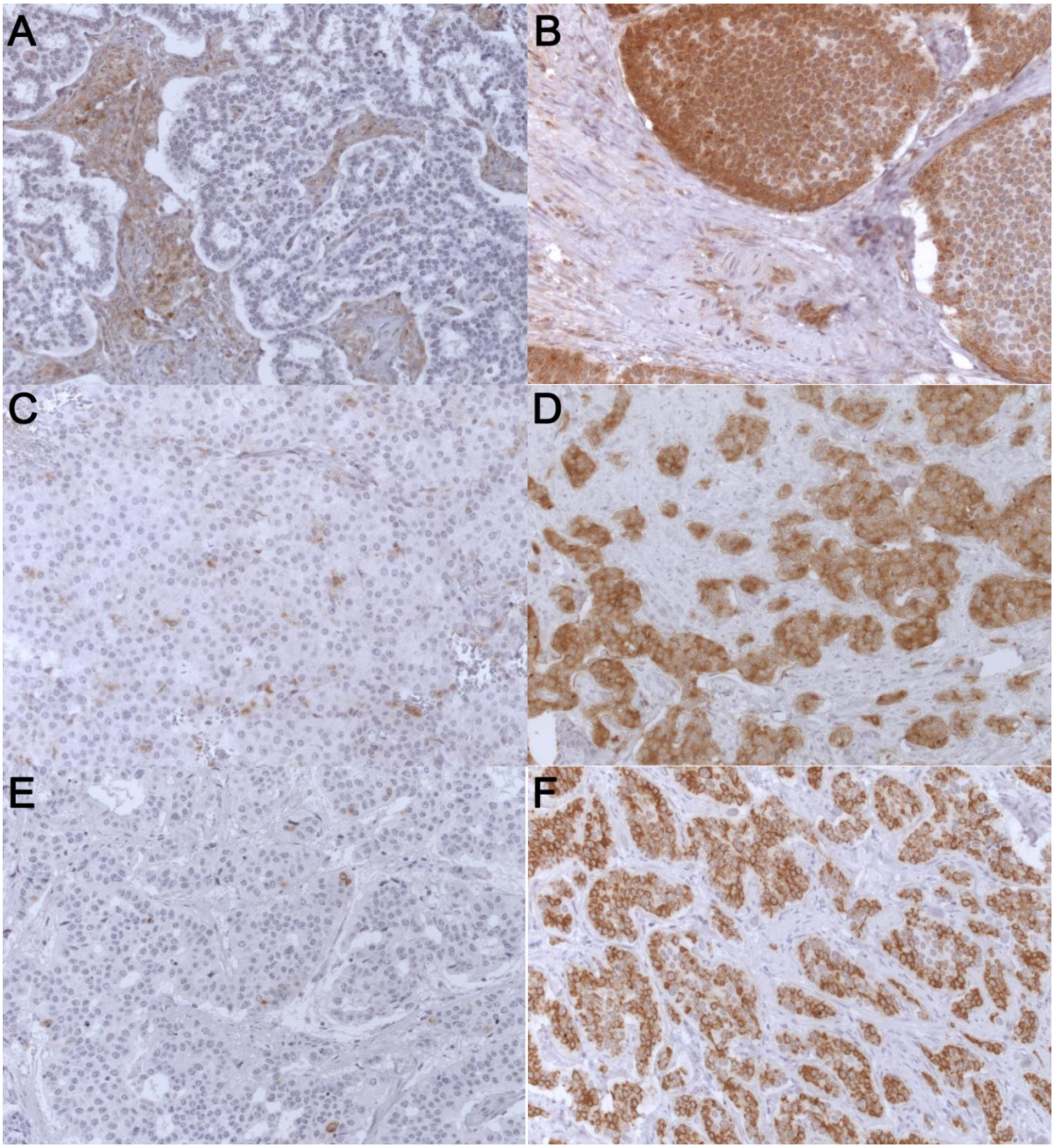

Figure 22: Immunohistochemical stainings of AKT2, p-AKT, and p-mTOR in SI-NETs
Picture (A) depicts an AKT2 negative, (B) an AKT2 positive, (C) a p-AKT negative, (D) a p-AKT positive, (E) a p-mTOR negative, and (F) a p-mTOR positive case. Magnification: 200x

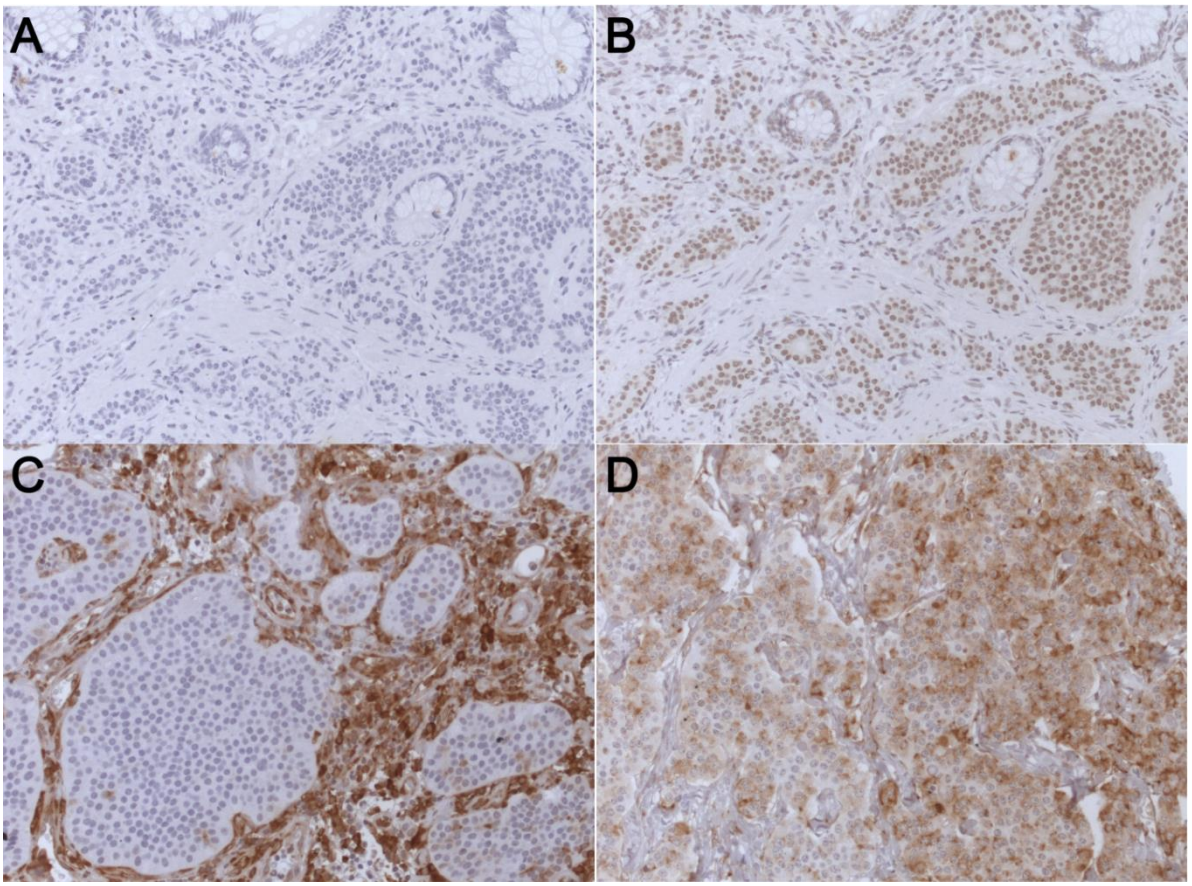

Figure 23: Immunohistochemical stainings of mTOR downstream molecules in SI-NETs
Picture (A) depicts a p-4E-BP1 positive case with use of a complementary peptide and (B) without peptide. (C) shows a p-S6 negative and (D) a p-S6 positive case. Magnification: 200x

Copy number gains of the PI3K/AKT/mTOR pathway are not associated with protein expression or activation

In order to identify possible associations between copy number gains and the protein expression and activation status, Pearson's Chi-square test was applied. Copy number gains in primary tumors, lymph node, and distant metastases alone or together were analyzed against immunohistochemical stainings of p-mTOR, p-S6, and p-4E-BP1 (both cut-offs), as well as against any activation of the three proteins. Finally, multivariate analysis was performed to address the association between any gains in the pathway and the protein expression achieved by IHC (Appendix Table 31).

No significant association between gene gains and subsequent protein expression could be determined. In some cases, even the opposite event occurred, so that the

protein expression was inversely correlated with the amplification of the gene, suggesting that the amplifications do not result in enhanced protein expression.

V. Discussion

Parts of the discussion described on page 111-118 are already published in [50].

Part 1: Chromosome 18

Neuroendocrine tumors of the gastroenteropancreatic system (GEP-NETs) comprise a multiplicity of different neoplasms that differ in tumor biology and prognosis [5]. What they have in common, however, is their origin in single neuroendocrine cells or neuroendocrine islets of the diffuse neuroendocrine system. Although SI-NETs are slow-growing neoplasms, they are nevertheless tumors with a morbidity rate that cannot be neglected (23.5% after 10 years for G1 and 30.3% for G2, respectively [8]).

Loss of (a part) of Chr18 found in approximately 70% of SI-NETs has been shown in several previous studies to be a common event in SI-NETs, and seems to be an early event of tumorigenesis. No other frequent genetic alterations or putative affected pathways have been implicated in the tumorigenesis of SI-NETs as yet. A number of studies (reviewed in [39]) investigated the possible effect of Chr18 loss. However, there is no comprehensive data on Chr18-related alterations at transcriptional level in SI-NETs. One conceivable possibility is the loss of tumor suppressor activity of Chr18-related tumor suppressors. The first part of my doctoral thesis focused on the investigation of six putative tumor suppressors on Chr18 using RNA or protein-based assays, comparing SI-NETs with and without Chr18 losses.

First, the most relevant Chr18-related tumor suppressors, SMAD2 and SMAD4, which are important signal transduction molecules in the TGFβ pathway, were evaluated [40]. SMAD4 is functionally inactivated in different types of cancer such as pancreatic adenocarcinomas [44], metastatic colorectal cancer [42] and small intestine adenocarcinomas [46]. SMAD2 has also been described as being altered in a variety of cancers, although to a lesser extent than SMAD4 [43, 45].

Western blot analyses confirmed that the loss of SMAD2 and SMAD4 protein expression is not commonly found in a cohort of 14 SI-NETs. Previous work done by the working group of Prof. Sipos revealed 100% expression of SMAD2 in 87 FFPE

samples by IHC; SMAD4 was only lost in three out of these 87 tumor samples. These findings correlate with data from Löllgen et al., who analyzed a small panel of seven neuroendocrine tumors of the midgut by SMAD4 immunohistochemistry and found no loss of SMAD4 protein expression in these samples [110]. The western blot results support the previous findings; indicating that SMAD2 and SMAD4 do not play a role in the tumorigenesis of SI-NETs.

In 1990, DCC (deleted in colorectal cancer) was identified to be frequently deleted in colorectal carcinoma [47]. Meanwhile, reduced expression of DCC has been described in a variety of cancers [111, 112]. *DCC* encodes a netrin-1 receptor, which induces apoptosis in the absence of netrin-1 [48]. Abridged expression of DCC could result in less apoptosis and thus give rise to tumor progression. DCC is a 158.5 kDa transmembrane protein with at least 18 splice variants (7 being protein coding). Since no reliable anti-DCC antibodies for IHC exist, DCC expression was assessed using qRT-PCR of different exon boundaries and western blot assays with peptide competition. qRT-PCR of *DCC* revealed no difference in expression between the two cohorts (38 with and 13 samples without loss of Chr18). Western blot showed a loss/reduced expression of DCC in 29% (6/21) SI-NETs. The specificity of the assay was verified with a biological positive control (IMR-32 cell line) competition of the reaction with corresponding peptide and the mass spectrometry of the positive control. The mechanism of loss of DCC has yet to be unraveled. Possible explanations are alternative splicing. The DCC gene is composed of 29 exons. Exons 1-7 encode for the four immunoglobulin domains, exons 8-21 for the fibronectin-type III domains, and exons 22-29 for the intracellular domain (Figure 24).

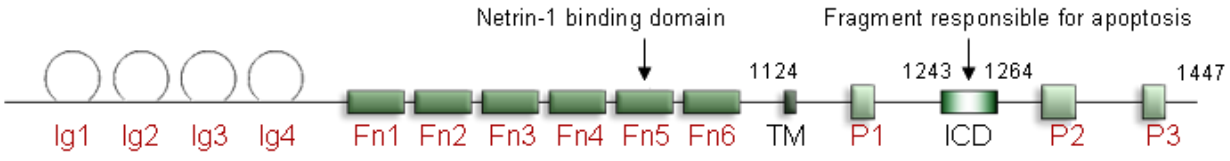

Figure 24: Domains of the DCC protein
Ig: immunoglobulin, Fn: fibronectin-type III, TM: transmembrane domain, ICD: intracellular domain, P: conserved domains (www.atlasgeneticsoncology.org)

Alternative splicing resulting in abnormal DCC transcript has already been described in colon cancer [113, 114]. One splice site occurs between exon 17 and 18, which encodes for the region between fibronectin domain 4 and 5. qRT-PCR was performed to address this specific exon boundary as well as the exon boundary of exon 3 and 4, which encodes for Ig domains of the protein (Figure 24). Reale et al. reported that loss of the splicing site between two fibronectin domains leads to inactivation of DCC [114]. Another publication on alternative splicing of DCC in cancer found, that colon cancer cell lines only express the proximal (exon 2) and distal exons (exons 28-29); exons in the center of the gene were confirmed to be absent [113]. This finding correlated with loss of protein expression in the cell lines. The qRT-PCR analysis of our SI-NET samples revealed *DCC* to be low to not expressed (Cp values 33-35) with no expression difference between the two intron-spanning primer pairs. This marked reduction of mRNA expression and possibly alternatively spliced gene could therefore result in reduced protein expression, as was detected in 29% of our SI-NET samples, comparable to the findings in colon cancer.

Another silencing mechanism of DCC, which was described in head and neck squamous as well as esophagus cancer, is the methylation of the *DCC* promoter CpG island [115, 116]. Further studies will shed light on the mechanisms, which lead to loss/reduction of protein expression in our SI-NET cohort.

Remarkably, Francis et al. reported the highest rate (29%) of intronic alterations in the *DCC* gene out of all putative tumor suppressor candidates on Chr18, rendering this gene even more interesting [2].

TCEB3C encodes for Elongin A3, a transcription elongation factor identified in 2002 [61]. *TCEB3C* is a maternally imprinted gene on Chr18 [60] and hence only one mutational hit is required to fulfill the Knudson's two-hit hypothesis. Edfeldt and colleagues were able to show that *TCEB3C* is epigenetically repressed in the human SI-NET cell line CNDT2.5 due to histone and DNA methylation. They found that 77% of human tumor samples with only one *TCEB3C* copy were completely or mostly negative for Elongin A3 IHC staining. However, one primary tumor, a lymph node metastasis and a liver metastasis with two gene copies displayed also (partly) negative staining [62].

qRT-PCR of *TCEB3C* in 69 FFPE samples revealed significant downregulation in SI-NET with loss of Chr18 compared to samples with two copies (p=0.01). However, no reduction or loss of protein expression was detected in 21 fresh frozen samples. These results indicate that reduced mRNA expression was not associated with a relevant loss of protein; however only one cryo-conserved sample with retained Chr18 status was available for western blot analysis. It is possible, that the evaluation of more 2xChr18 SI-NET samples by western blot could detect a difference in protein expression between 1xChr18 and 2xChr18 samples. Nevertheless, all 1xChr18 SI-NETs depicted strong Elongin A3 expression, reducing the impact of the differential qRT-PCR findings.

CABLES is a cell cycle regulatory protein that plays a role in proliferation and differentiation [53]; the encoding gene was found to be silenced in ovarian, colorectal, endometrial, and non-small lung cancer [54-57]. qRT-PCR of *CABLES* exhibited a slight downregulation of *CABLES* (p=0.03) in SI-NET samples with Chr18 loss compared to tumors with diploid Chr18 in our cohort of 69 FFPE samples. However, similar to the Elongin A3 results, all samples showed strong protein expression in western blot analysis, suggesting the qRT-PCR findings to be of reduced relevance for the protein expression in general. An interesting observation was that all SI-NET samples depicted an additional band at ~55 kDa in the western blot, whereas the positive control cell line HEK293 only depicted the normal doublet band (~67 kDa). It has been reported, that the *CABLES* gene undergoes aberrant splicing in tumors, which can result in the loss of the CDK-binding domain, thereby demolishing the interaction with CDKs [59]. Normally, CDK2 is involved in the G_1-S transition and DNA replication. Its activity is inhibited by Wee1 tyrosine 15 phosphorylation, which is dramatically enhanced by CABLES [1]. Loss of the CDK-binding domain could therefore result in faster progression through the cell cycle, finally leading to uncontrolled cell growth and enhanced tumor formation. Analysis of the transcriptome and proteasome could shed light on the question if all samples suffered from the same aberrant splicing event and if the CDK-binding domain is really impaired. This will be subject of our further investigations.

Zukerberg and colleagues reported a (partial) loss of CABLES in 92% (23/25) of SI-NETs by IHC [58]. The loss did not correlate with grade/stage/survival data. Whether the loss of CABLES expression was caused by the loss of Chr18 was not evaluated in

this study. They also found loss of CABLES in NETs from other sites, which are not associated with loss of Chr18 (e.g. lung), indicating that chromosomal deletion is not the mechanism of CABLES inactivation. It would be interesting to test whether epigenetic silencing could be the reason for the frequent loss of CABLES in NETs of other origin than small intestine.

PMAIP1 is a pro-apoptotic gene, whose protein functions in a p53-dependent manner [52]. In 2008, PMAIP1 was identified as a potential tumor suppressor in pancreatic cancer by comparative cDNA microarray analysis [51]. In our cohort of 69 FFPE samples, qRT-PCR of *PMAIP1* revealed high Cp values, suggesting that *PMAIP1*-mRNA is low abundant in SI-NETs irrespective of their Chr18 status. The protein PMAIP1 was not expressed in the eight samples investigated by western blot. This finding would make PMAIP1 an interesting candidate. However, due to the small sample size the explanatory power is slightly reduced. On the other hand, a 100% loss of a tumor suppressor during tumorigenesis is highly unlikely. Another explanation for the finding could be that PMAIP1 is not present in neuroendocrine cells at all. Preliminary experiments of the working group of Prof. Sipos could show that this is true for Maspin, which is only expressed in mucin-producing cells of the normal ileal mucosa and absent in the neuroendocrine cells. Unfortunately, no supportive antibody for PMAIP1 immunofluorescence staining was available, making the application of a double staining (synaptophysin and PMAIP1) unfeasible.

In summary, the systematic search for putative tumor suppressor proteins, which could get lost during tumorigenesis in SI-NETs, revealed DCC as the sole promising candidate in 29% of SI-NETs, although the mechanism of loss remains unclear.

The design of the project has strengths and limitations which need to be addressed to value the results accordingly. The strengths include the comprehensive approach of all Chr18-related events and the thorough examinations of the putative tumor suppressors at protein level. The power of the study is limited by the low number of frozen tissue samples (8-21); however, most of the tumor suppressors exhibited an unequivocal expression profile, so that it was possible to draw clear conclusions. The second limitation lies in the lack of high value antibodies for immunohistochemistry, making it

impossible to investigate high numbers of FFPE samples and to study co-localization of tumor suppressors in normal NE cells.

The next step was the search for novel putative tumor suppressor candidates located on Chr18. SNP array analysis and exome sequencing were conducted to identify additional genetic events on the remaining copy of Chr18, such as LOH, which could lead to the inactivation of tumor suppressor genes. SNP array analysis revealed loss of Chr18 in six of eight analyzable tumors, one tumor depicted a mosaic pattern and one tumor had two copies of Chr18. In the samples with loss / mosaic status of Chr18 no additional loss could be detected, indicating that the second hit of a Chr18 tumor suppressor does not underlie a genetic mechanism. Remaining possibilities are epigenetic events or post-translational modifications, which could affect the protein structure/stability. Since partial losses of Chr9 and 12 were also detected in one primary tumor and one pair of primary tumor and matching metastasis, respectively, further studies should concentrate on potential tumor suppressors located in these areas.

Recently, Karpathakis et al. described three different subtypes of SI-NETs, concerning their molecular pattern. The largest group was defined by loss of Chr18, CIMP negativity, and presence of *CDKN1B* mutation. It was associated with older age at onset and longer PFS, compared to the other subgroups, suggesting a less aggressive phenotype. In contrast, patients with multiple CNVs (Chr18 loss, gain of Chr4, 5, 20) had a younger age of onset in combination with a shorter PFS, indicating a more aggressive phenotype [96]. This subgroup is contrary to the grouping of Nilsson et al., where Chr18 loss seems to be exclusive of chromosomal gains [39]. Our SNP array analysis revealed tumors of three patients (the two primaries Tu1 and Tu7, and the matching metastases Tu1 Met and Tu7 Met, and Tu2) to harbor Chr18 loss and gain of Chr4 and 20. The two pairs of primary and metastasis also depicted gain of Chr5. So, these patients of our collective seem to fit in the prognostic least favorable group with multiple CNVs defined by Karpathakis et al. In contrast, Tu4 and Tu5 Met depicted Chr18 loss as sole alteration, whereas Tu3 had a mosaic pattern regarding Chr18. Our findings support the fact that Chr18 loss can occur as single chromosomal variation in SI-NETs, or appears in combination with other CN variations (gains and losses).

Five SI-NETs, that showed complete (n=4) or partial (n=1) loss of Chr18, were analyzed by exome sequencing. No SNVs or InDels in known tumor suppressor genes were detected. To extend this search, a data comparison with the supplementary data set of the study by Banck et al. [3] was conducted. Again, no relevant additional losses (SNVs in all six tumor suppressors investigated) were detected.

Regarding other Chr18-related genes, three somatic mutations by exome sequencing that could be validated by Sanger sequencing were found. One patient carried SNVs in the *CABYR* and *NFATC1* genes, whereas a 3-base pair deletion in *PIEZO2* was present in another patient. The three remaining patients showed no genetic alterations in Chr18 genes. NFATC1 becomes activated by calcium flux, resulting in translocation from the cytoplasm to the nucleus, where it promotes *de novo* gene transcription. It seems to play a role in various cancer types, e.g. by overexpression and/or promotion of tumor angiogenesis [117]. *NFATC1* could therefore represent an interesting candidate gene for tumor progression of SI-NETs, which is why it was further analyzed in a set of 30 SI-NET FFPE samples by Sanger sequencing of all functional gene regions (Dr. Laura Stoß). No additional somatic *NFATC1* mutations were found in this cohort of tumors, suggesting that *NFATC1* mutations are not a common event in SI-NETs. Piezos are large transmembrane proteins conserved among various species. PIEZO2 is involved in rapidly adapting mechanically activated currents in somatosensory neurons [118]. It is not known, whether PIEZO2 plays a role in tumor progression. CABYR, a calcium-binding tyrosine phosphorylation regulated fibrous sheath protein, was initially reported to be testis-specific and subsequently shown to be present in brain tumors, pancreatic, and lung cancer [119]. CABYR is a CT (cancer/testis) antigen widely expressed in diverse cancer cells [120]. 42 carcinoid endocrine tumors of the small intestine showed no mutations in CABYR (Cosmic, Wellcome Trust Sanger Institute). Mutations (31) and CNVs (1225 entries) in this gene seem to be common in different kinds of tumors, e.g. breast, large intestine, lung, and pancreas (Cosmic, Wellcome Trust Sanger Institute).

These results, in line with recent data from Banck et al. [3] and Verdugo et al. [121], indicate clearly, that SI-NETs do not harbor recurrent somatic mutations. Data comparison with Banck et al. revealed *ADCY5* to be the only gene mutated in both data

sets. However, only the SNV found in our collective was predicted to be damaging. Therefore, mutations of *ADCY5* seem to reflect passenger mutations, similar to all other mutations detected (including the *PML* mutations, detected in our tumor samples), with no driving impact on SI-NET development in general.

In summary, the question arises as to how one can explain the effect of the Chr18 loss in SI-NETs. One possible mechanism is haploinsufficiency of one of the putative tumor suppressors. Of the six putative tumor suppressor genes, it has been shown that SMAD4 haploinsufficiency significantly alters TGF-β and BMP (Bone morphogenetic protein) signaling, and that a SMAD4 dose-dependent transcriptional regulation of target genes of the TGF-β and Wnt signaling pathways in a *SMAD4*-mutant mouse model exists [122]. A second possible mechanism may be explained by the study of Solimini et al. They were able to show that pro-proliferative genes (GO genes) are often enriched and anti-proliferative genes (STOP genes) are underrepresented by hemizygous deletions in malignant tumors [123]. In other words, multiple haploinsufficiencies probably contribute to proliferative fitness of cancers. This hypothesis may at least in part explain the significance of Chr18 loss in SI-NETs. In conclusion, this study on loss of putative tumor suppressor proteins on Chr18 was able to show, that DCC is the only tumor suppressor that is lost in 29% of SI-NETs, in contrast to retained expression of SMAD2, SMAD4, CABLES (aberrant splicing?), and Elongin A3. PMAIP1 is possibly not expressed at all in SI-NETs. This finding should be interpreted as a feature of neuroendocrine cells in small intestine in general, rather than as a complete loss of these molecules during tumorigenesis. No recurrent Chr18 alterations could be found by exome sequencing of SI-NETs (in line with data from [2, 3, 121]), which could identify new potential tumor suppressors. Further studies should concentrate on Chr18-related alterations of transcriptome or proteome signatures to shed light on more complex events such as potential haploinsufficiencies of tumor suppressors or transcriptional/posttranscriptional events such as alternative splicing of Chr18 transcripts. Recently, a transcriptome analysis of 33 ileal NETs defined three clinical relevant subgroups of tumors [124], but unfortunately differences between tumors with and without loss of Chr18 were not part of the analysis and therefore remain to be elucidated.

Part 2: PI3K/AKT/mTOR-pathway

In 2013, Banck et al. published the genomic landscape of neuroendocrine tumors of the small intestine [3]. Apart from showing that SI-NETs are genetically stable tumors, they detected an accumulation of amplifications in the PI3K/AKT/mTOR pathway.

Amplifications may lead to constant activation of this pathway, resulting in enhanced proliferation, cell survival and angiogenesis [66], promoting tumorigenesis. Since surgery is the sole curative therapy for SI-NETs and only possible in 20% of patients [97], new approaches are strongly needed. A series of FDA approved drugs is available for mutated or amplified genes involved in different pro-tumorigenic pathways in a broad range of tumor types. However, only few studies focused on GEP-NETs in regard of the use of these drugs.

In 2009, Pitt and colleagues showed that the PI3K inhibitor LY294002 (which binds the p110δ catalytic subunit thereby preventing AKT1 phosphorylation), as well as small interfering RNA (siRNA) targeting AKT1, lead to suppression of cell growth in the pancreatic carcinoid cell line BON-1 [125].

Another group did a druggable approach by analyzing different genes/proteins on mutational and expression level [126]. They found 35% of SI-NETs to harbor low grade EGFR amplifications (aneuploid tumors with >2.47 signals/nucleus), suggesting anti-EGFR tyrosine kinase inhibitors (TKI) and monoclonal antibodies to be potential drugs for GEP-NETs.

Finally, the RADIANT-4 study showed, that advanced, non-functional neuroendocrine tumors of the gastrointestinal tract benefit from everolimus, a potent mTOR inhibitor, in regard of prolonged progression-free survival [4].

Therefore, the second part of my doctoral thesis focused on the PI3K/AKT/mTOR pathway: Six genes, namely *PIK3CD*, *AKT1*, *AKT2*, *PDGFRα*, *PDGFRβ*, and *mTOR* were analyzed by FISH. Low level amplifications (partially in combination with increased reference chromosome signals) were detectable in 4-14% in primary tumors, 9-27% in lymph node metastases, and 8-36% in distant metastases (Figure 16). Statistical analysis revealed higher frequencies of CN gains in tumors of advanced, metastatic

stage (p=0.028) and more invasive tumors (p=0.014). Additionally, for *AKT1* (p=0.005), *AKT2* (p=0.014), *PDGFRα*, and *PDGFRβ* (both p<0.000) significantly higher proportions of amplifications were found in the metastases (lymph node and distant metastases combined) compared to primary tumors.

We sometimes observed co-amplification of the centromere signal with the target signal by FISH; the CN data from Banck et al. [3] and our SNP array results revealed the amplified genes to be included in huge regions which are affected in total by CN gains, in contrast to single gene specific amplifications.

The frequent association of gene specific signals with CN gains of the reference chromosomes has already been described for *AKT1* and *AKT2* in lung carcinomas, resulting in mean ratios of 1.29 and 1.66, respectively [63]. The authors reported that single *AKT* amplifications were rare, but that polysomy seems to be a frequent deregulation in these tumors. However, they found a significant correlation between gene gains and protein overexpression.

No significant association could be found between gains on DNA level and protein expression in our investigation of the PI3K/AKT/mTOR pathway. One possible explanation might be that the gains have no impact on single gene level but on chromosomal level. As described before, SI-NETs often harbor gains of a number of (parts of) chromosomes (e.g. Chr4, 5, 14, and 20). So, amplifications of single genes could be passenger effects of gains of whole chromosomes. This hypothesis is supported by the fact, that nearly all of the patients with *PI3K/AKT/mTOR*-amplified tumors harbored amplifications in more than one gene. Interestingly, one tumor (I105) exhibited loss of one gene specific signal for five out of the six genes, indicating loss of Chr1 (*mTOR*, *PIK3CD*), Chr4 (*PDGFRα*), Chr5 (*PDGFRβ*), and Chr14 (*AKT1*). *AKT2*, which is located on Chr19, was not affected. This specific rearrangement pattern affecting the chromosomes commonly underlying CN gains in SI-NETs, points out, that these tumors are driven by alterations on chromosomal level, rather than by gains of single genes. However, CN gains of regions in which genes of pro-tumorigenic pathways are located, can result in enhanced gene function, although no specific amplification exists. This has also been shown for CN gains of *HER2* in breast cancer,

with normal *HER2*:Chr17 ratios due to Chr17 polysomy [127]. In a retrospective study it could be shown, that polysomy is no counter argument against trastuzumab medication. IHC results were of better prognosis for treatment response compared to *HER2*:Chr17 ratios [128]. Other reports state that polysomy does not necessarily lead to protein overexpression [129]. The authors ask, if the absolute *HER2* gene copy number may be the best predictor for trastuzumab response, irrespective of underlying polysomy or amplification.

Since no significant association between CN gains and protein expression could be found in our cohort of SI-NETs, similar questions should be addressed. The most important question is if/why the extra chromosome copies could/should hamper or block the effect of the additional gene copies. In metastatic colorectal cancer (mCRC) a similar situation occurs concerning *EGFR* amplifications / co-amplification with Chr7, since “true” amplifications – defined as more than 2x *EGFR* signals compared to the CEP7 signals – are rarely seen in these tumors. Nevertheless, the *EGFR* amplification is used as predictive biomarker for response prediction of the therapy with anti-EGFR monoclonal antibodies, such as cetuximab, in *KRAS* wildtype mCRC [130]. More retrospective studies on effectiveness of monoclonal antibodies in cancers with gene amplification accompanying chromosome polysomy and the dependence of the drug impact on protein overexpression could help resolve the question of drug application in tumors with this kind of alterations.

For head and neck squamous cell carcinoma it has been shown, that CN gain or amplifications of 3q26, harboring *PIK3CA* amongst other genes, are early and frequent aberrations [131]. This alteration was significantly associated with a lower differentiation grade and a higher tumor stage, comparable to our findings regarding CN variations in the PI3K/AKT/mTOR pathway and the association with more invasive and advanced, metastatic tumors. Suh et al. could even demonstrate, that CN gains of *PIK3CA* is a poor prognostic factor for disease-free survival in liposarcomas, in contrast to *PIK3CA* mutations [132].

Others found, that gene amplifications do not necessarily result in protein overexpression, suggesting that epigenetic events might play a role in the

transcriptional control of amplified genes [133]. Since we observed, that gene gains and protein expression were not – partly even inversely – correlated in SI-NETs, such mechanisms could play a role here as well.

All these publications underline the results which were achieved by analyzing genes of the PI3K/AKT/mTOR pathway by FISH and protein expression of downstream molecules by IHC. CN gains were present in 12-24% of our cohort, revealing slightly higher frequencies than the ones detected by the study of Banck et al., and seem to define a subgroup of advanced and more invasive tumors of higher UICC-stages. Since especially this group is in need of new anti-cancer drugs, it would be interesting to test, whether monoclonal antibodies or inhibitors of these targets have an effect on tumor dissemination and invasiveness. Although no association between CN gains and overall survival could be detected, inhibition of the PI3K/AKT/mTOR pathway could slow down tumor cell growth and thereby tumor progression and formation of metastases. The usefulness of these findings for future therapeutic interventions remains to be seen.

The analysis of the PI3K/AKT/mTOR pathway by FISH and IHC has its strength and limitations, which are important to have in mind for the interpretation of the results. The great sample size achieved by using TMAs for the analysis is an advantage, which results in greater power of the statistical evaluation. Therefore, the finding of a significant association between accumulation of CN variations and more developed/invasive tumor stages is a reliable result. The second strength is the thorough investigation of this pathway by analyzing key players by FISH and IHC. We therefore could rule out, that the CN gains result in overexpression of the respective (downstream) effector proteins. One possible explanation for this finding is, that the gene gains were partially accompanied by chromosome polysomy, so that the alteration affects not one specific gene, but a greater area on the respective chromosome. However, the interaction of different affected genes could give rise to altered protein expression not yet detected and subsequent changed signaling cascades. Another explanation for the missing translation of gene amplifications into protein overexpression might be that epigenetic events regulate the transcription of amplified genes.

One drawback of the study is the heterogeneity of tumor tissues owing to the usage of TMAs. Therefore, the fixation of the biopsies of different tissue blocks can vary greatly, so that some samples had to be excluded from the evaluation due to low sample quality. One disadvantage lies in the FISH analysis itself, since the evaluation is time-consuming due to counting the gene specific and the reference chromosome signals separately of 30-100 cells per sample. Based on the fact, that a certain observer bias is also not dismissed, a second assessor is to be recommended.

Concluding remarks

This thesis focused on the genetic alterations in SI-NETs, since up to know only little is known about driver mutations giving rise to these tumors.

We could demonstrate that the common Chr18 loss seems to result in a partial loss of the tumor suppressor protein DCC. Another interesting finding regarding Chr18-associated tumor suppressors, is the fact, that CABLES depicted additional isoforms in the western blot analysis of SI-NETs, possibly as a result of aberrant splicing. These two candidates will be subject of further investigations in our lab.

The PI3K/AKT/mTOR pathway is deregulated in 12-24% of our SI-NET samples. Although the gene amplifications were not reflected by protein overexpression, the alterations defined a subgroup of more advanced and invasive tumors. Since especially patients with tumors of these stages are in urgent need of new anti-cancer drugs, inhibitors of the PI3K/AKT/mTOR pathway should be tested in functional gastrointestinal NETs.

Another outcome of this study is the possible use of Chr18 loss and CN gains as distinct tumor markers for SI-NETs. Unpublished data of our work group suggest the usefulness of these variations for distinguishing SI-NETs from appendiceal NETs (a-NET). A- and SI-NETs are phenotypical similar tumors (sharing the same embryonic origin), but whereas SI-NETs show high malignant behavior, manifesting in early lymph node and distant metastases, a-NETs are indolent tumors and often found incidentally. The 5-year survival rate of a-NETs ranges between 74% and 95% [134, 135]. We suggest that the mortality rate of a-NETs might be overrated due to false disease coding and imprecise data on causes of death. Usage of Chr18 FISH in combination

with analysis of CN gains (by FISH or SNP array) could help to improve the data and making a precise diagnosis, since these alterations were not present in our cohort of 15 a-NETs (unpublished data).

VI. References

1. Wu, C.L., et al., *Cables enhances cdk2 tyrosine 15 phosphorylation by Wee1, inhibits cell growth, and is lost in many human colon and squamous cancers.* Cancer Res, 2001. **61**(19): p. 7325-32.
2. Francis, J.M., et al., *Somatic mutation of CDKN1B in small intestine neuroendocrine tumors.* Nat Genet, 2013. **45**(12): p. 1483-6.
3. Banck, M.S., et al., *The genomic landscape of small intestine neuroendocrine tumors.* Journal of Clinical Investigation, 2013. **123**(6): p. 2502-2508.
4. Yao, J.C., et al., *Everolimus for the treatment of advanced, non-functional neuroendocrine tumours of the lung or gastrointestinal tract (RADIANT-4): a randomised, placebo-controlled, phase 3 study.* Lancet, 2015.
5. Modlin, I.M., et al., *Gastroenteropancreatic neuroendocrine tumours.* Lancet Oncology, 2008. **9**(1): p. 61-72.
6. Frilling, A., et al., *Neuroendocrine tumor disease: an evolving landscape.* Endocr Relat Cancer, 2012. **19**(5): p. R163-85.
7. Cancer, T.I.A.f.R.o., *WHO Classification of Tumours of the Digestive System*. 4th ed. 2010.
8. Jann, H., et al., *Neuroendocrine tumors of midgut and hindgut origin: tumor-node-metastasis classification determines clinical outcome.* Cancer, 2011. **117**(15): p. 3332-41.
9. Chopin-Laly, X., et al., *Neuroendocrine neoplasms of the jejunum: a heterogeneous group with distinctive proximal and distal subsets.* Virchows Arch, 2013. **462**(5): p. 489-99.
10. Massironi, S., et al., *Neuroendocrine tumors of the gastro-entero-pancreatic system.* World J Gastroenterol, 2008. **14**(35): p. 5377-84.
11. Tsikitis, V.L., B.C. Wertheim, and M.A. Guerrero, *Trends of incidence and survival of gastrointestinal neuroendocrine tumors in the United States: a seer analysis.* J Cancer, 2012. **3**: p. 292-302.
12. Kulke, M.H., et al., *Future directions in the treatment of neuroendocrine tumors: consensus report of the National Cancer Institute Neuroendocrine Tumor clinical trials planning meeting.* J Clin Oncol, 2011. **29**(7): p. 934-43.
13. Kloppel, G., *Classification and pathology of gastroenteropancreatic neuroendocrine neoplasms.* Endocrine-Related Cancer, 2011. **18 Suppl 1**: p. S1-16.
14. Modlin, I.M., K.D. Lye, and M. Kidd, *A 5-decade analysis of 13,715 carcinoid tumors.* Cancer, 2003. **97**(4): p. 934-959.

15. Wang, G.G., et al., *Comparison of genetic alterations in neuroendocrine tumors: frequent loss of chromosome 18 in ileal carcinoid tumors.* Modern Pathology, 2005. **18**(8): p. 1079-1087.
16. Anlauf, M., et al., *[Neuroendocrine neoplasms of the distal jejunum and ileum].* Pathologe, 2014. **35**(3): p. 283-93; quiz 294.
17. Wong, H.H. and P. Chu, *Immunohistochemical features of the gastrointestinal tract tumors.* J Gastrointest Oncol, 2012. **3**(3): p. 262-84.
18. Ramage, J.K., et al., *Guidelines for the management of gastroenteropancreatic neuroendocrine (including carcinoid) tumours (NETs).* Gut, 2011. **61**(1): p. 6-32.
19. Eriksson, B., et al., *Consensus guidelines for the management of patients with digestive neuroendocrine tumors--well-differentiated jejunal-ileal tumor/carcinoma.* Neuroendocrinology, 2008. **87**(1): p. 8-19.
20. Group, B.D.W., *Biomarkers and surrogate endpoints: preferred definitions and conceptual framework.* Clin Pharmacol Ther, 2001. **69**(3): p. 89-95.
21. Arnold, R., et al., *Plasma chromogranin A as marker for survival in patients with metastatic endocrine gastroenteropancreatic tumors.* Clin Gastroenterol Hepatol, 2008. **6**(7): p. 820-7.
22. O'Toole, D., et al., *ENETS Consensus Guidelines for the Standards of Care in Neuroendocrine Tumors: biochemical markers.* Neuroendocrinology, 2009. **90**(2): p. 194-202.
23. Marotta, V., et al., *Limitations of Chromogranin A in clinical practice.* Biomarkers, 2012. **17**(2): p. 186-91.
24. Niederle, B., et al., *ENETS Consensus Guidelines Update for Neuroendocrine Neoplasm of the Jejunum and Ileum.* Neuroendocrinology, 2016.
25. Wiedenmann, B., et al., *Synaptophysin: a marker protein for neuroendocrine cells and neoplasms.* Proc Natl Acad Sci U S A, 1986. **83**(10): p. 3500-4.
26. Kasprzak, A., M. Zabel, and W. Biczysko, *Selected markers (chromogranin A, neuron-specific enolase, synaptophysin, protein gene product 9.5) in diagnosis and prognosis of neuroendocrine pulmonary tumours.* Pol J Pathol, 2007. **58**(1): p. 23-33.
27. Tellez, M.R., et al., *A single fasting plasma 5-HIAA value correlates with 24-hour urinary 5-HIAA values and other biomarkers in midgut neuroendocrine tumors (NETs).* Pancreas, 2013. **42**(3): p. 405-10.
28. Bajetta, E., et al., *Chromogranin A, neuron specific enolase, carcinoembryonic antigen, and hydroxyindole acetic acid evaluation in patients with neuroendocrine tumors.* Cancer, 1999. **86**(5): p. 858-65.

29. De Lott, L.B., et al., *CDX2 is a useful marker of intestinal-type differentiation: a tissue microarray-based study of 629 tumors from various sites.* Arch Pathol Lab Med, 2005. **129**(9): p. 1100-5.
30. Heverhagen, A.E., et al., *Embryonic transcription factors CDX2 and Oct4 are overexpressed in neuroendocrine tumors of the ileum: a pilot study.* Eur Surg Res, 2013. **51**(1-2): p. 14-20.
31. Mizutani, G., et al., *Expression of Somatostatin Receptor (SSTR) Subtypes (SSTR-1, 2A, 3, 4 and 5) in Neuroendocrine Tumors Using Real-time RT-PCR Method and Immunohistochemistry.* Acta Histochem Cytochem, 2012. **45**(3): p. 167-76.
32. Kaufmann, O., T. Georgi, and M. Dietel, *Utility of 123C3 monoclonal antibody against CD56 (NCAM) for the diagnosis of small cell carcinomas on paraffin sections.* Hum Pathol, 1997. **28**(12): p. 1373-8.
33. Khan, M.S., et al., *Circulating tumor cells as prognostic markers in neuroendocrine tumors.* J Clin Oncol, 2013. **31**(3): p. 365-72.
34. Ehlers, M., et al., *Circulating tumor cells in patients with neuroendocrine neoplasms.* Horm Metab Res, 2014. **46**(10): p. 744-5.
35. Lollgen, R.M., et al., *Chromosome 18 deletions are common events in classical midgut carcinoid tumors.* International Journal of Cancer, 2001. **92**(6): p. 812-815.
36. Kulke, M.H., et al., *High-resolution analysis of genetic alterations in small bowel carcinoid tumors reveals areas of recurrent amplification and loss.* Genes Chromosomes & Cancer, 2008. **47**(7): p. 591-603.
37. Andersson, E., et al., *High-resolution genomic profiling reveals gain of chromosome 14 as a predictor of poor outcome in ileal carcinoids.* Endocrine-Related Cancer, 2009. **16**(3): p. 953-966.
38. Cunningham, J.L., et al., *Common Pathogenetic Mechanism Involving Human Chromosome 18 in Familial and Sporadic Ileal Carcinoid Tumors.* Genes Chromosomes & Cancer, 2011. **50**(2): p. 82-94.
39. Nilsson, O., *Profiling of ileal carcinoids.* Neuroendocrinology, 2013. **97**(1): p. 7-18.
40. Heldin, C.H. and A. Moustakas, *Role of Smads in TGFbeta signaling.* Cell Tissue Res, 2012. **347**(1): p. 21-36.
41. Lebrun, J.-J., *The Dual Role of TGF in Human Cancer: From Tumor Suppression to Cancer Metastasis.* ISRN Molecular Biology, 2012. **2012**: p. 28.
42. Miyaki, M., et al., *Higher frequency of Smad4 gene mutation in human colorectal cancer with distant metastasis.* Oncogene, 1999. **18**(20): p. 3098-103.

43. Maliekal, T.T., et al., *Loss of expression, and mutations of Smad 2 and Smad 4 in human cervical cancer.* Oncogene, 2003. **22**(31): p. 4889-97.
44. Hahn, S.A., et al., *DPC4, a candidate tumor suppressor gene at human chromosome 18q21.1.* Science, 1996. **271**(5247): p. 350-353.
45. Takagi, Y., et al., *Somatic alterations of the SMAD-2 gene in human colorectal cancers.* Br J Cancer, 1998. **78**(9): p. 1152-5.
46. Blaker, H., et al., *Genetics of adenocarcinomas of the small intestine: frequent deletions at chromosome 18q and mutations of the SMAD4 gene.* Oncogene, 2002. **21**(1): p. 158-64.
47. Fearon, E.R., et al., *Identification of a chromosome 18q gene that is altered in colorectal cancers.* Science, 1990. **247**(4938): p. 49-56.
48. Mehlen, P., et al., *The DCC gene product induces apoptosis by a mechanism requiring receptor proteolysis.* Nature, 1998. **395**(6704): p. 801-4.
49. Chen, E.I. and J.R. Yates, *Maspin and tumor metastasis.* IUBMB Life, 2006. **58**(1): p. 25-9.
50. Nieser, M., et al., *Loss of Chromosome 18 in Neuroendocrine Tumors of the Small Intestine: The Enigma Remains.* Neuroendocrinology, 2016.
51. Ishida, M., et al., *The PMAIP1 gene on chromosome 18 is a candidate tumor suppressor gene in human pancreatic cancer.* Dig Dis Sci, 2008. **53**(9): p. 2576-82.
52. Yakovlev, A.G., et al., *BOK and NOXA are essential mediators of p53-dependent apoptosis.* J Biol Chem, 2004. **279**(27): p. 28367-74.
53. Zukerberg, L.R., et al., *Cables links Cdk5 and c-Abl and facilitates Cdk5 tyrosine phosphorylation, kinase upregulation, and neurite outgrowth.* Neuron, 2000. **26**(3): p. 633-46.
54. Park do, Y., et al., *The Cables gene on chromosome 18q is silenced by promoter hypermethylation and allelic loss in human colorectal cancer.* Am J Pathol, 2007. **171**(5): p. 1509-19.
55. Sakamoto, H., et al., *Mechanisms of Cables 1 gene inactivation in human ovarian cancer development.* Cancer Biol Ther, 2008. **7**(2): p. 180-88.
56. Tan, D., et al., *Loss of cables protein expression in human non-small cell lung cancer: a tissue microarray study.* Hum Pathol, 2003. **34**(2): p. 143-9.
57. Zukerberg, L.R., et al., *Loss of cables, a cyclin-dependent kinase regulatory protein, is associated with the development of endometrial hyperplasia and endometrial cancer.* Cancer Res, 2004. **64**(1): p. 202-8.
58. Arnason, T., et al., *Loss of Cables Expression in Neuroendocrine Tumors (NETs) of the Gastrointestinal Tract, Pancreas, and Lung.* Nature Abstracts Laboratory Investigation, 2013.

59. Zhang, H., et al., *Aberrant splicing of cables gene, a CDK regulator, in human cancers.* Cancer Biol Ther, 2005. **4**(11): p. 1211-5.
60. Li, S.S., S.L. Yu, and S. Singh, *Epigenetic states and expression of imprinted genes in human embryonic stem cells.* World J Stem Cells, 2010. **2**(4): p. 97-102.
61. Yamazaki, K., et al., *Identification and biochemical characterization of a novel transcription elongation factor, Elongin A3.* J Biol Chem, 2002. **277**(29): p. 26444-51.
62. Edfeldt, K., et al., *TCEB3C a putative tumor suppressor gene of small intestinal neuroendocrine tumors.* Endocr Relat Cancer, 2014. **21**(2): p. 275-84.
63. Dobashi, Y., et al., *Molecular alterations in AKT and its protein activation in human lung carcinomas.* Hum Pathol, 2012. **43**(12): p. 2229-40.
64. Phillips, J.J., et al., *PDGFRA amplification is common in pediatric and adult high-grade astrocytomas and identifies a poor prognostic group in IDH1 mutant glioblastoma.* Brain Pathol, 2013. **23**(5): p. 565-73.
65. Parsons, D.W., et al., *Colorectal cancer: mutations in a signalling pathway.* Nature, 2005. **436**(7052): p. 792.
66. Holmes, D., *PI3K pathway inhibitors approach junction.* Nat Rev Drug Discov, 2011. **10**(8): p. 563-4.
67. Ramos, A.H., et al., *Amplification of chromosomal segment 4q12 in non-small cell lung cancer.* Cancer Biol Ther, 2009. **8**(21): p. 2042-50.
68. Nupponen, N.N., et al., *Platelet-derived growth factor receptor expression and amplification in choroid plexus carcinomas.* Mod Pathol, 2008. **21**(3): p. 265-70.
69. Tsao, A.S., et al., *Immunohistochemical overexpression of platelet-derived growth factor receptor-beta (PDGFR-beta) is associated with PDGFRB gene copy number gain in sarcomatoid non-small-cell lung cancer.* Clin Lung Cancer, 2011. **12**(6): p. 369-74.
70. Knobbe, C.B. and G. Reifenberger, *Genetic alterations and aberrant expression of genes related to the phosphatidyl-inositol-3'-kinase/protein kinase B (Akt) signal transduction pathway in glioblastomas.* Brain Pathol, 2003. **13**(4): p. 507-18.
71. Mizoguchi, M., et al., *Genetic alterations of phosphoinositide 3-kinase subunit genes in human glioblastomas.* Brain Pathol, 2004. **14**(4): p. 372-7.
72. Altomare, D.A. and J.R. Testa, *Perturbations of the AKT signaling pathway in human cancer.* Oncogene, 2005. **24**(50): p. 7455-64.
73. Arranz, E., et al., *Incidence of homogeneously staining regions in non-Hodgkin lymphomas.* Cancer Genet Cytogenet, 1996. **87**(1): p. 1-3.

74. Cheng, J.Q., et al., *Amplification of AKT2 in human pancreatic cells and inhibition of AKT2 expression and tumorigenicity by antisense RNA.* Proc Natl Acad Sci U S A, 1996. **93**(8): p. 3636-41.
75. Xu, X., et al., *Akt2 expression correlates with prognosis of human hepatocellular carcinoma.* Oncol Rep, 2004. **11**(1): p. 25-32.
76. Sabatini, D.M., *mTOR and cancer: insights into a complex relationship.* Nat Rev Cancer, 2006. **6**(9): p. 729-34.
77. Wendel, H.G., et al., *Survival signalling by Akt and eIF4E in oncogenesis and cancer therapy.* Nature, 2004. **428**(6980): p. 332-7.
78. Mamane, Y., et al., *eIF4E--from translation to transformation.* Oncogene, 2004. **23**(18): p. 3172-9.
79. Cheng, H., et al., *RICTOR Amplification Defines a Novel Subset of Patients with Lung Cancer Who May Benefit from Treatment with mTORC1/2 Inhibitors.* Cancer Discov, 2015. **5**(12): p. 1262-70.
80. Asati, V., D.K. Mahapatra, and S.K. Bharti, *PI3K/Akt/mTOR and Ras/Raf/MEK/ERK signaling pathways inhibitors as anticancer agents: Structural and pharmacological perspectives.* Eur J Med Chem, 2016. **109**: p. 314-41.
81. LoPiccolo, J., et al., *Targeting the PI3K/Akt/mTOR pathway: effective combinations and clinical considerations.* Drug Resist Updat, 2008. **11**(1-2): p. 32-50.
82. Zhang, B., et al., *microRNAs as oncogenes and tumor suppressors.* Developmental Biology, 2007. **302**(1): p. 1-12.
83. Li, S.C., et al., *Global microRNA profiling of well-differentiated small intestinal neuroendocrine tumors.* Mod Pathol, 2013. **26**(5): p. 685-96.
84. Choi, H.J., et al., *MicroRNA expression profile of gastrointestinal stromal tumors is distinguished by 14q loss and anatomic site.* Int J Cancer, 2010. **126**(7): p. 1640-50.
85. Korkmaz, A., et al., *Epigenetic mechanisms in human physiology and diseases.* J Exp Integr Med, 2011. **1**(3): p. 139-147.
86. Inbar-Feigenberg, M., et al., *Basic concepts of epigenetics.* Fertil Steril, 2013. **99**(3): p. 607-15.
87. Paska, A.V. and P. Hudler, *Aberrant methylation patterns in cancer: a clinical view.* Biochem Med (Zagreb), 2015. **25**(2): p. 161-76.
88. Chan, A.O., et al., *CpG island methylation in carcinoid and pancreatic endocrine tumors.* Oncogene, 2003. **22**(6): p. 924-34.
89. Liu, L., et al., *Epigenetic alterations in neuroendocrine tumors: methylation of RAS-association domain family 1, isoform A and p16 genes are associated with metastasis.* Mod Pathol, 2005. **18**(12): p. 1632-40.

90. Fotouhi, O., et al., *Global hypomethylation and promoter methylation in small intestinal neuroendocrine tumors: an in vivo and in vitro study.* Epigenetics, 2014. **9**(7): p. 987-97.
91. Verdugo, A.D., et al., *Global DNA methylation patterns through an array-based approach in small intestinal neuroendocrine tumors.* Endocr Relat Cancer, 2014. **21**(1): p. L5-7.
92. Ehrlich, M., *DNA hypomethylation in cancer cells.* Epigenomics, 2009. **1**(2): p. 239-59.
93. Hoffmann, M.J. and W.A. Schulz, *Causes and consequences of DNA hypomethylation in human cancer.* Biochem Cell Biol, 2005. **83**(3): p. 296-321.
94. Rodriguez, J., et al., *Genome-wide tracking of unmethylated DNA Alu repeats in normal and cancer cells.* Nucleic Acids Res, 2008. **36**(3): p. 770-84.
95. Choi, I.S., et al., *Hypomethylation of LINE-1 and Alu in well-differentiated neuroendocrine tumors (pancreatic endocrine tumors and carcinoid tumors).* Mod Pathol, 2007. **20**(7): p. 802-10.
96. Karpathakis, A., et al., *Prognostic Impact of Novel Molecular Subtypes of Small Intestinal Neuroendocrine Tumor.* Clin Cancer Res, 2015.
97. Bornschein, J., et al., *Gastrointestinal neuroendocrine tumors.* Deutsche Medizinische Wochenschrift, 2008. **133**(28-29): p. 1505-1510.
98. Bruns, C., et al., *SOM230: a novel somatostatin peptidomimetic with broad somatotropin release inhibiting factor (SRIF) receptor binding and a unique antisecretory profile.* Eur J Endocrinol, 2002. **146**(5): p. 707-16.
99. Patel, Y.C. and C.B. Srikant, *Somatostatin receptors.* Trends Endocrinol Metab, 1997. **8**(10): p. 398-405.
100. Li, S.C., et al., *The somatostatin analogue octreotide inhibits growth of small intestine neuroendocrine tumour cells.* PLoS One, 2012. **7**(10): p. e48411.
101. Duran-Prado, M., et al., *Identification and characterization of two novel truncated but functional isoforms of the somatostatin receptor subtype 5 differentially present in pituitary tumors.* J Clin Endocrinol Metab, 2009. **94**(7): p. 2634-43.
102. van der Zwan, W.A., et al., *GEPNETs update: Radionuclide therapy in neuroendocrine tumors.* Eur J Endocrinol, 2015. **172**(1): p. R1-8.
103. Pavel, M.E., et al., *Everolimus plus octreotide long-acting repeatable for the treatment of advanced neuroendocrine tumours associated with carcinoid syndrome (RADIANT-2): a randomised, placebo-controlled, phase 3 study.* Lancet, 2011. **378**(9808): p. 2005-12.

104. Buchholz, M., et al., *A multistep high-content screening approach to identify novel functionally relevant target genes in pancreatic cancer.* PLoS One, 2015. **10**(4): p. e0122946.
105. Noell, S., et al., *Water Channels Aquaporin 4 and -1 Expression in Subependymoma Depends on the Localization of the Tumors.* PLoS One, 2015. **10**(6): p. e0131367.
106. Albertson, D.G., *Gene amplification in cancer.* Trends Genet, 2006. **22**(8): p. 447-55.
107. Li, H., et al., *The Sequence Alignment/Map format and SAMtools.* Bioinformatics, 2009. **25**(16): p. 2078-2079.
108. Partridge, A.W., A.G. Therien, and C.M. Deber, *Missense mutations in transmembrane domains of proteins: phenotypic propensity of polar residues for human disease.* Proteins, 2004. **54**(4): p. 648-56.
109. Sakharkar, M.K., V.T. Chow, and P. Kangueane, *Distributions of exons and introns in the human genome.* In Silico Biol, 2004. **4**(4): p. 387-93.
110. Lollgen, R.M., et al., *Chromosome 18 deletions are common events in classical midgut carcinoid tumors.* Int J Cancer, 2001. **92**(6): p. 812-5.
111. Miyamoto, H., et al., *Loss of heterozygosity at the p53, RB, DCC and APC tumor suppressor gene loci in human bladder cancer.* J Urol, 1996. **155**(4): p. 1444-7.
112. Reyes-Mugica, M., et al., *Loss of DCC expression and glioma progression.* Cancer Res, 1997. **57**(3): p. 382-6.
113. Huerta, S., et al., *Human colon cancer cells deficient in DCC produce abnormal transcripts in progression of carcinogenesis.* Dig Dis Sci, 2001. **46**(9): p. 1884-91.
114. Reale, M.A., et al., *Expression and alternative splicing of the deleted in colorectal cancer (DCC) gene in normal and malignant tissues.* Cancer Res, 1994. **54**(16): p. 4493-501.
115. Carvalho, A.L., et al., *Deleted in colorectal cancer is a putative conditional tumor-suppressor gene inactivated by promoter hypermethylation in head and neck squamous cell carcinoma.* Cancer Res, 2006. **66**(19): p. 9401-7.
116. Park, H.L., et al., *DCC promoter hypermethylation in esophageal squamous cell carcinoma.* Int J Cancer, 2008. **122**(11): p. 2498-502.
117. Mancini, M. and A. Toker, *NFAT proteins: emerging roles in cancer progression.* Nat Rev Cancer, 2009. **9**(11): p. 810-20.
118. Coste, B., et al., *Piezo1 and Piezo2 are essential components of distinct mechanically activated cation channels.* Science, 2010. **330**(6000): p. 55-60.

119. Li, H., et al., *The expression and effects the CABYR-c transcript of CABYR gene in hepatocellular carcinoma.* Bull Cancer, 2012. **99**(3): p. E26-33.
120. Tseng, Y.T., et al., *Expression of the sperm fibrous sheath protein CABYR in human cancers and identification of alpha-enolase as an interacting partner of CABYR-a.* Oncol Rep, 2011. **25**(4): p. 1169-75.
121. Delgado Verdugo, A., et al., *Exome Sequencing and CNV Analysis on Chromosome 18 in Small Intestinal Neuroendocrine Tumors: Ruling Out a Suspect?* Horm Metab Res, 2015. **47**(6): p. 452-5.
122. Alberici, P., et al., *Smad4 haploinsufficiency: a matter of dosage.* Pathogenetics, 2008. **1**(1): p. 2.
123. Solimini, N.L., et al., *Recurrent hemizygous deletions in cancers may optimize proliferative potential.* Science, 2012. **337**(6090): p. 104-9.
124. Andersson, E., et al., *Expression profiling of small intestinal neuroendocrine tumors identifies subgroups with clinical relevance, prognostic markers and therapeutic targets.* Mod Pathol, 2016. **29**(6): p. 616-29.
125. Pitt, S.C., H. Chen, and M. Kunnimalaiyaan, *Inhibition of phosphatidylinositol 3-kinase/Akt signaling suppresses tumor cell proliferation and neuroendocrine marker expression in GI carcinoid tumors.* Ann Surg Oncol, 2009. **16**(10): p. 2936-42.
126. Gilbert, J.A., et al., *Molecular markers for novel therapies in neuroendocrine (carcinoid) tumors.* Endocr Relat Cancer, 2010. **17**(3): p. 623-36.
127. Hanna, W.M., et al., *HER2 in situ hybridization in breast cancer: clinical implications of polysomy 17 and genetic heterogeneity.* Mod Pathol, 2014. **27**(1): p. 4-18.
128. Hofmann, M., et al., *Central HER2 IHC and FISH analysis in a trastuzumab (Herceptin) phase II monotherapy study: assessment of test sensitivity and impact of chromosome 17 polysomy.* J Clin Pathol, 2008. **61**(1): p. 89-94.
129. Schiavon, B., J. Vassallo, and R. Rocha, *Is polysomy 17 an important phenomenon to predict treatment with trastuzumab in breast cancer?* Applied Cancer Research, 2011. **31**(4): p. 138-142.
130. Sartore-Bianchi, A., et al., *Standardisation of EGFR FISH in colorectal cancer: results of an international interlaboratory reproducibility ring study.* J Clin Pathol, 2012. **65**(3): p. 218-23.
131. Woenckhaus, J., et al., *Genomic gain of PIK3CA and increased expression of p110alpha are associated with progression of dysplasia into invasive squamous cell carcinoma.* J Pathol, 2002. **198**(3): p. 335-42.
132. Kim, J.H., et al., *Prognostic implications of PIK3CA amplification in curatively resected liposarcoma.* Oncotarget, 2016.

133. Imoto, I., et al., *SNO is a probable target for gene amplification at 3q26 in squamous-cell carcinomas of the esophagus.* Biochem Biophys Res Commun, 2001. **286**(3): p. 559-65.
134. Hauso, O., et al., *Neuroendocrine tumor epidemiology: contrasting Norway and North America.* Cancer, 2008. **113**(10): p. 2655-64.
135. Yao, J.C., et al., *One hundred years after "carcinoid": epidemiology of and prognostic factors for neuroendocrine tumors in 35,825 cases in the United States.* J Clin Oncol, 2008. **26**(18): p. 3063-72.

VII. Appendix

Table 26: Clinical characteristics
M: male, f: female, X: not assessable, NA: not available

Case	Site of primary tumor	Age at diagnosis	Sex	Cohort	T	N	M	UICC Stage	MIB-1	Grade	PHH3	CEP18	Tissue type
1	Ileum	70	m	3	3	2	1	IIIB	0.90	1	0.47	1	FFPE
2	Ileocecal valve	51	f	2	3	1	X	IIIB	0.70	1	0.09	1	FFPE
3	Ileum	50	f	1	3	0	X	IIB	0.75	1	0.01	2	FFPE
4	Ileocecal valve	65	m	2	2	1	X	IIIB	0.40	1	0.23	1	FFPE
5	Ileum	71	m	3	3	1	1	IV	1.01	1	0.19	1	FFPE
7	Ileum	67	m	2	2	1	X	IIIB	0.46	1	0.12	1	FFPE
8	Ileocecal valve	66	m	2	2	X	X	IIA	0.54	1	0.11	1	FFPE
9	Ileocecal valve	77	f	1	3	0	X	IIB	0.42	1	0.02	1	FFPE
10	Ileum	67	m	3	3	2	1	IV	6.13	2	0.17	2	FFPE
11	Ileum	48	m	2	3	1	X	IIIB	0.21	1	0.09	2	FFPE
13	Ileum	73	m	1	3	0	X	IIB	0.59	1	0.00	2	FFPE
14	Ileocecal valve	63	f	2	3	1	X	IIIB	0.98	1	0.20	2	FFPE
15	Jejunum	75	m	1	3	X	X	IIB	0.90	1	0.05	1	FFPE
16	Ileocecal valve	45	f	2	3	1	X	IIIB	1.10	1	0.11	2	FFPE
17	Ileum	53	f	2	2	1	X	IIIB	1.89	1	0.12	1	FFPE
18	Ileum	57	f	2	1	1	X	IIIB	0.88	1	0.08	1	FFPE
19	Ileum	56	f	3	4	1	1	IV	0.37	1	0.59	2	FFPE
20	Ileum	68	f	2	NA	NA	NA	NA	0.60	1	0.22	1	FFPE
21	Ileocecal valve	45	m	3	3	2	1	IV	0.24	1	0.06	1	FFPE
22	Ileum	58	m	1	1	0	X	I	NA	NA	NA	1	FFPE
23	Jejunum	76	f	3	3	0	1	IV	0.60	1	0.21	1	FFPE
24	Ileum	48	f	2	3	2	X	IIIB	1.09	1	0.07	1	FFPE
25	Jejunum	63	m	2	3	1	X	IIIB	1.09	1	0.53	1	FFPE
26	Ileum	74	f	1	2m	0	X	IIA	0.49	1	0.11	2	FFPE
27	Ileum	77	m	2	3m	1	X	IIIB	0.77	1	0.20	2	FFPE
28	Ileum	44	f	2	3	1	X	IIIB	1.30	1	0.06	1	FFPE
29	Jejunum	86	m	2	4	1	X	IIIB	0.78	1	0.16	2	FFPE
30	Jejunum	66	f	2	3	1	X	IIIB	0.63	1	0.14	1	FFPE + cryo
31	Jejunum	66	m	3	3	0	1	IV	0.90	1	0.07	1	FFPE
32	Ileum	69	m	2	3	1	X	IIIB	1.02	1	0.06	2	FFPE + cryo
33	Terminal ileum	40	m	2	3	1		IIIB	4.03	2	1.18	1	FFPE
34	Ileum	46	w	1	1	X	X	I	2.78	2	0.09	2	FFPE
38	NA	56	NA	2	NA	NA	NA	NA	0.25	1	0.12	2	FFPE
39	NA	60	NA	3	NA	NA	NA	NA	0.61	1	0.41	2	FFPE
48	NA	56	NA	2	NA	NA	NA	NA	3.88	2	0.46	1	FFPE

52	Ileum	80	m	3	3	1	X	IIIB	1.49	1	0.02	mosaicism	FFPE
53	Terminal ileum	29	f	1	1	0	0	I	1.07	1	0.04	1	FFPE
54	Jejunum	60	NA	1	3	0	0	IIB	0.30	1	0.00	1	FFPE
55	Terminal ileum	20	NA	1	3	X	X	IIB	0.99	1	0.09	1	FFPE
56	Terminal ileum	46	NA	3	2	1	1	IV	0.21	1	NA	2	FFPE
57	Ileum	58	NA	1	3	X	X	IIB	0.49	1	0.11	2	FFPE
58	Small intestine	69	NA	1	1	x	x	I	0.82	1	0.00	mosaicism	FFPE
59	Terminal ileum	74	NA	1	1	0	X	I	0.36	1	0.13	1	FFPE
60	Small intestine	64	NA	1	3	X	X	IIB	1.49	1	0.10	1	FFPE
61	Terminal ileum	54	NA	2	3	1	X	IIIB	1.71	1	0.04	1	FFPE
62	Terminal ileum	47	NA	1	1	0	X	I	0.78	1	0.03	1	FFPE
63	Small intestine	68	NA	3	3	1	1	IV	0.85	1	0.16	1	FFPE
64	Ileum	54	NA	1	2m	X	X	IIA	1.34	1	0.06	1	FFPE
65	Terminal ileum	36	NA	2	2	1	X	IIIB	1.60	1	0.11	1	FFPE
66	Terminal ileum	60	NA	2	2	1	X	IIIB	0.68	1	0.09	1	FFPE
67	Terminal ileum	81	NA	2	2	1	X	IIIB	1.69	1	0.48	1	FFPE
68	Small intestine	62	NA	1	2	0	X	IIA	0.42	1	0.05	2	FFPE
89	Terminal ileum	65	f	2	2	1	X	IIIB	0.78	1	0.08	1	FFPE
91	Terminal ileum	74	m	3	4	1	1	IV	1.08	1	0.03	1	FFPE
92	Ileum	39	m	1	2	X	X	IIA	0.58	1	0.09	2	FFPE
93	Ileocecal valve	71	f	3	3	1	1	IV	1.46	1	0.16	1	FFPE
96	Small intestine	66	NA	3	2m	X	1	IV	3.43	2	0.26	1	FFPE
97	Terminal ileum	62	NA	2	3	1	X	IIIB	0.72	1	0.02	1	FFPE
98	Ileum	75	NA	2	3	1	X	IIIB	2.94	2	0.45	1	FFPE
99	Terminal ileum	54	f	3	2	1	1	IV	2.68	2	0.16	2	FFPE
100	Terminal ileum	65	f	2	3	1	X	IIIB	0.97	1	0.05	1	FFPE
101	Terminal ileum	65	m	1	1	X	X	I	1.36	1	0.08	2	FFPE
103	Small intestine	84	f	1	4m	0	X	IIIA	1.57	1	0.07	1	FFPE
104	Terminal ileum	53	m	2	2	1	X	IIIB	1.32	1	0.45	1	FFPE
105	Small intestine	73	m	3	4	0	1	IV	NA	NA	0.37	1	FFPE
106	Small intestine	38	m	3	3	1	1	IV	7.09	2	0.25	mosaicism	FFPE
107	Terminal ileum	60	f	2	3	1	X	IIIB	1.71	1	0.11	1	FFPE
109	Terminal ileum	49	NA	3	3	1	1	IV	0.27	1	0.30	1	FFPE
110	Small intestine	87	NA	2	2	1	X	IIIB	1.05	1	0.30	2	FFPE
111	Ileum	73	NA	3	4	1	1	IV	1.26	1	0.44	mosaicism	FFPE
112	Terminal ileum	38	f	2	3	1	X	IIIB	1.60	1	0.09	2	FFPE
113	Terminal ileum	84	NA	2	4	1	X	IIIB	0.84	1	0.05	mosaicism	FFPE
115	Ileum	52	NA	2	2	1	X	IIIB	0.44	1	0.40	mosaicism	FFPE
116	Ileum	77	f	2	2m	1	X	IIIB	NA	NA	0.10	1	FFPE
117	Distal ileum	63	NA	3	2	1	1	IV	0.25	1	0.23	1	FFPE
118	Ileum	56	f	3	4m	1	1	IV	1.19	1	0.80	1	FFPE
119	Small intestine	77	NA	2	2m	1	X	IIIB	0.70	1	0.09	mosaicism	FFPE

120	Terminal ileum	44	NA	2	2	1	X	IIIB	1.62	1	0.49	1	FFPE
121	Ileum	64	NA	2	3m	1	X	IIIB	0.94	1	0.36	1	FFPE
122	Terminal ileum	70	NA	2	3	1	X	IIIB	1.05	1	0.16	1	FFPE
123	Distal jejunum, terminal ileum	67	NA	3	2	1	1	IV	0.44	1		NA	FFPE
124	Jejunum/ileum	45	f	3	3	1	1	IV	1.85	1	0.00	1	FFPE
125	Terminal ileum	77	m	2	3	1	X	IIIB	0.03	1	1.12	NA	FFPE
126	Small intestine	72	f	2	3	1	X	IIIB	0.03	1	0.10	NA	FFPE
127	Small intestine	67	f	2	3	1	X	IIIB	NA	NA	NA	NA	FFPE
130	Small intestine	70	f	2	3	1	X	IIIB	0.00	1	NA	NA	FFPE
133	Small intestine	58	m	2	2	1	X	IIIB	1.60	1	0.56	mosaicism	FFPE
134	Ileocecal valve	60	f	2	3	1	X	IIIB	0.13	1	0.00	NA	FFPE
136	Terminal ileum	67	f	3	3	1	1	IV	0.18	1	0.71	NA	FFPE
137	Small intestine	73	m	3	3	1	1	IV	0.57	1	0.15	NA	FFPE
138	Small intestine	70	f	3	3	1	1	IV	1.95	1	0.54	mosaicism	FFPE
140	Ileum	46	f	2	2	1	X	IIIB	1.60	1	0.35	NA	FFPE
141	Ileum	69	m	3	3	1	1	IV	NA	NA	NA	NA	FFPE
142	Small intestine	60	m	3	3	1	1	IV	0.34	1	0.00	1	FFPE
144	Small intestine	28	m	NA	NA	NA	NA	NA	7.24	2	0.04	NA	FFPE
146	Small intestine	56	m	3	3	1	1	IV	1.28	1	0.09	NA	FFPE
147	Small intestine	59	f	NA	NA	NA	NA	NA	0.34	1	0.10	1	FFPE
148	Small intestine	53	m	NA	NA	NA	NA	NA	NA	NA	NA	1	FFPE
149	Terminal ileum	67	f	3	3	1	1	IV	0.70	1	0.10	mosaicism	FFPE
152	Ileum	73	f	3	3	1	1	IV	0.90	1	NA	1	FFPE
153	Small intestine	47	f	NA	NA	NA	NA	NA	0.08	1	0.01	1	FFPE
156	Ileum	62	m	3	3	1	1	IV	4.82	2	0.03	1	FFPE
157	Terminal ileum	45	m	1	1	0	x	I	0.00	1	0.08	1	FFPE
158	Small intestine	52	f	3	3	1	1	IV	1.76	1	0.06	1	FFPE
160	Small intestine	71	f	NA	NA	NA	NA	NA	NA	NA	NA	NA	FFPE
161	Ileum	42	m	3	3	1	1	IV	1.91	1	2.14	1	FFPE
162	Small intestine	68	m	3	3	1	1	IV	1.30	1	NA	1	FFPE
163	Jejunum	68	m	2	3	1	X	IIIB	1.26	1	0.31	1	FFPE
166	Terminal ileum	43	f	3	3	1	1	IV	1.45	1	0.82	1	FFPE
168	Ileum	40	m	3	3	1	1	IV	0.52	1	1.19	1	FFPE
169	Terminal ileum	44	m	3	3	1	1	IV	1.10	1	0.10	1	FFPE
172	Small intestine	70	m	2	2	1	X	IIIB	0.43	1	0.08	1	FFPE
173	Small intestine	65	f	NA	NA	NA	NA	NA	1.54	1,00	0.15	1	FFPE
174	Small intestine	52	f	NA	NA	NA	NA	NA	NA	NA	1.31	1	FFPE
176	Small intestine	52	m	NA	NA	NA	NA	NA	6.91	2,00	0.71	mosaicism	FFPE
177+178	Ileum	67	m	2	3	1	X	IIIB	1.30	1	1.31	1	FFPE
180	Ileum	63	m	3	2	1	1	IV	11.67	2,00	1.11	mosaicism	FFPE
183	Ileum	55	m	2	2	1	X	IIIB	2.35	2	0.50	1	FFPE

184	Small intestine	56	f	3	3	1	1	IV	1.14	1	0.10	1	FFPE
186	Ileum	65	m	2	3	1	X	IIIB	1.01	1	0.87	1	FFPE
188	Ileum	70	m	3	3	1	1	IV	10.65	2	0.44	1	FFPE
189	Ileum	70	f	3	2	1	1	IV	1.79	1,00	0.78	NA	FFPE
190	Ileum	45	f	3	3	1	1	IV	1.79	1	0.78	1	FFPE
192	Ileum	65	m	3	3	1	1	IV	0.64	1	0.18	mosaicism	FFPE
193	Ileum	43	f	1	2	0	X	IIA	0.53	1	0.05	mosaicism	FFPE
194	Ileum	68	f	2	3	1	X	IIIB	0.98	1	0.66	mosaicism	FFPE
195	Ileum	58	m	3	3	1	1	IV	NA	NA	NA	mosaicism	FFPE
196	Ileum	45	f	2	1	1	X	IIIB	2.28	2	0.72	1	FFPE
197	Terminal ileum	61	f	3	2	1	1	IV	1.00	1	NA	mosaicism	FFPE
198	Ileum	50	f	3	3	1	1	IV	1.31	1	0.07	mosaicism	FFPE
199	Small intestine	55	f	1	3	X	X	I	0.49	1	0.21	mosaicism	FFPE
201	Terminal ileum	72	m	3	3	1	1	IV	1.07	1	0.22	1	FFPE
202	Small intestine	59	m	3	3	1	1	IV	3.36	2	0.49	1	FFPE
207	Ileum	87	m	2	3	1	X	IIIB	2.39	2	0.27	1	FFPE
254	Ileum	66	f	1	2m	0	X	IIA	0.75	1	0.11	1	FFPE + cryo
255	Terminal ileum	69	f	2	3	1	X	IIIB	3.13	2	0.33	1	FFPE + cryo
256	Unknown	74	f	NA	NA	NA	NA	NA	1.27	1	0.21	1	FFPE + cryo
257	Ileum	52	f	3	2m	1	1	IV	1.97	1	0.33	1	FFPE + cryo
258	Ileum	26	f	1	3	X	X	IIB	1.94	1	0.10	1	FFPE + cryo
259	Ileum	66	m	2	2	1	X	IIIB	6.65	2	0.37	mosaicism	FFPE + cryo
260	Ileum	70	f	2	3	1	X	IIIB	0.87	1	0.17	1	FFPE + cryo
Tu1 Met	Small intestine	NA	NA	3	1	1	1	IV	NA	NA	NA	1	Cryo
Tu3	Ileum	72	f	2	2	2	0	IIIB	NA	1	NA	mosaicism	Cryo
Tu4	Ileum	72	f	2	3	1	0	IIIB	NA	1	NA	1	Cryo
Tu7 Met	Small intestine	NA	NA	3	4	1	1	IV	NA	NA	NA	1	Cryo
Tu5 Met	Small intestine	NA	NA	2	3	1	X	IIIB	NA	NA	NA	1	Cryo
BB1	Ileum	71	f	3	3	1	1	IV	1.00	1	NA	1	Cryo
GR1	Duodenum	52	f	1	1	0	X	I	1.00	1	NA	1	Cryo
GR2	Jejunum	45	m	1	4	0	X	I	1.00	1	NA	1	Cryo
GR3	Duodenum	57	m	1	3	0	X	I	1.00	1	NA	1	Cryo
GR4	Ileum	85	m	2	4	1	X	IIIB	1.00	1	NA	1	Cryo
GR5	Small intestine	78	f	2	4	1	X	IIIB	1.00	1	NA	1	Cryo
MB1	Ileum	45	f	2	3	1	X	IIIB	NA	1	NA	1	Cryo
MB2	Ileum	44	f	3	3	1	1	IV	NA	1	NA	1	Cryo
MB3	Ileum	69	m	2	2	1	0	IIIB	NA	1	NA	1	Cryo
MB4	Ileum	64	f	3	3	1	1	IV	NA	1	NA	1	Cryo
MB5	Ileum	47	m	2	2	1	0	IIIB	NA	1	NA	1	Cryo
MB6	Ileum	74	f	3	3	1	1	IV	NA	1	NA	1	Cryo
MB7	Ileum	49	m	3	3	1	1	IV	NA	1	NA	1	Cryo

Table 27: Expression of immunohistochemical markers
P: Primary tumor, LN: lymph node metastasis, DM: distant metastasis, neg: negative, pos: positive, NA: not available; samples in grey were excluded from further analyses.

Case	P, LN, DM	Synaptophysin (0-3)	SSTR2 (0-3)	CDX2 (-: neg, (+): weak pos, +: pos)	Serotonin (0-3)
I001	P	3	3	(+)	3
I001	LN	3	3	+	3
I002	P	2	1+	NA	0
I002	LN	3	2	+	2
I003	P	3	3	+	1
I004	P	3	1+	NA	3
I005	DM	3	0	+	1
I005	P	2	3	+	2
I005	LN	3	1+	+	2
I007	P	3	NA	NA	3
I008	P	1	3	-	3
I009	P	3	3	+	3
I010	P	2	1+	NA	1
I010	LN	2	3	+	2
I011	P	2	3	+	3
I013	P	2	3	+	3
I014	P	3	0	-	2
I015	P	2	3	+	1
I016	P	3	2+	+	3
I016	LN	3	3	+	3
I017	LN	2	3	+	3
I017 Normal liver	P	0	NA	-	0
I018	P	3	3	+	3
I018	LN	3	3	+	3
I019	P	2	0	+	3
I019	LN	3	2+	+	3
I020 No tumor	LN	0	NA	-	-
I020	P	1	3	+	3
I021	P	2	3	+	3
I022	P	2	0	+	3
I023 No tumor	P	0	NA	-	0
I024	LN	3	3	+	1
I024	P	2	3	+	2
I025	P	2	3	+	3
I026	P	2	3	+	3
I027	LN	3	0	+	0
I027 Normal liver	P	0	NA	-	0
I028	P	3	1+	+	3

I029	LN	3	3	+	2
I029	P	3	2+	+	3
I030	LN	2	0	NA	1
I030	P	3	3	+	3
I031	P	2	1+	+	1
I031	DM	3	3	+	3
I032	LN	3	0	+	0
I032	P	3	3	+	3
I033	P	3	3	+	3
I034	P	2	3	+	3
I038	LN	3	1	+	1
I038	P	2	3	NA	2
I039	LN	3	1	+	0
I039	P	1	2+	+	3
I048	P	2	3	+	0
I048	LN	3	0	+	1
I052	P	2	3	+	3
I053	P	2	3	+	3
I054	P	1	NA	+	0
I055	P	3	3	+	2
I056	LN	3	3	+	1
I056	P	3	2	+	2
I057	P	2	3	+	3
I058	P	NA	3	+	1
I059	P	1	3	+	3
I060	P	2	1	+	3 (focal)
I061	LN	0	NA	+	1
I061	P	2	3	+	3
I062	P	2	0	+	1
I063	LN	3	2	+	2
I063	DM	3	0	+	2
I063	P	2	2	+	3
I064	P	2	3	+	3
I065	P	1	3	+	3
I065	LN	2	2+	+	3
I066	P	2	1	+	3
I067	P	3	2	+	3
I068	P	2	3	+	3
I089	P	0	0	+	2
I089	LN	3	1+	+	3
I091	DM	3	0	+	0
I091	LN	2	1	+	2

I091	P	1	1+	+	3
I092 Detached from slide	P	NA	NA	-	3
I093	LN	3	3	+	1
I093	P	3	3	+	3
I093	DM	3	2+	+	3
I095	P	2	3	+	1
I096	P	3	3	+	3
I097	LN	3	1+	+	2
I097	P	3	0	+	3
I098	P	1	3	+	3
I098	LN	2	0	-	3
I099	P	1	3	+	3
I099	LN	1	3	+	3
I099	DM	1	3	+	3
I100	P	2	3	+	3
I100	LN	1	0	-	3
I101	P	2	3	+	3
I103	P	2	2	+	3
I104	LN	0	NA	+	0
I104	P	1	3	+	3
I105	P	0	0	-	0
I105	DM	0	0	-	0
I106	P	3	3	+	3
I106	DM	3	3	+	3
I107	LN	2	2+	+	3
I107 No tumor	P	0	NA	+	0
I109	P	2	3	+	3
I109	LN	2	1+	+	3
I110	P	2	3	+	1
I111	P	2	0	+	3
I112	P	2	1+	NA	0
I112	LN	2	0	+	2
I113	P	2	0	+	1
I113	LN	3	0	+	3
I115	P	1	0	+	3
I116	P	0	0	-	0
I117	P	3	3	+	3
I117	DM	3	3	+	3
I118	LN	3	2+	+	1
I118	P	3	3	+	3
I119	P	2	3	+	2
I120	P	2	3	+	3

I121	LN	3	3	+	0
I121	P	3	1+	+	3
I122	P	1	3	+	3
I123	LN	2	3	+	1
I123	P	1	3	+	1
I124	LN	2	3	+	3
I124	P	1	0	+	3
I125	P	1	2+	-	0
I125	LN	0	0	-	1
I126	LN	1	1	-	0
I126	P	1	3	(+)	3
I127	LN	3	3	+	0
I130	LN	1	0	-	1
I130	P	1	0	-	1
I133	LN	2	3	+	3
I133	P	3	0	(+)	3
I134	P	2	0	NA	1
I136	LN	2	0	NA	0
I136	P	1	1+	-	3
I137	LN	1	0	+	3
I137	P	1	3	+	3
I138	LN	2	3	+	0
I138	P	2	3	+	1
I140	P	2	3	+	3
I141	LN	1	3	+	3
I141	P	1	3	+	3
I142	LN	3	2	+	0
I142	P	2	3	+	1
I144	LN	0	0	-	0
I144	P	0	0	-	0
I146	LN	2	0	+	0
I146	P	1	3	+	2
I147	P	2	0	+	1
I148	LN	2	3	+	2
I149	LN	1	NA	+	0
I149	DM	1	0	-	2
I152	P	2	0	+	2
I153	P	3	3	-	0
I153	DM	1	NA	+	2
I156	DM	2	2+	+	3
I157	P	0	3	+	3
I158	DM	3	3	NA	0

I158	LN	2	1	NA	0
I158	P	3	3	+	1
I160	P	3	3	+	3
I161	P	2	0	+	2
I161	LN	1	3	(+)	3
I162	P	3	2+	+	2
I162	LN	3	2	NA	3
I163	LN	3	3	+	1
I163	P	3	3	+	2
I166	LN	3	NA	-	-
I166	P	3	1+	+	3
I168	LN	3	0	+	0
I168	P	2	2+	+	1
I169	P	3	2	+	1 (focal)
I169	DM	2	2	+	2
I172	LN	NA	0	+	1
I172	P	2	2	+	1
I173	LN	3	0	(+)	1
I173	P	3	1+	+	3
I174	LN	3	1+	+	0
I176	LN	3	1+	(+)	1
I178	P	3	3	+	3
I178 No tumor	LN	0	NA	-	0
I180	P	2	3	+	3
I180	LN	3	3	+	3
I183	LN	3	3	+	3
I183	P	2	3	+	3
I184	P	1	0	(+)	3
I186	LN	2	0	+	1
I186	P	2	0	+	3
I188	P	3	3	+	3
I189	P	2	1	+	0
I189	LN	2	3	+	1
I190	LN	3	1+	+	2
I190	P	2	3	+	3
I192	P	3	0	+	0
I192	LN	3	1	+	2
I193	P	3	3	+	3
I194	P	3	0	+	3
I195	LN	3	0	+	0
I195	P	3	3	+	3
I196	LN	3	3	+	2

I196	P	2	3	+	3
I197	LN	3	1+	+	2
I198	LN	3	2	+	1
I198	DM	3	2	+	1
I198	P	3	3	+	3
I199	P	2	3	+	3
I201	P	2	0	+	2
I202	LN	3	2+	+	3
I202	P	2	3	+	3
I207	LN	2	1	+	3
I207	P	2	3	+	3

Table 28: Quality data of exome sequencing
A) Mean coverage on target of the five SI-NETs and the corresponding normal tissues, B) Underrepresented bases (coverage <10 /<30)
Tu: tumor, Met: metastasis, N: corresponding normal tissue

A)	**Tu1 Met**	**Tu3**	**Tu4**	**Tu7 Met**	**Tu5 Met**
Mean coverage on target:	96.17	92.49	87.17	79.93	133.92
	N1	**N3**	**N4**	**N7**	**N1**
Mean coverage on target:	126.81	119.16	129.69	142.97	129.02

B)	**Tu1 Met**		**Tu3**		**Tu4**		**Tu7 Met**		**Tu5 Met**	
Underrepresented	bases	[%]	bases	[%]	bases	[%]	bases	[%]	bases	[%]
Cov<10	6395223	12.44	6138145	11.94	6422059	12.50	7006239	13.63	4252238	8.27
Cov<30	13806402	26.86	13698051	26.65	14497542	28.21	15639855	30.43	9734268	18.94
	N1		**N3**		**N4**		**N7**		**N1**	
Underrepresented	bases	[%]	bases	[%]	bases	[%]	bases	[%]	bases	[%]
Cov<10	5096674	9.92	5321044	10.35	5056319	9.84	4782423	9.30	4883694	9.50
Cov<30	11428300	22.24	11914443	23.18	11108916	21.61	10222034	19.89	11126732	21.65

Table 29: Alterations of the five SI-NET samples identified by exome sequencing
The numbers in parenthesis are alterations without rs-numbers (common SNPs). Ess.: essential

Sam-ple	Total	3‘	5‘	Down-stream	Inter-genic	Intro-nic	Synonymous coding	Up-stream	Within non-coding gene	Ess. Splice site / Splice site
1	443 (315)	18 (12)	13 (9)	2	16 (8)	181 (123)	52 (36)	7 (5)	22 (15)	6 (4) / 8 (6)
2	451 (301)	19 (15)	13 (5)	9 (7)	16 (11)	201 (132)	49 (35)	12 (7)	25 (9)	1 (-)/ 6 (3)
3	479 (315)	26 (19)	6 (4)	7 (4)	26 (11)	188 (131)	40 (28)	11 (7)	33 (12)	- (1) / 12 (8)
4	510 (343)	26 (19)	7 (5)	4 (3)	28 (14)	209 (147)	52 (29)	10 (5)	36 (16)	4 (3) / 12 (8)
5	321 (189)	15 (9)	5 (1)	11 (8)	34	128 (77)	24 (11)	12 (8)	21 (10)	2 (-)/ 14 (13)

Table 30: Counts and ratio of FISH signals in samples with CN alterations
P: primary tumor, LN: lymph node metastasis, DM: distant metastasis
A) *PIK3CD*

Samples	P *PIK3CD* Ratio	Count gene signal P *PIK3CD*	Count reference signal P *PIK3CD*	LN *PIK3CD* Ratio	Count gene signal LN *PIK3CD*	Count reference signal LN *PIK3CD*	DM *PIK3CD* Ratio	Count gene signal DM *PIK3CD*	Count reference signal DM *PIK3CD*
I001				1.25	75	60			
I002									
I003									
I004									
I005	1.16	74	64						
I007									
I008	1.28	37	29						
I009									
I010									
I011									
I013									
I014									
I015									
I016									
I017				1.26	43	34			
I018	1.23	69	56						
I019									
I020									
I021									
I024									
I025									
I026									

I027									
I028									
I029				1.38	88	64			
I030									
I031									
I033	1.43	83	58						
I034									
I038									
I039				1.04	77	74			
I048									
I052									
I053									
I055									
I056									
I059									
I060									
I061									
I062									
I063									
I064									
I065									
I066									
I068									
I089									
I091									
I093									
I095									
I096									
I097									
I098									
I099									
I100									
I101									
I103									
I104									
I106							1.44		
I107				1.25					
I109									
I110									
I112									
I113									
I117									

I118				1.25	85	68			
I120									
I121				1.58	104	66			
I122									
I123				1.29	81	63			
I124									
I127									
I133									
I138				1.23	81	66			
I141									
I142	1.20	12	10						
I144									
I146									
I147									
I148									
I149				1.40	88	63	1.56	103	66
I152									
I153	1.44	92	46						
I156									
I157									
I158									
I160									
I161	1.00	30	30						
I162				1.48	72	63			
I163									
I166									
I168	1.16	73	63						
I169									
I172									
I173									
I174				1.63	104	64			
I176									
I178									
I180									
I183									
I184	1.38	88	64						
I186									
I188									
I189									
I190									
I192									
I193									

I194									
I195									
I196									
I197									
I198									
I199									
I201									
I202	1.36	90	66						
I207	1.26	77	61						

B) *AKT1*

Samples	P *AKT1* Ratio	Count gene signal P *AKT1*	Count reference signal P *AKT1*	LN *AKT1* Ratio	Count gene signal LN *AKT1*	Count reference signal LN *AKT1*	DM *AKT1* Ratio	Count gene signal DM *AKT1*	Count reference signal DM *AKT1*
I001									
I002									
I003									
I004									
I005									
I007									
I008	1.57	119	76						
I009									
I010									
I011									
I013									
I014									
I015									
I016	1.25	79	63						
I017									
I018									
I019									
I020	1.39	89	64						
I021									
I024									
I025									
I026									
I027									
I028									
I029									
I030									

I031									
I033									
I034									
I038									
I039				1.54	106	69			
I048									
I052	1.29	85	66						
I053									
I055									
I056									
I059									
I060									
I061									
I062									
I063									
I064									
I065									
I066									
I068									
I089									
I091									
I093									
I095									
I096									
I097									
I098									
I099									
I100									
I101									
I103									
I104									
I106	1.24	78	63				1.21	82	68
I107									
I109									
I110									
I112									
I113									
I117							1.22	83	68
I118				1.19	83	70			
I120									
I121									
I122									

I123				1.21	76	63			
I124									
I127									
I133									
I138				1.31	109	83			
I141									
I142									
I144									
I146									
I147									
I148									
I149									
I152									
I153									
I156									
I157									
I158							1.21	85	70
I160	1.61	108	67						
I161									
I162				1.34	95	71			
I163									
I166									
I168				1.14	75	66			
I169									
I172									
I173									
I174									
I176									
I178									
I180	1.29	88	68	1.41	103	73			
I183									
I184									
I186									
I188	1.28	88	69						
I189				1.30	87	67			
I190									
I192	1.05	80	76	1.31	89	68			
I193									
I194									
I195	1.37	89	65	1.21	85	70			
I196									
I197				1.60	88	55			

I198									
I199									
I201									
I202									
I207									

C) *AKT2*

Samples	P *AKT2* Ratio	Count gene signal P *AKT2*	Count reference signal P *AKT2*	LN *AKT2* Ratio	Count gene signal LN *AKT2*	Count reference signal LN *AKT2*	DM *AKT2* Ratio	Count gene signal DM *AKT2*	Count reference signal DM *AKT2*
I001									
I002									
I003	1.11	78	70						
I004									
I005									
I007									
I008	1.26	49	39						
I009									
I010									
I011									
I013									
I014									
I015									
I016									
I017									
I018									
I019									
I020									
I021									
I024									
I025									
I026									
I027									
I028									
I029									
I030									
I031									
I033									
I034									
I038									

I039									
I048									
I052									
I053									
I055									
I056									
I059									
I060									
I061									
I062									
I063									
I064									
I065									
I066									
I068									
I089									
I091									
I093									
I095									
I096									
I097									
I098									
I099									
I100									
I101									
I103									
I104									
I106	1.08	86	80				1.05	81	77
I107									
I109									
I110									
I112									
I113									
I117									
I118	1.07	87	81	1.23	70	57			
I120									
I121									
I122									
I123				1.23	70	57			
I124									
I127									
I133									

I138				1.14	83	73			
I141									
I142									
I144									
I146									
I147									
I148									
I149									
I152									
I153									
I156									
I157									
I158									
I160									
I161									
I162				1.37	89	65			
I163									
I166									
I168				1.23	79	64			
I169									
I172									
I173									
I174				1.26	81	64			
I176									
I178									
I180									
I183									
I184									
I186									
I188	1.00	78	78						
I189				1.17	81	69			
I190									
I192	1.34	39	29	1.11	78	70			
I193									
I194									
I195				1.05	67	64			
I196									
I197									
I198				1.12	83	74	1.33	96	72
I199									
I201									
I202	1.21	88	73						

I207									

D) PDGFRα

Samples	P *PDGFRα* Ratio	Count gene signal P *PDGFRα*	Count reference signal P *PDGFRα*	LN *PDGFRα* Ratio	Count gene signal LN *PDGFRα*	Count reference signal LN *PDGFRα*	DM *PDGFRα* Ratio	Count gene signal DM *PDGFRα*	Count reference signal DM *PDGFRα*
I001				1.15	78	68	1.20	89	74
I002									
I003									
I004									
I005									
I007									
I008									
I009									
I010									
I011									
I013									
I014									
I015									
I016									
I017									
I018									
I019									
I020									
I021									
I024									
I025									
I026									
I027									
I028									
I029									
I030									
I031									
I033									
I034									
I038									
I039									
I048									
I052									

I053									
I055									
I056									
I059									
I060									
I061									
I062									
I063									
I064									
I065									
I066									
I068									
I089									
I091									
I093									
I095									
I096									
I097									
I098									
I099									
I100									
I101									
I103									
I104									
I106									
I107									
I109									
I110									
I112									
I113									
I117									
I118									
I120									
I121				1.11	84	76			
I122									
I123									
I124									
I127									
I133									
I138				1.29	93	72			
I141									
I142									

I144									
I146									
I147									
I148									
I149							1.07	88	82
I152									
I153									
I156									
I157									
I158							1.06	75	71
I160									
I161									
I162				1.39	100	72			
I163									
I166									
I168				1.16	80	69			
I169									
I172									
I173									
I174									
I176									
I178									
I180									
I183									
I184									
I186									
I188									
I189									
I190	1.09	87.00	80	1.03	90	87			
I192				1.07					
I193									
I194									
I195	1.10	80.00	73	1.14	89	78			
I196									
I197									
I198									
I199									
I201									
I202									
I207									

E) *PDGFRβ*

Samples	Count signal P *PDGFRβ*	Count signal LN *PDGFRβ*	Count signal DM *PDGFRβ*
I001		75	
I002			
I003	93		
I004			
I005			
I007			
I008	81		
I009			
I010	79	81	
I011			
I013			
I014	68		
I015	9		
I016			
I017			
I018			
I019			
I020			
I021			
I024			
I025			
I026			
I027			
I028			
I029			
I030			
I031			80
I033			
I034			
I038			
I039		90	
I048			
I052	84		
I053			
I055			
I056			
I059			

I060			
I061			
I062			
I063			
I064			
I065			
I066			
I068			
I089			
I091			
I093			
I095			
I096			
I097	68		
I098			
I099			
I100			
I101			
I103	77		
I104	9		
I106			
I107			
I109			
I110			
I112	73	74	
I113			
I117			78
I118			
I120			
I121			
I122			
I123			
I124			
I127			
I133		80	
I138	71	91	
I141			
I142	68	70	
I144			
I146		75	
I147			
I148			

I149		96	113
I152			
I153	71		
I156			
I157			
I158		85	90
I160			
I161			
I162		79	
I163			
I166	79	77	
I168			
I169			
I172	63		
I173	76	82	
I174		73	
I176		82	
I178		9	
I180	80		
I183			
I184			
I186			9
I188			
I189		69	
I190	79	78	
I192	94	85	
I193			
I194			
I195	66	78	
I196			
I197			
I198			79
I199			
I201			
I202	84	69	
I207			

F) *mTOR*

Samples	P *mTOR* Ratio	Count gene signal P *mTOR*	Count reference signal P *mTOR*	LN *mTOR* Ratio	Count gene signal LN *mTOR*	Count reference signal LN *mTOR*	DM *mTOR* Ratio	Count gene signal DM *mTOR*	Count reference signal DM *mTOR*
I001									
I002									
I003									
I004									
I005	1.22	95	78						
I007									
I008	1.18	91	77						
I009	1.23	74	60						
I010									
I011									
I013	1.31	81	62						
I014	1.27	85	67						
I015									
I016									
I017									
I018									
I019									
I020									
I021									
I024									
I025									
I026									
I027									
I028									
I029	1.08	66	61	1.43	90	63			
I030									
I031									
I033									
I034									
I038									
I039									
I048									
I052	1.19	86	72						
I053									
I055									
I056									

I059									
I060									
I061									
I062									
I063									
I064									
I065									
I066									
I068									
I089									
I091									
I093									
I095									
I096									
I097									
I098									
I099									
I100				-					
I101									
I103									
I104									
I106	1.19	94	79						
I107									
I109									
I110									
I112									
I113									
I117									
I118	1.36	90	66						
I120									
I121	1.04	76	73	1.46	99	68			
I122									
I123									
I124									
I127									
I133									
I138				1.23	81	66			
I141									
I142									
I144									
I146									
I147									

I148									
I149							1.39	96	69
I152									
I153	1.15	84	73						
I156									
I157									
I158									
I160									
I161									
I162				1.19	96	81			
I163									
I166									
I168									
I169									
I172				-					
I173	1.50	73	64						
I174				1.21	74	61			
I176									
I178									
I180									
I183									
I184	1.30	86	66						
I186									
I188									
I189									
I190	1.00	60	60						
I192									
I193									
I194									
I195									
I196									
I197									
I198									
I199									
I201									
I202	1.58	89	62						
I207									

Table 31: Statistical analysis of the association between gains in the PI3K/AKT/mTOR pathway and subsequent protein expression and activation.
CN: copy number, P: primary tumor, LN: lymph node metastasis, DM: distant metastasis.

Protein expression	p-mTOR any 0-3 vs. 4-12	p-mTOR any 0-6 vs. 7-12	p-S6 any 0-3 vs. 4-12	p-S6 any 0-6 vs. 7-12	p-4E-BP1 any 0-3 vs. 4-12	p-4E-BP1 any 0-6 vs. 7-12	any 0-3 vs. 4-12
Gene CN variation							
P *AKT1*	0.463	0.856	0.602	0.602	0.382	0.28	0.408
LN *AKT1*	0.263	0.671	0.271	0.271	0.225	0.581	0.436
DM *AKT1*	1	-	0.252	0.252	0.188	0.569	0.279
any *AKT1*	0.199	0.908	0.363	0.363	0.489	0.097	0.709
P *AKT2*	0.197	0.932	0.735	0.735	0.211	0.814	0.24
LN *AKT2*	0.063	0.813	0.565	0.565	0.326	0.708	0.209
DM *AKT2*	0.153	-	0.335	0.335	0.585	0.87	0.104
any *AKT2*	0.003*	0.261	0.362	0.362	0.794	0.156	0.113
P *PDGFRα*	0.253	0.92	0.732	0.732	0.051	0.783	0.434
LN *PDGFRα*	0.22	0.754	0.468	0.468	0.32	0.522	0.847
DM *PDGFRα*	0.067	-	0.19	0.19	0.028*	0.64	0.166
any *PDGFRα*	0.419	0.342	0.129	0.129	0.087	0.765	0.751
P *PDGFRβ*	0.605	0.394	0.909	0.909	0.056	0.694	0.223
LN *PDGFRβ*	0.491	0.31	0.437	0.437	0.343	0.983	0.682
DM *PDGFRβ*	0.928	-	0.803	0.803	0.36	0.439	0.923
any *PDGFRβ*	0.446	0.144	0.35	0.35	0.352	0.273	0.19
P *mTOR*	0.483	0.602	0.928	0.928	0.413	0.397	0.451
LN *mTOR*	0.46	0.876	0.758	0.758	0.648	0.74	0.395
DM *mTOR*	0.165	-	0.377	0.377	0.14	0.73	0.64
any *mTOR*	0.961	0.889	0.693	0.693	0.953	0.766	0.418
P *PIK3CD*	0.841	0.224	0.254	0.254	0.685	0.4	0.349
LN *PIK3CD*	0.093	0.645	0.046	0.046	0.593	0.542	0.678
DM *PIK3CD*	0.028*	-	0.715	0.715	0.715	-	0.4
any *PIK3CD*	0.15	0.836	0.793	0.793	0.703	0.114	0.481
any gain in	0.058	0.965	0.409	0.409	0.036	0.094	0.094

pathway (no vs. gain)							
any gain in pathway (no vs. 1x vs multiple)	0.217	0.149	0.693	0.693	0.075	0.218	0.2
any gain in pathway (no vs. 1x vs. 2x vs. 3x+)	0.089	0.283	0.36	0.36	0.142	0.344	0.285
any gain in pathway (no vs. 1x vs. 2x vs. 3x vs. 4x+)	0.161	0.432	0.519	0.519	0.227	0.358	0.408
any gain in pathway (no vs. 1x vs. 2x vs. 3x vs. 4x vs. 5x)	0.127	0.577	0.609	0.609	0.159	0.497	0.382
lower vs. higher gains (0-2 vs. >3)	0.128	0.218	0.874	0.874	0.415	0.483	0.439